

INFORMATION TO USERS

This manuscript has been reproduced from the microfilm master. UMI films the text directly from the original or copy submitted. Thus, some thesis and dissertation copies are in typewriter face, while others may be from any type of computer printer.

The quality of this reproduction is dependent upon the quality of the copy submitted. Broken or indistinct print, colored or poor quality illustrations and photographs, print bleedthrough, substandard margins, and improper alignment can adversely affect reproduction.

In the unlikely event that the author did not send UMI a complete manuscript and there are missing pages, these will be noted. Also, if unauthorized copyright material had to be removed, a note will indicate the deletion.

Oversize materials (e.g., maps, drawings, charts) are reproduced by sectioning the original, beginning at the upper left-hand corner and continuing from left to right in equal sections with small overlaps. Each original is also photographed in one exposure and is included in reduced form at the back of the book.

Photographs included in the original manuscript have been reproduced xerographically in this copy. Higher quality 6" x 9" black and white photographic prints are available for any photographs or illustrations appearing in this copy for an additional charge. Contact UMI directly to order.

UMI

A Bell & Howell Information Company
300 North Zeeb Road, Ann Arbor MI 48106-1346 USA
313/761-4700 800/521-0600



EPR Study on Vanadium Model Compounds Containing Nitrogen and Sulfur Heteroatoms

BY

Mohamed Omer Hamad AL-Turabi

A Dissertation Presented to the
FACULTY OF THE COLLEGE OF GRADUATE STUDIES
KING FAHD UNIVERSITY OF PETROLEUM & MINERALS
DHAHRAN, SAUDI ARABIA

In Partial Fulfillment of the
Requirements for the Degree of

DOCTOR OF PHILOSOPHY
In
CHEMISTRY

June 1998

UMI Number: 9915358

UMI Microform 9915358
Copyright 1999, by UMI Company. All rights reserved.

**This microform edition is protected against unauthorized
copying under Title 17, United States Code.**

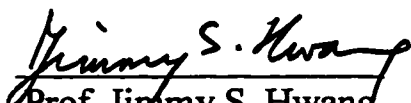
UMI
300 North Zeeb Road
Ann Arbor, MI 48103


KING FAHD UNIVERSITY OF PETROLEUM AND MINERALS
DHAHRAN 31261, SAUDI ARABIA


COLLEGE OF GRADUATE STUDIES

This Dissertation, written by **Mohamed Omer Hamad**, under the direction of his Dissertation Advisor and approved by his Dissertation Committee, has been presented to and accepted by the Dean of the College of Graduate Studies, in partial fulfillment of the requirements for the degree of **DOCTOR OF PHILOSOPHY in Chemistry**


Dissertation Committee



Prof. Jimmy S. Hwang
Dissertation Advisor

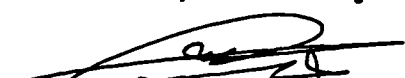

Dr. Abdul-Rahman A. Al-Arfaj
Member


Prof. Abdulaziz A. Al-Suwaiyan,
Member


Prof. Uwe K. Klein
Member


Prof. Fida F. Al-Adel
Member


Dr. Abdul-Rahman A. Al-Arfaj
Chairman, Chemistry Department


Dr. Abdallah M. Al-Shehri
Dean, College of Graduate studies

Date: 29/6/48



**TO THOSE WHO MADE IT POSSIBLE
MY PARENTS, WIFE & SON**

ACKNOWLEDGEMENT

Acknowledgment is due to King Fahd University of Petroleum and Minerals (KFUPM), for extending all the facilities and providing financial support.

I wish to express my sincere appreciation and gratitude to my advisor and chairman of my dissertation committee,.

Prof. Jimmy Hwang for his kind supervision endless encouragement and support. I would like also to express my appreciation and thanks to the committee members of my dissertation, Prof. Uwe Klein, Prof. Abdulaziz A. Al-Suwaiyan, Dr. Abdulrahman Al-Arfaj, Prof. Fida Al-Adel for their time reviewing the manuscript and for their valuable suggestions and remarks.

I wish to thank the Chemistry Department, and the Chairman Dr. Abdulrahman Al-Arfaj for extending all the facilities and support to conduct this research work. I am also thankful to Prof. M. S. Hussain the graduate advisor and Dr A. Abdennabi the former graduate advisor.

Thanks are also due to Prof. S. M. Sultan, Prof. S. A. Ali, Dr. M. Morsy, Mr. H. B. Balkhoyor, Mr. M. Saleem, Mr. W. Faroogi, Mr. Mir M. Hassan, Mr. I. Ismail for their help during this research work.

Finally, a word of appreciation and gratitude should go to my family whose support and understanding made this achievement possible.

TABLE OF CONTENTS

LIST OF TABLES	ix
LIST OF FIGURES	xi
ENGLISH ABSTRACT	xv
ARABIC ABSTRACT.....	xvii
CHAPTER ONE	1
1.1. INTRODUCTION.....	1
1.2. OBJECTIVES	8
CHAPTER TWO	9
2. THEORETICAL BACKGROUND	9
2.1. ELECTRON SPIN RESONANCE	9
2.2. DETERMINATION OF THE MAGNETIC PARAMETERS	12
2.3. THE EFFECTS OF ROTATIONAL MOTION ON EPR	
SPECTRA.....	19
2.3.1. <i>Fast Tumbling</i>	21

2.3.2. <i>Slow Tumbling</i>	24
2.4. THE TRANSLATIONAL DIFFUSION CONSTANT	30
CHAPTER THREE	32
3. APPARATUS AND PROCEDURE	32
3.1. THE EPR SPECTROMETER.....	32
3.1.1. <i>General Description</i>	32
3.1.2. <i>The Microwave Bridge</i>	35
3.1.3. <i>The EPR Cavity</i>	37
3.2. VACUUM SYSTEM	38
3.3. ESR SAMPLE PREPARATION	38
3.3.1. <i>V1 in toluene</i>	38
3.3.2. <i>V2 in toluene</i>	40
3.3.3. <i>V3 in methylene chloride</i>	40
3.3.4. <i>V4 in methylene chloride</i>	41
3.4. DATA COLLECTION AND EPR SPECTROMETER	
OPERATION:	41
3.5. DIFFUSION EXPERIMENT.....	44
3.5.1. <i>Capillary Diffusion Cell</i>	44
3.5.2. <i>3.5.2 Sample Preparation</i>	44
3.5.3. <i>Measurement and Data Collection</i>	47
CHAPTER FOUR	48
4. THE MAGNETIC PARAMETERS STUDY	48
4.1. DETERMINATION OF THE MAGNETIC PARAMETERS	48

4.1.1. <i>Isotropic Magnetic Parameters:</i>	48
4.1.2. <i>Anisotropic Magnetic Parameters</i>	53
4.2. ELECTRONIC AND STRUCTURAL STUDY	61
4.2.1. <i>Crystal Field Approximation:</i>	61
4.2.2. <i>Molecular Orbital Approach</i>	65
4.3. APPLICATION TO NON-PORPHYRIN VANADIUM SPECIES IN ASPHALTENS.....	76
CHARTER 5.....	81
5. TRANSLATIONAL DIFFUSION STUDY.....	81
5.1. THE DIFFUSION CONSTANT	82
5.1.1. <i>For V1 in Toluene</i>	82
5.1.2. <i>For V2 in toluene</i>	84
5.1.3. <i>For V3 in methylene chloride:</i>	84
5.1.4. <i>For V4 in methylene chloride:</i>	89
5.2. THE HYDRODYNAMIC RADIUS:.....	93
CHAPTER VI.....	94
6. MOTIONAL ANALYSIS :	94
6.1. MOTIONAL NARROWING ANALYSIS :.....	94
6.2. SLOW TUMBLING.....	119
6.3. ALLOWED-VALUES EQUATION (AVE)	139
6.4. STOKES-EINSTEIN MODEL	143
6.5. ANISOTROPIC INTERACTION PARAMETER (K):	146
6.6. STICKINESS FACTOR (S).....	160

CHAPTER VII.....	166
7. CONCLUSION	166
REFERENCES.....	171

LIST OF TABLES

Table 4.1 : Isotropic Magnetic Parameters:	54
Table 4.2 : Anisotropic Magnetic Parameters:.....	60
Table 4.3 : Molecular orbitals coefficients	72
Table 4.4 : P and K values	73
Table 5.1. Results from Translational Diffusion Experiment:.....	93
Table 6.1: Experimental Values of B & C for V1 at different Temperatures:	102
Table 6.2: Experimental Values of B & C for V2 at different Temperatures:	103
Table 6.3: Experimental Values of B & C for V3 at different Temperatures:	112
Table 6.4: Experimental Values of B & C for V4 at different Temperatures	113
Table 6.5 The Axis and the Anisotropy of Rotation of the Studied Systems	117
Table 6.6 Computational Data.....	121
Table 6.7 : AVE Parameters and Results :	142
Table 6.8 : Stokes-Einstein Model Results :	144
Table 6.9 : η , η/T and τ_R Values for v1 in toluene	148
Table 6.10 : η , η/T and τ_R Values for v2 in toluene	150

Table 6.11 : η , η/T and τ_R Values for ν_3 in CH_2Cl_2	152
Table 6.12 : η , η/T and τ_R Values for ν_4 in CH_2Cl_2	153
Table 6.13 : Anisotropic Interaction Results	162

LIST OF FIGURES

Scheme 1.1.a : Bis-(S-methyl-3-isopropylidenehydrazinecarbodithioato)	
oxovanadium(IV), V1.....	3
Scheme 1.1.b: Bis-(S-methyl-3-cyclohexylidene-hydrazinecarbodithioato)	
oxovanadium(IV), V2.....	3
Scheme 1.2. a) S-mehtyl-N-salicylidene-hydrazinecarbothioato-phenan	
throline-oxovanadium(IV), V3.....	4
Scheme 1.2 .b) S-mehtyl-N-5-me thoxysalicylidenehydrazine-carbothioato-	
phenanthorline-oxovanaium (IV), V4.....	4
Figure 2.1: A typical x-band spectrum of Oxovanadium (IV) at room	
temperature with DPPH as internal standard.	15
Figure 2.2: A typical x-band spectrum of Oxovanadium (IV) at 77K.....	17
Figure 2.3: Generalized energy level and transition scheme for	
oxovanadium (IV).....	29
Figure 3.1: A schematic representation of a Bruker EPR spectrometer	35
Figure 3.2: Block diagram of EPR spectrometer microwave bridge.....	37

Figure 3.3: A schematic representation of the capillary diffusion apparatus.	47
Figure 4.1.a: X-band spectrum of v1 in toluene at room temperature with DPPH as internal standard.	50
Figure 4.1.b: X-band spectrum of v2 in toluene at room temperature with DPPH as internal standard.	51
Figure 4.1.c: X-band spectrum of v3 in toluene at room temperature with DPPH as internal standard.	52
Figure 4.1.d: X-band spectrum of v4 in toluene at room temperature with DPPH as internal standard.	53
Figure 4.2.a: Rigid limit spectrum of v1 in toluene.	56
Figure 4.2.b: Rigid limit spectrum of v2 in toluene.	57
Figure 4.2.c: Rigid limit spectrum of v3 in methylene chloride.	58
Figure 4.2.d: Rigid limit spectrum of v4 in methylene chloride	59
Figure 4.3: Splitting of the vanadium d levels with C_{4v} symmetry	63
Figure 4.4: A typical oxovanadium(IV) general geometry.	67
Figure 4.5: Correlation between A_0 and g_0 values for a variety of square pyramidal vanadyl (IV) complexes	78

Figure 4.6: Correlation between g_{\parallel} and A_{\parallel} values for a variety of square pyramidal vanadyl (IV) complexes	80
Figure 5.1: EPR experimental spectra at different time intervals during the diffusion process of V1 in toluene.	84
Figure 5.2: Total ESR intensities as a function of time for V1 in toluene during the diffusion experiment.	86
Figure 5.3: EPR experimental spectra at different time intervals during the diffusion process of V2 in toluene.	87
Figure 5.4: Total ESR intensities as a function of time for V2 in toluene during the diffusion experiment.	88
Figure 5.5: EPR experimental spectra at different time intervals during the diffusion process of V3 in methylene chloride.	89
Figure 5.6: Total ESR intensities as a function of time for V3 in methylene chloride during the diffusion experiment.	91
Figure 5.7: EPR experimental spectra at different time intervals during the diffusion process of V4 in methylene chloride.	92
Figure 5.8: Total ESR intensities as a function of time for V4 in methylene chloride during the diffusion experiment.	93
Figure 6.1: Variable temperature spectra of v1 in toluene at 9GHz.	95

Figure 6.2: Variable temperature spectra of ν_2 in toluene at 9GHz.	98
Figure 6.3: B vs C for ν_1 in toluene at different temperature.....	105
Figure 6.4: B vs C for ν_2 in toluene at different temperature.....	106
Figure 6.5: Variable temperature spectra of ν_3 in methylene chloride at 9GHz.	107
Figure 6.7: B vs C for ν_3 in CH_2Cl_2 at different temperature.....	115
Figure 6.8: B vs C for ν_4 in CH_2Cl_2 at different temperature.....	116
Figure 6.9: Variable temperature spectra of ν_1 in toluene at 9GHz.	123
Figure 6.10: Variable temperature spectra of ν_2 in toluene at 9GHz.	128
Figure 6.11: Variable temperature spectra of ν_3 in methylene chloride at 9GHz.	132
Figure 6.12: Variable temperature spectra of ν_4 in methylene chloride at 9GHz.	135
Figure 6.13: η (poise) / T (K) vs τ_R for ν_1 in toluene at 9GHz.	155
Figure 6.14: η (poise) / T (K) vs τ_R for ν_2 in toluene at 9GHz.	156
Figure 6.15: η (poise) / T (K) vs τ_R for ν_3 in methylene chloride at 9GHz.	158
Figure 6.16: η (poise) / T (K) vs τ_R for ν_4 in methylene chloride at 9GHz.	159

DISSERTATION ABSTRACT

Name : Mohamed Omer Hamad AL-Turabi

Title : EPR Study on Vanadium Model Compounds Containing Nitrogen and Sulfur Heteroatoms

Major : Physical Chemistry

Date : May 1998

Magnetic resonance study was carried out for four vanadium model compounds containing sulfur and nitrogen heteroatoms at 9GHz. These systems are Bis(S-methyl-3-isopropylidenehydrazinecarbodithio)oxovanadium(IV); (V1); and Bis(S-methyl-3-cyclohexylidenehydrazinecarbodithio)oxovanadium(IV); (V2) in toluene and S-methyl-N-salicylidene-hydrazinecarbo-thioatophenanthrolineoxovanadium(IV); V3; and S-methyl-N-5-methoxysalicylidenehydrazinecarbothioatophenanthroline-oxovanadium(IV); V4; in methylene chloride.

The magnetic parameters for these systems are determined and structural and electronic information are obtained. The obtained magnetic parameters suggest that the structure of these systems is five coordinated distorted square pyramidal. Also, it is found that for $VO(N_2S_2)$ systems are characterized by a more in-plane σ -bonding compared to $VO(N_3S)$ systems. Also, it is found that for $VO(N_3S)$ systems the unpaired electron is more localized on vanadium compared to $VO(N_2S_2)$ systems. Also, we found a good correlation between g_{\parallel} and A_{\parallel} values for varying complexes with

equatorial liquids of the type $\text{VO}(\text{N}_4)$, $\text{VO}(\text{N}_3\text{S})$, $\text{VO}(\text{N}_2\text{S}_2)$ and $\text{VO}(\text{S}_4)$. This will be useful in characterization of the non-porphyrin species of vanadium in asphaltenes.

The hydrodynamic radii of these systems, which are essential to the anisotropic interaction analysis, are obtained from the translational diffusion experiment to be 5.39, 5.70, 7.12 and 7.67 Å for V1 and V2 in toluene and V3 and V4 in methylene chloride respectively.

The variable temperature spectra were recorded and analyzed in both the motional narrowing and the slow motion regions. The anisotropy of rotation (N) and the correlation times, τ_R were obtained from this motional analysis. The fast motion limit analysis suggest that the four systems studied were undergoing axially symmetric rotational diffusion at y-axis with $N = 2.5, 1.7, 1.5$ and 1.7 ± 0.4 for V1, V2, V3 and 4 respectively. The spectra in the slow tumbling region were successfully simulated using the Brownian model. This is important for the calculation of the hydrodynamic molecular radius, r_o , based on the stick model.

Molecular reorientation for these systems were analyzed in terms of the hydrodynamic free space model for molecular relaxation in liquids. The motional analysis indicate that the solute-solvent interactions and r_o are constant in the temperature range studied. The stickiness factor is found to be 0.461, 0.636, 0.365 and 0.160 for V1, and V2 in toluene, and V3 and V4 in methylene chloride respectively. We found that quite remarkably that S approaches unity even on the molecular level. In conclusion, rough solute spheres exert torques more efficiently than elongated solutes, and the solutes exert torques more efficiently when the solvent used is more anisotropic

خلاصة الرسالة

اسم مقدم الرسالة : محمد عمر حمد الترابي

عنوان الرسالة : دراسات الرنين الإلكتروني البارامغناطيسي لمركبات الفانديوم
النمذجية المحتوية على النتروجين والكبريت .

التخصص : كيمياء طبيعية

التاريخ : يونيو 1998م

تم إجراء دراسة الرنين الإلكتروني البارامغناطيسي (EPR) لأربعة نظم من مركبات الفانديوم والتي تعتبر نموذج للمركبات التي تحتوى على الكبريت والنتروجين. النظام الأول هو ثنائي (S - ميثيل -3- ايزوبروبيل - هايدرازين - كاربودايثيوتو) اكسي الفانديوم في التولوين ، والثاني هو ثنائي (S - ميثيل -3- هكسيل حلقي - هايدرازين - كاربودايثيوتو) اكسي الفانديوم في التولوين ، والثالث هو S-ميثيل-N-ساليسيلدين-هايدرازين-كاربودايثيوتو-فنانثرولين، اكسي الفانديوم في كلوريد الميثيل ، أما النظام الرابع فهو S-ميثيل-N-O-مئوكسي-ساليسيلدين-هايدرازين-كاربودايثيوتو-فنانثرولين، اكسي الفانديوم في كلوريد الميثيل .

ولقد تم تعيين ودراسة المعاملات المغناطيسية لهذه النظم وقد أظهرت هذه الدراسة أن المركبات من النوع $VO(N_2S_2)$ تحتوى على روابط σ -bonding في المستوى القاعدي أقوى من تلك التي لدى النوع $VO(N_3S)$. وأن احتمالية تواجد الإلكترون غير المتزاوج على الفانديوم في النظم من النوع $VO(N_2S_2)$ أعلى مما هي عليه لدى النظم من النوع $VO(N_2S_2)$. وكذلك وجدت علاقة جيدة بين $A_{||}$ و $g_{||}$ للمركبات من النوع $VO(S_4)$ ، $VO(NS_3)$ ، $VO(N_2S_2)$ ، $VO(N_4)$ ونوع المركب . هذه العلاقة يمكن الاستفادة منها في تصنيف و معرفة الفانديوم في البترول الخام .

ولقد تم تحديد نصف القطر الهايدروديناميكي لهذه النظم بواسطة طريقة الانتشار خلال الأنبوب الشعرية كما يلي 29, 5 ، 70 ، 5 ، 12, 7 و 67, 7 انجس ترون للنظامي الأول والثاني في التولوين والثالث والرابع في كلوريد الميثيل على التوالي .

ولقد تم دراسة خطوط الطيف لهذه النظم عند درجات حرارة مختلفة وذلك في مدي الحركتين السريعة والبطيئة. ومن هذه الدراسة تم إيجاد معامل التباين الدوراني (N) ومحور الدوران وكذلك معامل الزمن الدوراني (τ_R). ولقد وجد من الدراسات مدي الحركة السريعة أن محور الدوران هو لكل هذه النظم هو المحور الصادي وقيمة مدي تباين الدوران هو 2,5 و $1,7 \pm 0,4$ للنظامين الأول والثاني في تولوين وهو 1,5 و $1,7 \pm 0,4$ للتالث والرابع في كلوريد الميثيل على التوالي. ثم تمت محاكاة خطوط الطيف في مدي الحركة البطيئة وذلك باستعمال نموذج براون ، و بناءً على ذلك تم حساب نصف القطر الهايدروديناميكي لهذه النظم عند حد الالتصاق الكامل.

و أخيراً فقد تم دراسة إعادة الدوران الجزيئي لهذه النظم بواسطة نظرية الحيز الهيدروديناميكي الخالي لتراخي الجزئيات في السوائل . ولقد وجد أن كل من التفاعل المتبادل بين المذاب والمذيب ونصف القطر الهايدروديناميكي لم يتغيرا في مدي درجات الحرارة الذي تمت دراسته . ولقد وجد أن قيمة معامل الالتصاق (S) تساوي 0,461 ، 0,636 ، 0,365 و 0,160 للنظامين الأول والثاني في التولوين والثالث والرابع في كلوريد الميثيل على التوالي .

ولقد أظهرت هذه الدراسة أن معامل الالتصاق تقترب من حد الالتصاق (S=1) على المستوى الجزيئي ، و أن المذابات الكروية غير المنتظمة تبذل عزوماً بفاعلية أكثر من المذابات المطولة ، وكذلك فإن المذابات تبذل عزوماً أكثر عندما تكون مذابة في مذيبات متباينة الشكل.

CHAPTER ONE

1.1 INTRODUCTION

Electron spin resonance (ESR) also known as electron paramagnetic resonance (EPR) is a branch of spectroscopy in which radiation of microwave frequency is absorbed by molecules, ions, or atoms possessing electrons with unpaired spins in an external magnetic field. EPR is a powerful spectroscopic technique for structural and dynamical investigations at the molecular level ¹⁻¹⁵. EPR structural investigations^{1,2} on the vanadyl ion can be applied to reveal important information like the environment of the vanadyl ion, the nature of the ligand types, and the distortion of the complex and association with other systems. Also EPR study provides some important molecular motion information like the anisotropy of rotation, the hydrodynamic radius, the correlation times, and the anisotropic interaction parameter ^{5,6,8-13}.

EPR magnetic parameters can be used in combination with the optical data to get information on the distortion and the electronic structures of the molecules^{1,2}. In fact, the order of the magnitude of the g-tensors give direct information on the structure of the system. Also, the g-tensors can be used in combination with the optical data to calculate the molecular orbital coefficients which reflect the bonding properties in the molecule. Furthermore, the hyperfine tensors can be used in combination with the

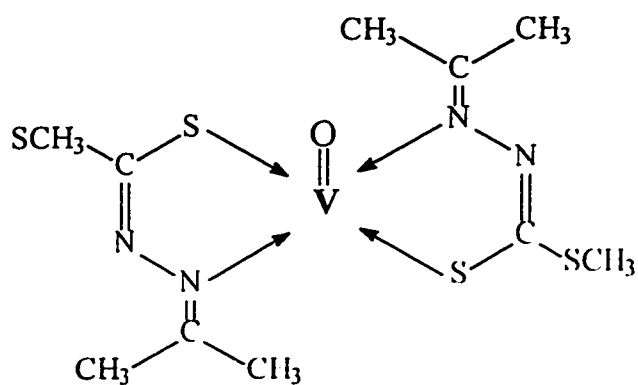
optical data to get some information on the unpaired electron delocalization. This information will be significant for determining the overall structure of metal-containing compounds in heavy crude oil ^{1,2}.

In literature there is a lot of interest in the application of EPR spectroscopy to vanadium systems to understand the nature of vanadium compounds present in petroleum ². However the non-porphyrin vanadium in crude oil is poorly understood. Knowledge about the chemical nature of vanadium is a prerequisite to understanding the role that vanadium ion plays in the origin of petroleum and to determine how to remove this element from petroleum product.

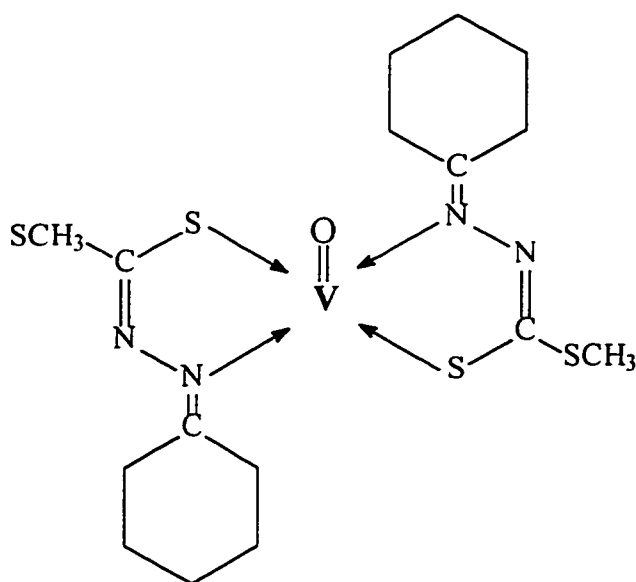
Yen ² proposed a method for the characterization of vanadium in oil by using the isotropic magnetic parameters. Yen ² found a linear relationship between A_0 and g_0 for VO^{2+} complexes for ligands made of varying compositions. Later, this method is improved by Holyk ^{14,15} who proposed the use of the anisotropic magnetic parameters rather than the isotropic magnetic parameters. Holyk ^{14,15} has shown that the correlation between $g_{||}$ and $A_{||}$ is perhaps more useful because $g_{||}$ depends directly on the in-plane ligand field and the range of the values for $g_{||}$ and $A_{||}$ is about twice that of g_0 and A_0 . However, as stated by Yen, this model would rest on a better foundation if data for $VO(NS_3)$, $VO(N_2S_2)$ and $VO(N_3S)$ model compounds were available.

Recently four vanadyl model compounds which contain sulfur and nitrogen have been synthesized.³ The names and structures of these four compounds, in which the coordination of the four donor atoms in the vanadyl complex consists of nitrogen and sulfur, are given in schemes 1.1 and 1.2. Since there is much interest in the vanadyl complexes containing

a) V1

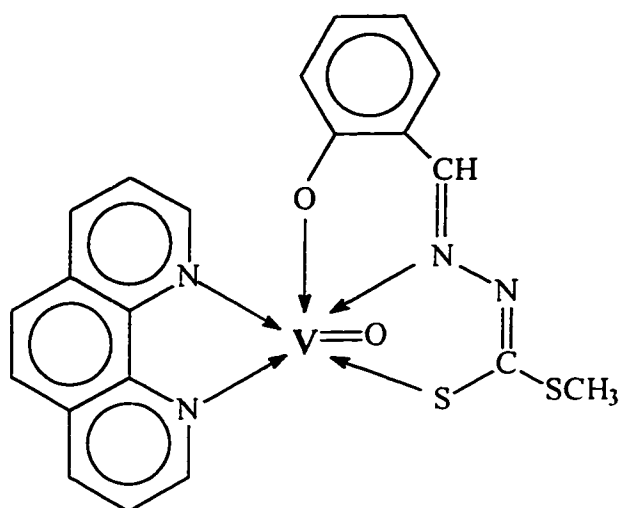


b) V2

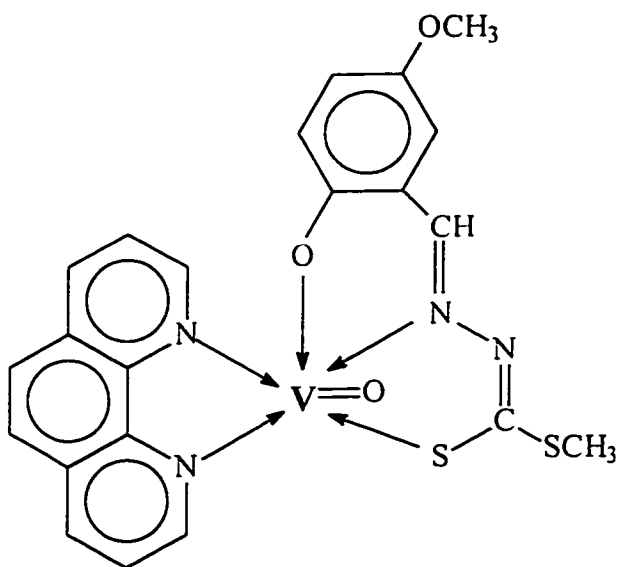


Scheme 1.1 a) Bis-(S-methyl-3-isopropylidene-hydrazine-carbodithioto) oxovanadium(IV); **V1**; b) Bis-(S-methyl-3-cyclohexylidene-hydrazine carbodithioto) oxovanadium(IV); **V2**;

a)



b)



Scheme 1.2 a) S-methyl-N-salicylidene-hydrazinecarbothioato-phenanthroline-oxovanadium(IV), V3; b) S-methyl-N-5-methoxy-salicylidene-hydrazinecarbothioato-phenanthroline-oxovanadium (IV), V4.

nitrogen and sulfur model compounds we will examine these four model compounds, V1, V2, V3 and V4. The reason for their choice is because these compounds have different sizes and corrugation ^{4,5}, and they have different ligand types, namely N₂S₂ and N₃S types.

The study of molecular dynamics in liquids is an active and exciting area in theoretical, computational, and experimental chemical physics ^{5,6,8-13}. EPR is a powerful spectroscopic technique for obtaining information at the molecular level, because EPR spectra of dilute solutions of spin probes in liquids are almost always showing single-particle properties. Moreover, the characteristic time scale of EPR experiments implies that they will be sensitive to motions of spin probes in liquids and diffusing probed macromolecules. Molecular motion modulates the EPR line shape due to its effects on the anisotropic magnetic parameters. The VO²⁺ probes are more sensitive to molecular motion than the more popular nitroxide spin probes because VO²⁺ probes do have (i) more anisotropic magnetic parameters, (ii) wider spectra scan range, and (iii) having more resonance lines which are free from inhomogeneous broadening presents in nitroxides.

In molecular dynamics investigations^{5,6,8-13} two regimes are distinguished, namely the motional narrowing region and the slow motion region. In the fast motion limit the motions of the probe molecules and solvent molecules are not so intimately coupled as much as it is in the slow motion. Thus molecular motion information can be obtained more directly in the slow tumbling when the two are intimately coupled. The motional narrowing analysis is more simple, however the slow tumbling study is more informative, more sensitive and adequate to study the motion by spin probes in viscous liquids and/or slowly diffusing spin-probed

macromolecules in solution. At present, the time scale of EPR slow motion region for nitroxide probes is extended to the range 10^{-11} - 10^{-10} s by working at high fields (90kG) and high frequencies (250MHz). Alternatively, this extension could be accomplished by using large vanadyl probes^{8,9}.

There are few EPR studies of $\text{VO}(\text{N}_2\text{S}_2)$ and $\text{VO}(\text{N}_3\text{S})$ model compounds in the fast motional region⁵. In previous work⁵ line shape analysis of V1 and V4 in the fast motional region were analyzed using magnetic parameters determined from positions of the resonant lines in the rigid limit spectra based on second order perturbation theory⁶. The most accurate determinations of the magnetic parameters are obtained by simulating the glass spectrum. Improved line shape analysis could be carried out by using simulated magnetic parameters. There are few slow-motional EPR studies for vanadyl complexes in the literature.^{8,9} The theory is based on a theoretical calculation of line shapes using the Stochastic Liouville equation (SLE) which includes nonsecular contributions.⁸ There is no EPR study for model compounds of vanadium bound to nitrogen and sulfur heteroatoms at the slow motion region. The vanadyl slow tumbling spectra is sensitive to model of rotation, hence the slow tumbling spectra of these systems will be analyzed for model dependence, i.e. which of the motional models (Brownian, moderate jump or free diffusion).

Also, this motional analysis yields information on the rotational correlation times, τ_R , over a wide temperature range from the fast motional limit to the slow tumbling region. The rotational correlation time, τ_R , has been plotted as a function of temperature and found to be linear in η/T , where T is the absolute temperature and η is the coefficient of shear

viscosity of the solvent. For spherical or linear solute molecules this correlation can be expressed as¹⁰

$$\tau_R = \frac{4}{3} \left(\frac{\pi r_o^3}{k_B} \right) \left(\frac{\eta}{T} \right) \kappa \quad (1.1)$$

where k_B is the Boltzmann constant, κ an experimentally determined dimensionless coupling parameter linking rotational and translational effects called the anisotropic interaction parameter^{11,12}, and $4\pi r_o^3/3$ a molecular hydrodynamic volume. The molecular hydrodynamic volume can be determined independently from measurement of the translational diffusion constant using the capillary diffusion cell.¹³ To calculate the molecular hydrodynamic volume from measurement of the diffusion constant the knowledge of model of molecular motion is essential. This model is obtained from the slow motion study.

In literature, very few work has been done on the anisotropic interaction parameter κ of vanadyl systems.¹⁰ Most of these studies are on κ solvent dependence. No much work were carried out to study the effect of solute size, and solute shape on the anisotropic interaction parameter, κ .¹⁰

In the remainder of this chapter, the principal objectives of this work are summarized. In chapter 2 a brief account of the magnetic properties of vanadium spin probes, and the theoretical background of the magnetic parameters determination, motional analysis, and the hydrodynamic radius determination are given. In chapter 3 the spectrometer and apparatus used in the experiment, and the experimental procedure are described. In chapter 4 the magnetic parameters are obtained and analyzed for structural information. In chapter 5 the hydrodynamic radii are obtained by capillary

diffusion experiment. In chapter 6 the variable temperature spectra are analyzed to obtain molecular motion information. In chapter 7 the conclusions are given.

1.2 OBJECTIVES

The main objectives of this work are (i) To determine the hyperfine and g-tensors from the room temperature and the rigid limit ESR spectra for some vanadium model compounds containing sulfur and nitrogen heteroatoms. (ii) To investigate the molecular and the electronic structure based on the determined magnetic parameters. (iii) To carry out fast motional analysis of the variable temperature ESR spectra to determine anisotropy of rotation (N), the z-axis, and the correlation times. (iv) To simulate the slow tumbling ESR spectra for the vanadyl complexes using the stochastic Liouville equation to see whether the anisotropy of rotation determined in the fast motional region could be carried over to the slow tumbling region and to determine if indeed it is a Brownian particle and to obtain the correlation time. (v) The hydrodynamic radius of the solvated solute in solution will be measured using the capillary diffusion technique. (vi) To investigate the effect of the solute size, and solute shape on the stickiness factor and the anisotropic interaction parameter for large molecules.

CHAPTER TWO

2.THEORETICAL BACKGROUND

2.1 ELECTRON SPIN RESONANCE

In EPR, different energy states arise from the interaction of the unpaired electron spin moment (given by $m_s = \pm 1/2$ for a free electron) with the magnetic field, the so called electronic Zeeman effect. The Zeeman Hamiltonian for the interaction of an electron with the magnetic field is given by

$$H = g \beta_e B S_z \quad (2.1)$$

where g is the g-tensor, β_e is the electron Bohr magneton, S_z is the spin operator, and B is the applied magnetic field strength. Thus transition can be induced between the two levels by an oscillating magnetic field having the frequency

$$\nu = \frac{g \beta_e B}{h} \quad (2.2)$$

where h is the Planck's constant.

EPR has proven to be a powerful technique for spectroscopic study of any system that possesses a net electron spin angular momentum. Typical

examples of systems that are amenable to study by EPR include free radicals produced by physical or chemical means in the solid, liquid or gaseous state; biradicals, molecules containing two unpaired electrons at sufficient separation such that unpaired electrons only weakly interact; triplet state molecules, which include ground state triplet molecules as well as triplet states produced by thermal or photochemical excitation; conduction electrons in metals; applications to biochemical and biomedical problems; semiconductors; and most of the transition metal ions.

The spin probe could be a paramagnetic metal ion of the transition or lanthanide series, or a nitroxide radical. One of the popular probes is the vanadyl spin probe. The vanadyl spin probe has paramagnetic properties due to the existence of an unpaired electron (d^1 -system). A number of factors contribute to the popularity of these spin probes, for example, many vanadyl probes can easily be obtained and purified; they are stable over a wide range of temperatures and do not, therefore, undergo appreciable changes in magnetic parameters with variation in temperature; they are readily soluble in many organic solvents; they have an electron spin of $1/2$ and its orbital contribution to the magnetic moment is largely quenched, they have only vanadium nuclear moment which contributes to the spectrum and they do not therefore involve any complications found in systems with several nuclear spins.¹⁶ Thus the subsequent theoretical analysis is simplified and the results are easier to interpret than for typical nitroxide spin probes with less symmetry.¹⁷ Also the characteristic eight-hyperfine-line EPR spectrum of vanadyl complexes provides a more severe testing of any theoretical analysis than a nitroxide spectrum with three hyperfine-lines

would provide. In addition, inhomogeneous broadening is usually negligible in the EPR spectra of vanadyl complexes.¹⁶

There are two techniques related to the vanadyl spin probes: the spin labeling and the spin probe techniques.¹⁸⁻²⁰ Spin labeling is a technique which involves covalent bonding of vanadyl probe to diamagnetic media like liquid crystals. For systems with no inherent paramagnetism, a great advantage is gained by introduction of some versatile probe containing a paramagnetic center. Line-width measurements of the EPR spectra of covalently bound spin label may give information on the mobility of macromolecules. The spin probe technique is a method whereby different paramagnetic centers are mixed with the diamagnetic host (unbound), and their tumbling behavior during relaxation and transition process in the diamagnetic host is studied. The spectral changes result from restrictions in the motional freedom imposed upon the probe by its microenvironment. The vanadyl spin probe studies have been performed in liquid and frozen media,²¹⁻²³ petroleum², poly(vinyl alcohol)gels,²⁴ liquid crystals, human serotransferrin²⁵ as well as many other biological systems.²⁶

EPR methods can be applied to reveal three of the most important types of structural information: (1) the environment of the vanadyl ion, (2) the nature of ligand types, and (3) the distortion of complexes and association with systems, as well as dynamical information.

2.2 DETERMINATION OF THE MAGNETIC PARAMETERS

The spin Hamiltonian, H_S , for the vanadyl paramagnetic systems is:^{19,20}

$$H_S = B \beta_e \mathbf{g} \cdot \mathbf{S} + \mathbf{S} \cdot \mathbf{A} \cdot \mathbf{I} + (\text{electron-electron dipole term}) + (\text{electron-electron exchange term}) + (\text{nuclear Zeeman term}) \quad (2.3)$$

The first term is the electron Zeeman term and the second term is the electron-nuclear hyperfine interaction term; where β_e is electron Bohr magneton, B is the laboratory magnetic field, \mathbf{g} the \mathbf{g} -tensors, \mathbf{S} is the electron spin angular momentum operator, \mathbf{A} is the electron-nuclear hyperfine tensor, and \mathbf{I} is the nuclear spin angular momentum operator. The nuclear Zeeman term is not important in most work²⁷ and will be omitted. For clarity small second order effects are not discussed here. The electron-electron dipole and exchange terms are significant only when very high concentration⁸ and single crystals studies²⁸ are considered.

The EPR spectra of these vanadyl complexes in liquid solutions can be described by the electron Zeeman and electron-nuclear hyperfine interactions included in the spin Hamiltonian:^{6,4}

$$H_S = \beta_e \mathbf{g} \cdot \mathbf{S} B + \hbar \mathbf{I} \cdot \mathbf{A} \cdot \mathbf{S} \quad (2.4)$$

where β_e is the Bohr magneton, \mathbf{S} is the electron spin operator, \mathbf{I} is the nuclear spin operator, B is the applied magnetic field, \mathbf{g} is the \mathbf{g} -value tensor and \mathbf{A} is the hyperfine interaction tensor of the ^{51}V nucleus.⁴

At the room temperature the allowed transitions, when a microwave field at frequency ω_0 is applied, occur at the field B which satisfies the resonance condition^{6,4}

$$\omega_0 = \frac{g_0 \beta_e B_M}{\hbar} + A_0 M + \frac{1}{2} A_0^2 \left[\frac{I(I-1) - M^2}{g_0 \beta_e B / \hbar} \right] \quad (2.5)$$

where ω_0 is the microwave frequency in radians per second, \hbar is the Planck's constant divided by 2π , $I = 7/2$, M is the nuclear spin magnetic moment, B_M is the resonant value of the magnetic field corresponding to M , A_0 is the isotropic hyperfine constant in radians per second:

$$A_0 = \frac{1}{3} (A_x + A_y + A_z) \quad (2.6)$$

and g_0 is the isotropic g-factor :

$$g_0 = \frac{1}{3} (g_x + g_y + g_z) \quad (2.7)$$

where g_x , g_y , and g_z and A_x , A_y , and A_z are the principal g- and A-tensors and x, y and z refer to the molecule fixed coordinates, and it has been assumed that g, A can be simultaneously diagonalized. The contact hyperfine constant A_0 can be obtained to second order by taking the difference of B_M for line and B_{-M}

for line -M :

$$A_0 = -g_0 \beta_e (B_M - B_{-M}) / 2M \hbar \quad (2.8)$$

Furthermore,

$$g_0 - g_s = g_s \left\{ \left[B_s - \frac{1}{2} (B_M - B_{-M}) \right] / \frac{1}{2} (B_M + B_{-M}) \right\} - 2 A_0^2 \hbar^2 [I(I-1) - M^2] / g_s \beta_e^2 (B_M + B_{-M})^2 \quad (2.9)$$

where g_s and B_s are the isotropic g-value and the resonant value of the magnetic field (in Gauss) for standard of known g-value, respectively. The standard used in this study is diphenylpicrylhydrazyl (DPPH), for which g_e value is 2.0037.

The first term in equations (2.3) and (2.4), the electron Zeeman term, represents the large interaction of the electron spin with the laboratory magnetic field. This term yields the useful relation:

$$h \nu = g_o \beta_e B \quad (2.10)$$

where ν is the microwave frequency of the EPR spectrometer.

The unpaired electron responsible for the EPR spectrum is confined largely to the vanadyl center. This unpaired electron interacts with the nuclear spin of ^{51}V ($I = 7/2$), the result is $(2I + 1)$ or 8 lines separated by a coupling constant with different intensities. This electron nuclear interaction is represented by the second term in equation (2.3).

It is apparent from the variation in the intensities of the lines that the line widths of the different hyperfine components are not equal and depend on the ^{51}V nuclear spin quantum number.^{6,4} This line width variation indicates that the anisotropic hyperfine and Zeeman interactions are not completely averaged out by the tumbling of the molecules in the liquid, and they contribute significantly to the lines widths.

The relationships of the important A_o and g_o parameters are shown in figure 2.1 along with the lines widths (ΔH) and the peak heights in a first derivative representation of the absorption curve. The EPR spectrum can be displayed in various ways, namely the absorption curve, the integral of the absorption curve, first and second derivatives of the absorption curve. The

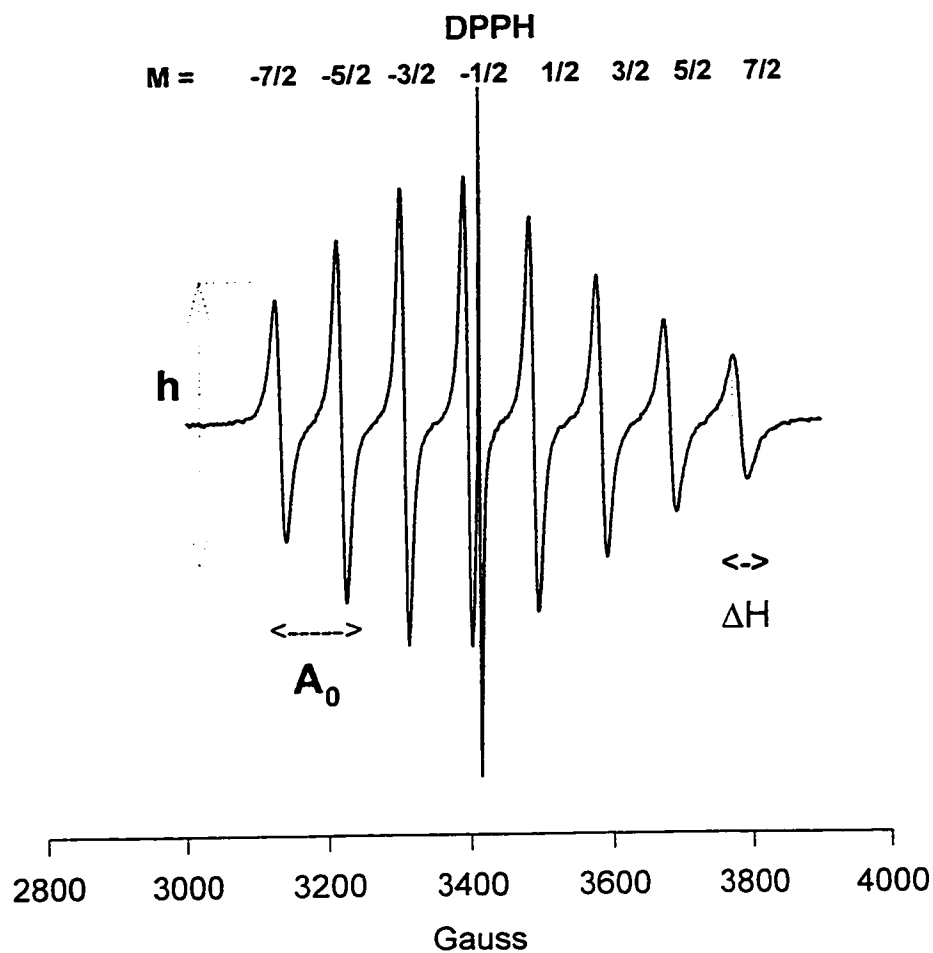


Figure 2.1: A typical X-band spectrum of Oxovanadium (IV) at room temperature with DPPH as internal standard.

first derivative is the most common representation in the literature. The spectra can also be recorded with the opposite phase from that in Fig. 2.1 (producing an upside-down effect). The choice of the phase and scan direction results in four possible permutations of the same spectrum. Although all the four permutations can be found in the spin labeling and the spin probing literature, the presentation most consistent with current trends in spectroscopy involves positive phase and increasing B from left to right. All spectra presented in this thesis follow this convention.

The glass EPR spectrum of a typical VO^{2+} (at 77 K) is illustrated in Fig. 2.2. This glass spectrum of vanadyl complexes is governed by:⁶

$$\omega_0 = \frac{g \beta_e B_M}{\hbar} + AM + \frac{(A_x^2 + A_y^2)(A_z^2 + A^2)}{8A^2} \frac{[I(I+1-M^2)]}{g \beta_e B_M / \hbar} \quad (2.11)$$

where

$$g = \left(g_z^2 \cos^2 \theta + g_x^2 \sin^2 \theta \cos^2 \phi + g_y^2 \sin^2 \theta \sin^2 \phi \right)^{\frac{1}{2}}$$

$$gA = \left(A_z^2 g_z^2 \cos^2 \theta + A_x^2 g_x^2 \sin^2 \theta \cos^2 \phi + A_y^2 g_y^2 \sin^2 \theta \sin^2 \phi \right)^{\frac{1}{2}}$$

θ is the angle between B and unique molecular axes, presumably the vanadyl VO-axis, and ϕ is the azimuthal angle. Note that the line for which $\theta = 0$ gives rise to the spectrum corresponding to g_z and A_z in the rigid limit spectrum, while those for which $\theta = \pi/2$, $\phi = 0$ and $\pi/2$ give rise to the doubled spectra which are corresponding to (g_x, A_x) and (g_y, A_y) in Fig. 2.2.

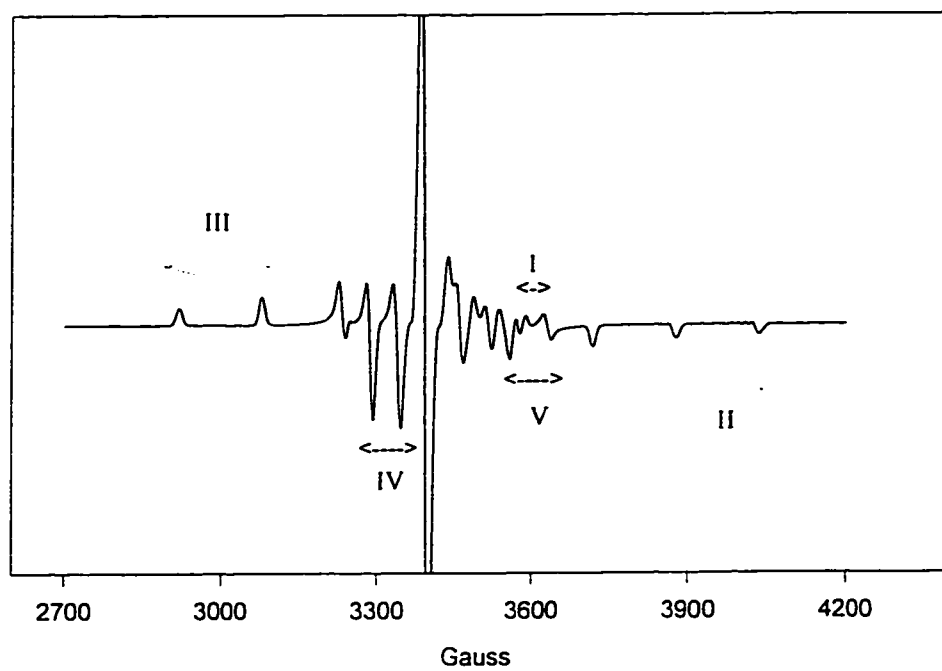


Figure 2.2: A typical X-band spectrum of Oxovanadium (IV) at 77K.

The anisotropic tensors can be determined from rigid limit spectra, Fig. 2.2, as Wilson and Kivelson have done for vanadyl acetylacetonate (VOAA).⁶ If we consider spacings I, II, III, IV and V in Fig. 2.2.; then

$$A_z = \frac{II + III}{2} \quad (2.12)$$

$$A_x + A_y = IV + V \quad (2.13)$$

$$I = \frac{\beta_e B^2 \delta g}{\hbar} + 4 c (7 / 2) \quad (2.14)$$

where B is the frequency in gauss units,

$$\delta g = \frac{1}{2}(g_x - g_y), \text{ and}$$

$$c = \frac{1}{2}(A_x - A_y)$$

The magnetic parameters could be obtained by measuring g_o and A_o from the liquid spectrum; g_z , $g_x - g_y$, A_z , and $A_x - A_y$ from the glass spectrum, and g_x , g_y , A_x and A_y and from this data and equations (2.6) and (2.7).⁶

Although the values of g_x , g_y , g_z and A_x , A_y , A_z can be calculated from the positions of the resonant lines in the glassy spectrum accurate determinations of the magnetic parameters should be obtained by simulating the glass spectrum. In this work the magnetic parameters are determined by simulation using the general method of Lefbre and Maruani⁷.

2.3 THE EFFECTS OF ROTATIONAL MOTION ON EPR SPECTRA

The EPR line shape is markedly dependent upon the rotational mobility of the paramagnetic spin probe. For example, in a nonviscous solvent nearly all vanadyl probes exhibit eight sharp lines. The rapid isotropic tumbling motion averages away all anisotropic effects, therefore sharp lines are obtained. If the rotational motion is slowed down by increasing the solvent viscosity, averaging is incomplete. The result is unequal broadening of the eight derivative lines. Molecular motion is not necessarily isotropic. Preferential motion about one axis is more likely to occur for any asymmetric spin probe, but the effects are particularly evident when surrounding medium is anisotropic. The EPR spectrum is very sensitive to the probe mobility. The best way to make use of this sensitivity is to describe the motion quantitatively in terms of the shape of the spectrum.

Both the anisotropic hyperfine electron-nuclear interaction and the anisotropic spin-orbit interaction in a spin probe depend on the mutual orientation of the external magnetic field and orbital of the unpaired electron. Rotations of the probe modulate these interactions, leading to fluctuations in local magnetic fields and changes of the EPR line widths. Rotational motion is characterized by correlation time (τ_R) which determines the effective frequency of rotation, (f_{eff} in Hz): $f_{\text{eff}} = 2\pi \tau_R^{-1}$.

The anisotropy of g and A tensors is applied in dynamic spin probe studies to get information about the motional state of the probe. Between the two limits of very rapid motion and a rigid glass, the spectra are quite

complex. This complexity provides much of the information that can be obtained about molecular motion using spin-probe techniques.

The spin Hamiltonian which describes the molecular tumbling can be divided into:^{6,8}

$$H = H_0 + H_1(\Omega) + \varepsilon(t) \quad (2.15)$$

where

$$H_0 = \beta_e g_0 B S_z + A_0 I \cdot S \quad (2.16)$$

where S_z is the electron spin along the Z-axis, S and I are the electron and the nuclear spin operator, B is the laboratory magnetic field, and β_e is electron Bohr magneton, and

$$H_1 = \beta_e B \cdot \underline{g} S + I \cdot \underline{A} \cdot S \quad (2.17)$$

where \underline{g} and \underline{A} contain the anisotropic components of the electron g-tensor and electron-nuclear dipole hyperfine tensor after the isotropic components g_0 and A_0 have been subtracted. These tensors are defined in terms of molecular fixed axes whose orientation varies with time with respect to the laboratory magnetic field due to molecular motion. Thus the time dependence of H_1 is modulated by the reorientational motion of the molecule (Ω); and

$$\hbar \varepsilon(t) = \frac{1}{2} \hbar \gamma_e B_1 [S_+ \exp(-i\omega t) + S_- \exp(i\omega t)] \quad (2.18)$$

where B_1 is the time dependent field; and

$$S_+ = S_x + iS_y$$

is the raising operator,

$$S_+ = S_x + iS_y$$

is the lowering operator, γ_e is the magnetogyric ratio of a free electron and ω is the microwave frequency. $\varepsilon(t)$ gives the interaction of the spin with the microwave radiation field which must be included in the Hamiltonian if the saturation effects are to be considered. Since saturation effects are known field which must be included in the Hamiltonian if the saturation effects are to be considered. Since saturation effects are known to be negligible for experimental spectra discussed in this work, only terms linear in $\varepsilon(t)$ must be considered.⁸

The term "fast" and "slow" refers to the randomly fluctuating part $H_1(t)$ of the spin Hamiltonian (where $H_1(t)$ has a time averaged value zero) in relation to a correlation time τ_R which characterizes the underlying stochastic process. Fast motional theories are applicable if $|H_1(t)| \tau_R \ll 1$ (where $H_1(t)$ is expressed in frequency units). On the other hand, the rigid limit is attained when $|H_1(t)| \tau_R \gg 1$. The correlation time data of vanadyl complexes is usually divided into three groups: Rapid rotations (10^{-11} - 10^{-10} sec); Slow rotations (10^{-10} - 10^{-7} sec); Very slow rotations (10^{-6} - 10^{-3} sec). The limits of these regions are essentially determined by the anisotropy of the magnetic interactions occurring in the probes.

2.3.1 Fast Tumbling

It is convenient at this point to define a line width parameter T_2 . If the peak to peak width is ΔH (in gauss), then $T_2^{-1} = \Delta H$. In general, the

dependence of T_2 upon M , the component of the nuclear spin along the direction of the applied magnetic field is given by:

$$T_2^{-1}(M) = A + BM + CM^2 + DM^3 + X \quad (2.19)$$

where A , B and C and D depend on the magnetic tensors and X takes into account other possible broadening mechanisms. The line width contributions have been extensively studied by many workers.^{16,29,30} For vanadyl systems, where the second order effects are large the line width contributions can be calculated by time-dependent perturbation as applied by Wilson and Kivelson⁶ to second order effects, or by SLE method as applied by Freed and Campell.⁸

In order to determine the anisotropy of rotation (N) and the axis of rotation, the motional narrowing analysis of Freed et al^{8,21,22} has been used. In practice, τ_R is obtained from B and C because of the uncertainty in A .⁸ The theoretical expressions for B and C coefficients are well described in the literature.^{21,22}

For isotropic Brownian diffusion $\tau_R = (6R)^{-1}$ where R is the rotational diffusion coefficient. For the eight lines spectrum for vanadyl probe, equ. (2.19) will give rise to three experimentally determined unknowns, A , B and C . Since the line width coefficients B and C are functions of τ_R values, in the case of two values of τ_R value not agreeing, the assumption of anisotropic rotation must be suspected. Fortunately, this restriction has been resolved by Freed and his co-workers.^{22,31} The cubic dependence of T_2^{-1} on M given in eq. (2.19) is retained, but the motion is described by a rotational tensor, R . This is often axially symmetric and is defined by two

components R_{\parallel} and R_{\perp} where R_{\parallel} is the rotational diffusion constant along the principal axis of rotation, and R_{\perp} is the rotational diffusion constant perpendicular to the principal axis of rotation. The anisotropy of rotation (N) is defined as the ratio of $R_{\parallel} / R_{\perp}$. Two related correlation times $\tau(0)$ and $\tau(2)$ are given by:

$$\tau(0) = (6 R_{\perp})^{-1} \quad (2.20)$$

$$\tau(2) = (2 R_{\perp} + 4 R_{\parallel})^{-1} \quad (2.21)$$

The expressions for B and C , assuming that the rotational diffusion tensor is axially symmetric, are listed as follows ^{10,32}.

$$C_0 = 8/3 - [1 + (\omega_a \tau_0)^2]^{-1} - \{3[1 + (\omega_0 \tau_0)^2]\}^{-1} \quad (2.22)$$

$$C_2 = 8/3 - [1 + (\omega_a \tau_2)^2]^{-1} - \{3[1 + (\omega_0 \tau_2)^2]\}^{-1} \quad (2.23)$$

$$C = [2/(3^{1/2} \gamma)] (0.8\pi^2) (D_0^2 \tau_0 C_0 + 2D_2^2 \tau_2 C_2) \quad (2.24)$$

$$B_0 = 16/3 + 4/[1 + (\omega_0 \tau_0)^2] \quad (2.25)$$

$$B_2 = 16/3 + 4/[1 + (\omega_0 \tau_2)^2] \quad (2.26)$$

$$B = [-2 / (3^{1/2} \gamma)] (0.1 \pi \omega_0) (g_0 D_0 \tau_0 B_0 + 2g_2 D_2 \tau_2 B_2) \quad (2.27)$$

where

$$\tau_0 = \tau_R N^{1/2}$$

$$\tau_2 = 3\tau_0 / (1 + 2N)$$

$$g_0 = (g_z' - g_i)(3/2)^{1/2}$$

$$g_2 = (g_x' - g_y') / 2$$

$$g_i = (g_x + g_y + g_z)/3$$

$$\omega_a = A_0 \gamma_p / 2$$

$$D_0 = (A_{Z'} - A_i)(\frac{1}{2} \gamma_p^{1/2} / 2\pi)(3/8)^{1/2} \text{ (in MHz)}$$

$$D_2 = (A_{X'} - A_{Y'})(\frac{1}{2} \gamma_p^{1/2} / 8\pi) \text{ (in MHz)}$$

$$\gamma_p = \gamma g_i / g_e \quad \text{where } g_e \text{ is the free electron } g \text{ value i.e } 2.0023.$$

$$A_i = (A_x + A_y + A_z)/3 \text{ (in G)}$$

These equations^{21,32} were adapted from the motional-narrowing analysis of Freed *et al*²². Reference should be made to the original literature^{22,23} and the more recent work¹⁰⁻¹¹ for details of this analysis.

2.3.2 Slow Tumbling

The motional region of slow rotations is interesting because many relaxation phenomena observed in this region at various temperatures. The changes in EPR spectra are complex because line widths, shape, and positions of spectral lines vary. The slow tumbling spectra were typical for those observed in the low temperature region. Several theoretical approaches^{8,9,22} have been used to calculate EPR spectra in the slow tumbling region,^{8,9,22} the most general one has been developed by Freed and his co-workers^{8,22} and is based on the Stochastic Liouville Method (SLE). The corresponding equation of motion for the spin density matrix is very simple in its formal appearance. However, the practical use is quite involved due to the fairly complicated coupling among the various spin variables, stochastic (bath) variables, and applied radiation fields.

The method involves the solution of the stochastic Liouville equation for $S_x(\Omega, t)$ ²²:

$$\frac{d}{dt}S_x(\Omega, t) = i[H(\Omega), S_x(\Omega, t) + \Gamma S_x(\Omega, t)] \quad (2.28)$$

where S_x is the X-component of the magnetization, Ω are the orientational angles, and Γ is a time independent Markoff's operator. For isotropic rotational diffusion, $\Gamma = D\Delta_R^2$ where D is the rotational diffusion constant and Δ_R^2 is the rotational Laplacian operator. The EPR line shape is Fourier transform of $S_x(\Omega, t)$. Eq. (2.28) is readily extended to include asymmetric g and A tensors as well as axially symmetric rotational diffusion. The method is capable of giving information about anisotropic rotation and a variety of models. Several model sensitive theories have been developed to explain motional data. Usually the following models are used:²²

- (a) Brownian rotational diffusion (an infinitesimal reorientation of a molecule with each collision with surrounding particles).
- (b) Jump diffusion; in which the molecule has fixed orientation for time t and then jump instantaneously to a new orientation (= "large jump" diffusion).
- (c) Free diffusion (the molecule reorients freely for the time t and then jump instantaneously to a new orientation). This model gives essentially the same results as moderate jump model.

The Stochastic Liouville method has been developed as a general approach to the calculation of EPR line shapes for the Vanadyl(IV) probe in particular, and for inorganic ions with spin $S = 1/2$. The total spin Hamiltonian, $H_s(\Omega)$, which is separated in a form convenient for a perturbation type treatment of the non secular contributions, is ⁸:

$$H_S(\Omega) = H_0 + H_1^{(\text{sec} + \text{pseudosec})}(\Omega) + H_1^{(\text{nonsec})}(\Omega) + \epsilon(t) \quad (2.29)$$

Now it is well established that ⁸:

- a) The vanadyl ion (a d¹ transition metal ion) is paramagnetic possessing an unpaired electron.
- b) In dilute solutions the primary magnetic interactions contributing to the spin Hamiltonian are due to interaction of this single electron moment with both the external magnetic field *viz.* the electron Zeeman interactions, and the ⁵¹V nuclear moment, I = 7/2 *viz.* the intramolecular electron-dipolar interaction.
- c) The principal axes of the g and A tensors are coincident, and
- d) the g and A tensors are nearly always axially symmetric.

If we take the advantage of this knowledge, as well as neglect the nuclear Zeeman term (this approximation commonly made for nitroxide for which the nuclear Zeeman term is more important, and it results in greatly reducing the number of coefficient equations to be solved), the spin Hamiltonian becomes ⁸:

$$H_0 = g_0 (\beta_e / \hbar) B S_z - 2 b I_z \quad (2.30.a)$$

$$H_1^{(\text{sec} + \text{pseudo sec})} = [F + D' I_z] D_{0,0}^2(\Omega) S_z + [D_{0,1}^2(\Omega) I_+ - D_{0,-1}^2(\Omega) I_-] D S_z \quad (2.30.b)$$

$$\begin{aligned}
H_1^{(nonsec)} = & [b + D'/4] D_{0,0}^2(\Omega) [I_+ S_- + I_- S_+] + \\
& \left[(3/8)^{1/2} F - D I_z \right] \left[D_{0,-1}^2(\Omega) S_- - D_{0,1}^2(\Omega) S_+ \right] \\
& D \left[D_{0,-2}^2(\Omega) I_- S_- + D_{0,2}^2(\Omega) I_+ S_+ \right]
\end{aligned} \tag{2.30.c}$$

$$\varepsilon(t) = \frac{1}{2} \gamma_e B_1 \left[S_+ e^{-i\omega t} + S_- e^{i\omega t} \right] \tag{2.30.d}$$

where the following definitions apply:

$$\begin{aligned}
b &= -|\gamma_e| A_o / 2 \\
F &= \frac{2}{3} \left(g_{\parallel} - g_{\perp} \right) \left(\beta_e / \hbar \right) B \\
D &= |\gamma_e| \left(A_{\parallel} - A_{\perp} \right) / (6)^{\frac{1}{2}} \\
D' &= - \left(\frac{8}{3} \right)^{\frac{1}{2}} D
\end{aligned}$$

$$\begin{aligned}
g_o &= \frac{1}{3} (g_{\parallel} + 2g_{\perp}) = \frac{1}{3} (g_x + g_y + g_z) \\
A_o &= \frac{1}{3} (A_{\parallel} + 2A_{\perp}) = \frac{1}{3} (A_x + A_y + A_z)
\end{aligned}$$

The $D_{0,m}^2(\Omega)$ are the orientation-dependent Wigner rotation matrices. S and I are the electron and nuclear spin operators respectively; g_{\parallel} , g_{\perp} and A_{\parallel} , A_{\perp} (in gauss) are the principal values of the g and A tensors; g_o and A_o (in gauss) are the isotropic g -value and A -value, $|\gamma_e|$ is the magnitude of the electron magnetogyric ratio, β_e is the Bohr magneton B is the magnitude of the externally applied magnetic field.

Now using the generalized energy level scheme given in Fig. 2.3 and type of transitions in the following scheme, 2.1.

scheme 2.1: Type of transition for oxovanadium(iv):

for $n = 0, m = 1, 1-1, \dots, -1+1, -1$	8 "allowed transitions"
for $n = 1, m = 1-1, 1-2, \dots, 1, -1$	7 "singly forbidden transitions"
.....	
.....	
for $n = 7, m = -1$	"multiply forbidden transition"

$$\Delta = 1, \Delta' = 1 \quad \text{for } n > 0$$

$$\Delta = 0, \Delta' = 2 \quad \text{for } n = 0$$

$$\text{further } \sum_{L'} \text{ is restricted to } L' = L, L \pm 2$$

and following the SLE formulation, Freed et. al⁸ obtained (in the absence of saturation) a generating equation for the set of coupled algebraic equations for the coefficient, $C_{K_m}^L$, which determine the ESR spectrum of the vanadyl(IV) probe. In their theoretical work Freed et. al⁸ presented the complete perturbation treatment, and took into account both shift and line-width contributions to the allowed and forbidden EPR transitions. Freed et. al work⁸ is a more comprehensive treatment than Bruno et al work⁹.

The procedure for solving Eq. (2.28) involves an expansion of the line shape terms of a complete orthogonal set of eigenfunctions of the Markovian rotational diffusion operator. The Wigner rotation matrices $D_{KM}(\Omega)$ with eigenvalues $E_{K,M}^L = \tau_{L,K}^{-1}$ given by

$$\tau_{L,K}^{-1} = R_{\perp} L(L+1) + (R_{\parallel} - R_{\perp}) K^2$$

General :
(Allowed Transitions)

$$\frac{|\frac{1}{2} \cdot m\rangle}{[2m+2I+1]} \longleftrightarrow \frac{|-\frac{1}{2} \cdot m\rangle}{[2m+2I+2]}$$

$m = I, I-1, \dots, -I$

Vanadyl (Allowed and Forbidden Transitions)

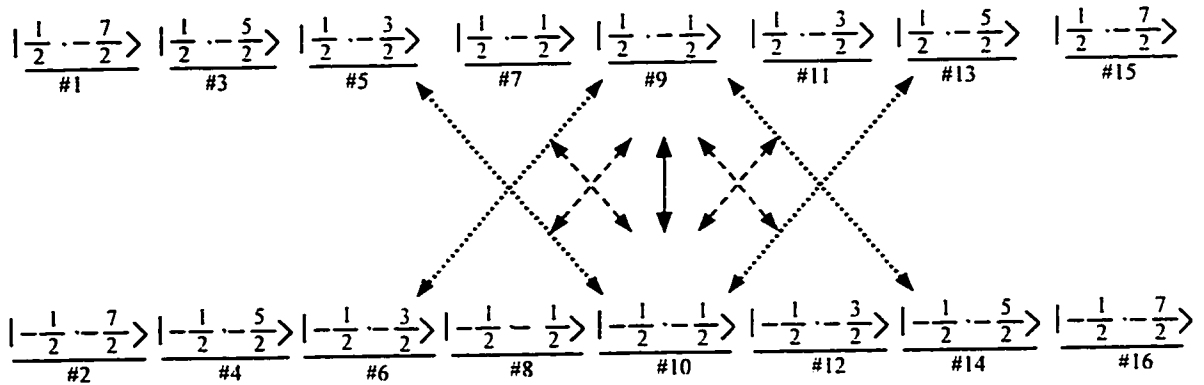


Figure 2.3: Generalized energy level and transition scheme. The notation is $|M_S, M_I = m\rangle$ for the energy levels, and these levels are numbered according to bracketed terms (e.g., $[2m+2I+1]$ for $I = 1$ and $m = +1$ corresponds to state 5). Typical allowed transitions (—), singly forbidden transitions (---), doubly forbidden transitions (.....).

$$\tau_{2,0}^{-1} = \tau(0)^{-1} = 6R_{\perp} \text{ and}$$

$$\tau_{2\pm 2}^{-1} = \tau(2)^{-1} = 2R_{\perp} + 4R_{\parallel}$$

provide such a set for axially symmetric Brownian rotational diffusion. Convergent solutions may be obtained by terminating the expansion at sufficiently large value of $L = n$, in general, the larger the value of $H_1(t) \tau_R$ larger the value of n must be. A more detailed discussion of convergence is given by Freed³³. For $|H_1(t) \tau_R| \ll 1$ convergence can be obtained with $n=2$. This yields essentially the same results as earlier relaxation theories^{6,15,29,33}.

2.4 THE TRANSLATIONAL DIFFUSION CONSTANT

The molecular volume of the paramagnetic species has been determined in the past using the Dreydinger model³⁴ and experimentally using techniques such as the porous disk method¹², the electron spin resonance/spin exchange method^{35,36}, and the capillary diffusion method¹³.

The translational diffusion constant can be determined at room temperature (22 ± 1 °C) by a capillary diffusion cell. The translational diffusion processes were monitored by electron spin resonance spectral intensities as a function of time. The total spectral intensity $I(t)$, which is the sum of the peak-to-peak heights of the eight hyperfine lines were plotted as a function of time. The theoretical intensities with time is given by the following diffusion equation¹³

$$\frac{I(t)}{I(0)} = \frac{8}{\pi^2 R} \sum_{n=0}^{\infty} (-1)^n f_n(t) \sin \left[\frac{(2n+1)\pi R}{2} \right]$$

where (2.26)

$$f_n(t) = \frac{1}{(2n+1)^2} \exp \left\{ \frac{-(2n+1)^2 \pi^2 D t}{4 \ell_t^2} \right\}$$

where $R = \ell_S / \ell_t$, $I(0)$ is the intensity at time zero, t is the time, and D the translational diffusion constant. A computer program can be used to get the best least-squares fit of the experimental points and the theoretical values obtained from Eq. (2.26). Using the Stokes-Einstein equation for translational diffusion, the hydrodynamic radius r_0 could be calculated.

$$D = \frac{k_B T}{6 \pi \eta r_0} \quad (2.27)$$

CHAPTER THREE

APPARATUS AND PROCEDURE

3.1 THE EPR SPECTROMETER

3.1.1 General Description

The EPR measurements were performed using Bruker Electron Spin Resonance spectrometer model ER 200E/D-SRC along with a micro-station (Bruker Data System ESP 3220) on which the ESP 300E Software (version 3.02) is installed. To accurately measure the microwave frequency and the field of the magnet a Hewlett Packard 5342A Microwave Frequency Counter and the NMR Gaussmeter ER 035M were used, respectively. The HP 5342A Microwave Frequency Counter gave a stable reading of at least eight digits. The Bruker Variable Temperature Unit ER 4111VT was used to vary the temperature of the cavity containing the sample. The accuracy of this unit is ± 1 degrees K. The bridge and cavity for the X-band are ER 045 MRBDH and ER 4105 DR, respectively.

Other accessories included Bruker ER 072 Power Supply, Bruker heat exchanger unit to cool both the magnet and the microwave bridge, a water cooling bath. The WIN-EPR software (version 921201 which is developed by Bruker for PC) is installed on a PC which is interfaced with the ESP 3220 micro-station. This makes possible the manipulation of the EPR data on any PC software after its transfer to the interfaced PC.

Figure 3.1 depicts a general schematic representation of a Bruker EPR spectrometer. The essential components of any spectrometer are: a source of electromagnetic radiation, a sample cavity, and a detector. The electromagnetic radiation source and the detector are in the microwave bridge. The sample is in a microwave cavity, which is a metal box that assist in amplifying weak signals from the sample. The magnet is to "tune" the electronic spin energy levels of the unpaired electron in the sample. In addition, the control device contains signal processing and control electronics, also called the console, and a computer or a micro-station. The computer is used for analyzing the data as well as coordinating all the units for acquiring a spectrum.

The main components of the console are a field controller ER 032 M, a signal channel ER 023 M, a microwave controller ER 048 H, and an NMR gaussmeter ER 035 M. Each component is built as a separate unit or a module. The ER 032 M field control module is used to control the magnetic field. The sweep width (in Gauss), the central field (in Gauss), and the sweep time (in seconds) are set through this controller. The ER 023 M signal channel module works by phase sensitive detection and applies

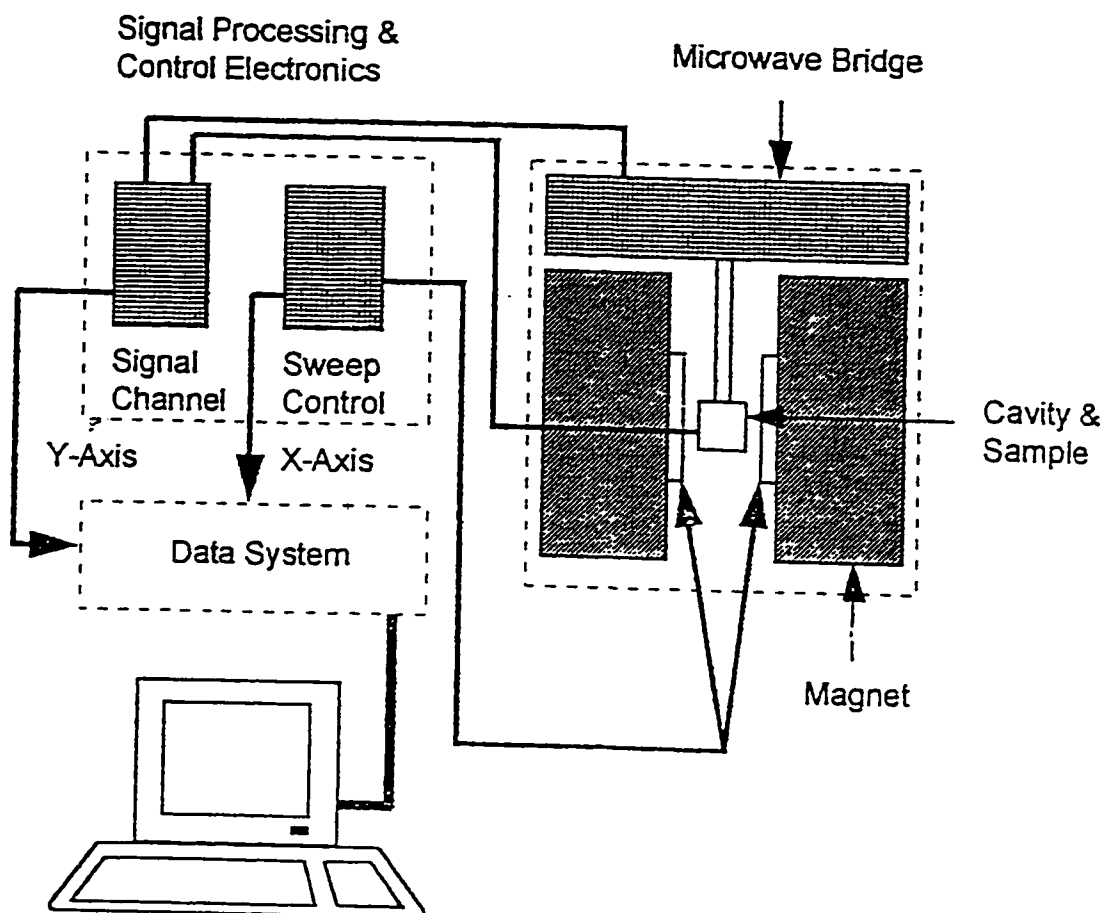


Figure 3.1: A schematic representation of a Bruker EPR spectrometer

magnetic field modulation to increase the sensitivity. Optimum settings of modulation amplitude, modulation frequency, and time constant are required to achieve good sensitivity and accurate results. Absolute calibration of field modulation amplitude for Bruker EPR cavities is achieved by a calibrated "tune box" supplied with each cavity type. The ER 048 H microwave controller is used to control the microwave bridge. The radiation output power level can be set in one dB steps and a direct true power reading in mW, μ W, and nW is possible on the ER 048 LED display.

3.1.2 The Microwave Bridge

The microwave bridge used to investigate the behavior X-band mentioned above. A block diagram of the microwave bridge is depicted in Figure 3.2. The microwave bridge contains the microwave source and the detector. The microwave source used in the bridge used in this study is a klystron. The attenuator, which blocks the flow of the microwave radiation, comes after the microwave source. The attenuator is used to control the amount of microwave power that the sample is exposed to it. The circulator controls the flow of radiation with help of the three ports. The incident microwave radiation passes only through the first and second ports to the sample in the cavity. The reflected microwave radiation is directed to the detector only through ports two and three. Therefore, the Bruker EPR spectrometer is a reflection spectrometer which measures the changes (due to absorption) in the amount of radiation reflected back from the microwave

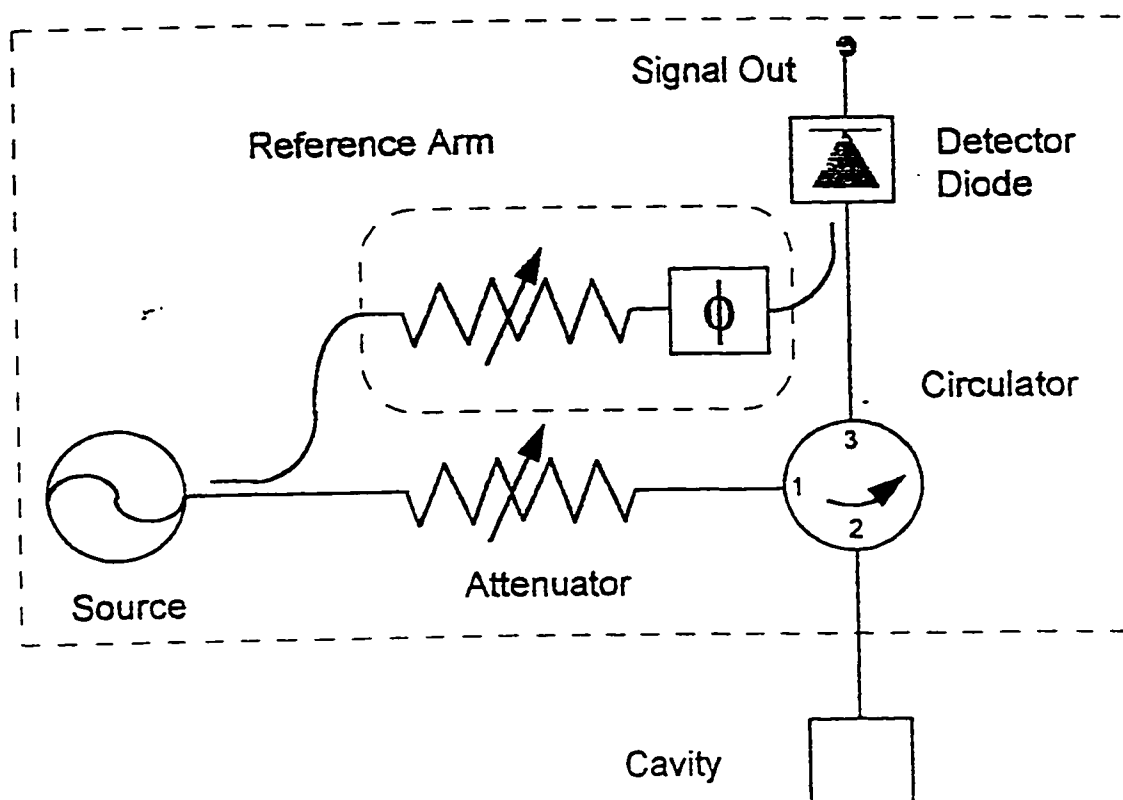


Figure 3.2: Block diagram of EPR spectrometer microwave bridge

cavity containing the sample. The detector is a Schottky barrier diode which converts the microwave power to an electrical current. For the diode to operate in the linear region, the detector current should be approximately 200 micro amperes. This is for optimal operating conditions. The reference arm supplies the detector with some extra microwave power or "bias". The second attenuator controls the power level so that the detector operates with optimal performance.

3.1.3 The EPR Cavity

Microwave EPR cavities are used to amplify weak signals from the sample. The cavity is a metal box that resonates with microwaves. At the resonance frequency of the cavity, the cavity stores the microwave energy and, therefore, no microwaves will be reflected back but will remain inside the cavity. The iris matches the impedance of the cavity and the wave guide, which is used to transfer microwaves from the microwave bridge to the cavity. The matching is achieved by adjusting the iris. The EPR signal results when the sample absorbs the microwave energy. Absorption by the sample alters the impedance of the cavity and the matching, or coupling, between the cavity and the waveguide is lost. Thus, the cavity is not critically coupled and the microwave radiation will be reflected back to the bridge. This will give rise to an EPR signal.

3.2 VACUUM SYSTEM

For meaningful EPR line width studies, the sample should be evacuated in order to get rid of oxygen present in the air which is paramagnetic and can interfere with the line width measurements from the paramagnetic sample of interest.

A normal system manufactured by Pope Scientific Inc. was used with slight modifications to suit our needs. One of the modifications is a QUICK FIT arrangement to insert and remove the sample easily. Also, to measure the vacuum readily, we used a digital vacuum gauge manufactured by Granville-Phillips.

Vacuum could be easily reached as low as 1 mTorr and all the samples were sealed when the vacuum was of that order.

3.3 EPR SAMPLE PREPARATION

3.3.1 V1 in toluene

V1 was obtained through private communications ^{3.a}. The synthesis was carried out following the procedure outlined in reference ^{3.b}.

Samples in the concentration range $(5 \pm 2) \times 10^{-4}$ M were prepared in toluene (spectroscopic grade purchased from Merck) without further purification. The sample of the above concentration was dripped inside a 2 mm ID Pyrex sample tube until the length comes to be about 2.7 cm, with the help of a very narrow mouthed dropper.

The sample is degassed to get rid of any dissolved oxygen and sealed. Good vacuum is needed for sample degassing. To get good vacuum one must put on the vacuum line for at least one hour before degassing the sample. The sample is degassed by freeze-pump-thaw procedure which is repeated several times for better degassing.

While sealing the sample, the following precautions are to be taken:

- (1) The length of the sample inside the sample tube must be well immersed inside liquid nitrogen, so that the heat of the torch does not reach the sample.
- (2) The sealing must be done just one to two centimetres above the surface of the sample.
- (3) The length of the sample inside the sample tube must be at least 2.7cm.

Since the sample tube is thin and under pressure, it must be removed very carefully from the vacuum system.

3.3.2 *V2 in toluene*

V2 was obtained through private communications.^{3.a} The synthesis was carried out following the procedure outlined in reference.^{3.b}

Samples in the concentration range $(5 \pm 2) \cdot 10^{-4}$ M were prepared in toluene (spectroscopic grade purchased from Merck) without further purification. Sample introduction to the sample tube, concentration check up, degassing and sealing were carried out in the same way as described for V1.

3.3.3 *V3 in methylene chloride*

V3 complex was obtained through private communications.^{3.a} The synthesis was carried out following the procedure outlined in reference.^{3.b} Samples in the concentration range $(5 \pm 3) \cdot 10^{-4}$ M were prepared in methylene chloride (spectroscopic grade purchased from Merck) without further purification.

Sample introduction into the sample tube, concentration check up, degassing and sealing were carried out in the same way as described for V1.

3.3.4 V4 in methylene chloride

V4 was obtained through private communications ^{3.a}. The synthesis was carried out following the procedure outlined in reference ^{3.b}. Samples in the concentration range $(5 \pm 3) \times 10^{-4}$ M were prepared in methylene chloride (spectroscopic grade purchased from Merck) without further purification. Sample introduction to the sample tube, concentration check up, degassing and sealing were carried out in the same way as described for VO $\{(\text{CH}_3)_2\text{C}=\text{NNCSSCH}_3\}_2$

3.4 DATA COLLECTION AND EPR SPECTROMETER OPERATION:

Following is a brief description of how to operate the EPR spectrometer:

- (i) Put on the chiller water for circulation, turn the console power on and bring the field set slowly to the central field value (≈ 3300 - 3400 G).
- (ii) The degassed sample tube is inserted into the microwave cavity; and the sample length is adjusted at the active region of the microwave cavity.
- (iii) In the microwave bridge bring the STANDBY setting to TUNE position, and set the microwave power to 32 dB. Calibrate the instrument and turn on the frequency counter.

(iv) Initial spectrometer parameters like scan speed, time constant, microwave power, modulation amplitude, etc. are interred.

(v) The "FREQUENCY" knob is used to center the dip on the oscilloscope.

The iris screw was used to produce a dip with maximum sharpness and deepness. Then, the "REF." button was pressed "ON" and the dip was again centered by fine adjustment of the "FREQUENCY" knob and the whole peak is maximized using the "REF. PHASE" knob. The two shoulders of the dip were made at their highest level, and equal. Then the "REF." button was switched "OFF" and the "OPERATE" button was switched "ON" followed by the "REF." button. The diode current was set equal to 200mA by adjusting the iris. The power was increased to 15dB while maintaining the diode current at 200mA by adjusting the level of the iris. This is called critical coupling.

(vi) Data Collection

The next step is acquiring a spectrum. Before the instrument can be used for spectrum acquisition, good parameter values must be selected and entered into the spectrometer. These parameters are: Modulation Amplitude (mA), Modulation Frequency (MF), Receiver Gain (RG), Conversion Time, Time Constant, Central Field (CF), Sweep Width (SW), and Phase. The instrument was then ready for spectrum acquisition.

Remote Control and Data Acquisition

Remote control of the Bruker EPR spectrometer and acquisition of data are performed using the ESP 300E software. The main menu of ESP 300E software contains such options as File handling, Acquisition,

Parameters, Data handling, Calibration, ... etc. Each option in the main menu and in the sub menus can be entered by selecting it using the arrows in the key board and hitting enter or directly by pressing the designated letter.

A brief description of the main options will clarify some of their functions. The option *File handling*, as the name implies, is for activities like opening files, saving files, entering operator's name and comment lines, and so forth. Through the *Acquisition* option the following activities can be performed: acquisition of spectra with the signal channel, deletion of spectra, transferring of spectrum and/or parameters from the active page to another page, and editing and execution of automation routines. The option *Parameters* is for setting the parameters of, for example, the field controller, the signal channel, and for downloading and uploading the parameters to and from the instrument.

Measurement parameters and the obtained spectra are stored in pages which can then be saved in the data station. The stored data can be analyzed with the ESP 300E software or transferred to PC for further analysis.

For variable temperature experiments, the temperature controlling unit must be properly connected. During high temperature studies the temperature is controlled via N₂ gas flowing through the heat exchanger. While for low temperature study, the heat exchanger is immersed in liquid N₂ and the cavity is purged with nitrogen gas to flush out the moisture. After the required temperature is chosen enough time is given for the temperature to become stable.

The glass spectra are obtained by inserting the sample in a liquid nitrogen dewar filled with liquid nitrogen. To avoid bubbling, put in a long sheet of filter paper. The filter paper should be kept away from the active region of the cavity. The glass spectra were taken while purging the cavity with nitrogen gas.

3.5 DIFFUSION EXPERIMENT

3.5.1 Capillary Diffusion Cell

The capillary diffusion cell, illustrated schematically in Figure 3.3,¹³ was made of 1 mm i.d. (inside diameter) heavy wall Pyrex tubing which was closed from one end and the other end was ground flat. The capillary was joined to a 11 mm o.d. tubing (A). A small distortion of the capillary at the joining spot is unavoidable. The chambers (B) and (C) are 10 ml graduated cylinders, and (E) is a male ground joint that fits into the vacuum system described earlier.

3.5.2 Sample Preparation

The procedure followed here is slightly different from the procedure described in the literature. A weighed amount of the sample, dissolved in a small amount of vacuum distilled solvent, was introduced into the chamber

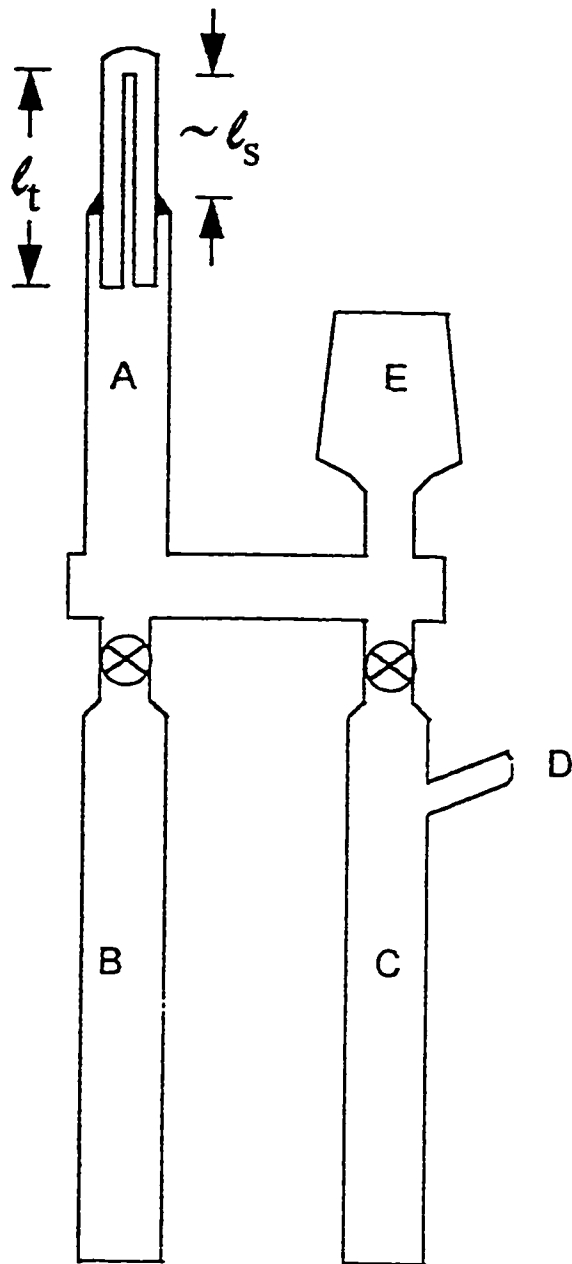


Figure 3.3: A schematic representation of the capillary diffusion apparatus.

(C) through a side arm (D). The side arm was then sealed with a torch. Dissolved oxygen in the solution was removed by several cycles of freeze-pump-thaw. The cell was connected to the vacuum system through the male ground joint (E). After that, the entire cell was evacuated, the solvent was vacuum distilled into the reservoirs (B) and (C) and the constriction below E was sealed under vacuum. Vacuum distillation consisted of two steps: after attaching the diffusion cell and another chamber that contains toluene into the vacuum system, both of them were immersed in liquid nitrogen and were entirely evacuated; then, liquid nitrogen was removed away from the solvent chamber, the solvent was allowed to vaporize under vacuum, and due to liquid nitrogen, toluene condensed in the diffusion cell. This process was repeated until enough toluene was collected in the diffusion cell¹⁰.

The concentration of the solution prepared in C was about $8.0 \times 10^{-4} \text{M}$. A small amount of the sample solution in C was transferred into the capillary, the excess solution was poured back into C, and A was washed with a small amount of pure toluene from B and the washed solution was poured back into C. Then, the pure solvent in B was introduced into the 11 mm o.d. tubing (A) above the open end of the capillary. Simultaneously, a portion of the capillary at the closed end was placed into the microwave cavity of the EPR spectrometer, and at this instant the time zero was recorded. The height of the cell in the cavity was also noted to assist in the estimation of ℓ_S .

3.5.3 Measurement and Data Collection

The measurements were performed at X-band (9GHz). At the beginning, the settings of the spectrometer were optimized and kept fixed throughout the diffusion experiment. The spectra were recorded every 4-6 hours. The diffusion experiment took about 3 weeks. The cell was left in the cavity undisturbed for the whole duration of the diffusion experiment.

CHAPTER FOUR

4.THE MAGNETIC PARAMETERS STUDY

4.1 DETERMINATION OF THE MAGNETIC PARAMETERS

4.1.1 Isotropic Magnetic Parameters:

The room temperature EPR spectra, with DPPH as an internal standard, were recorded at 9GHz for compounds V1 & V2 in toluene and V3 and V4 in methylene chloride and are shown in Figure 4.1. Each spectrum consists of eight lines arising from the interaction of a single unpaired electron ($S = \frac{1}{2}$) with the quenched orbital angular momentum of the vanadium nucleus of spin $I = 7/2$.

The isotropic hyperfine constant, A_0 and g_0 were obtained from B_M for line M and B_{-M} for line -M by equations (4.1) & (4.2)

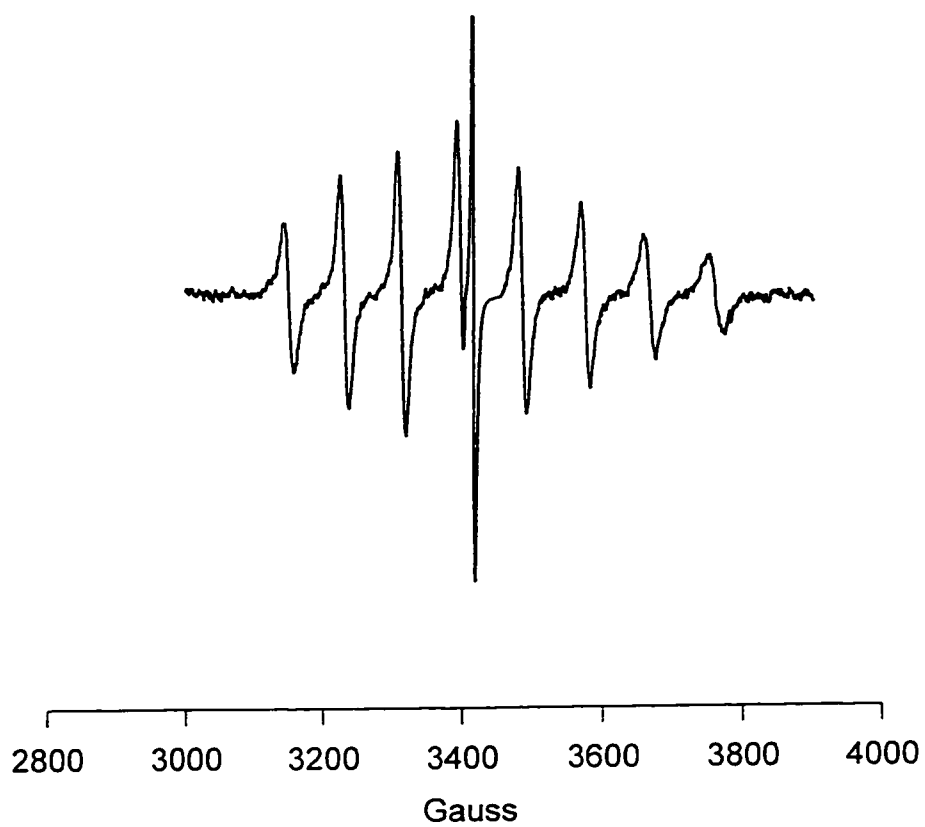


Figure 4.1.a: X-band spectrum of V1 in toluene at room temperature with DPPH as internal standard.

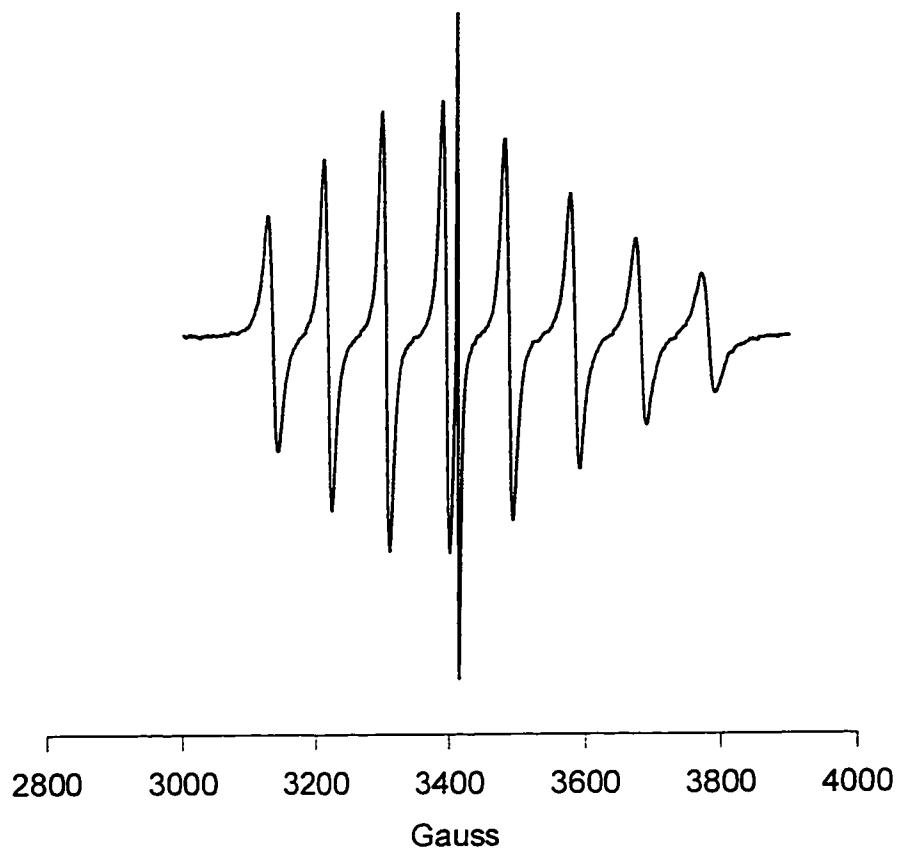


Figure 4.1.b: X-band spectrum of V2 in toluene at room temperature with DPPH as internal standard.

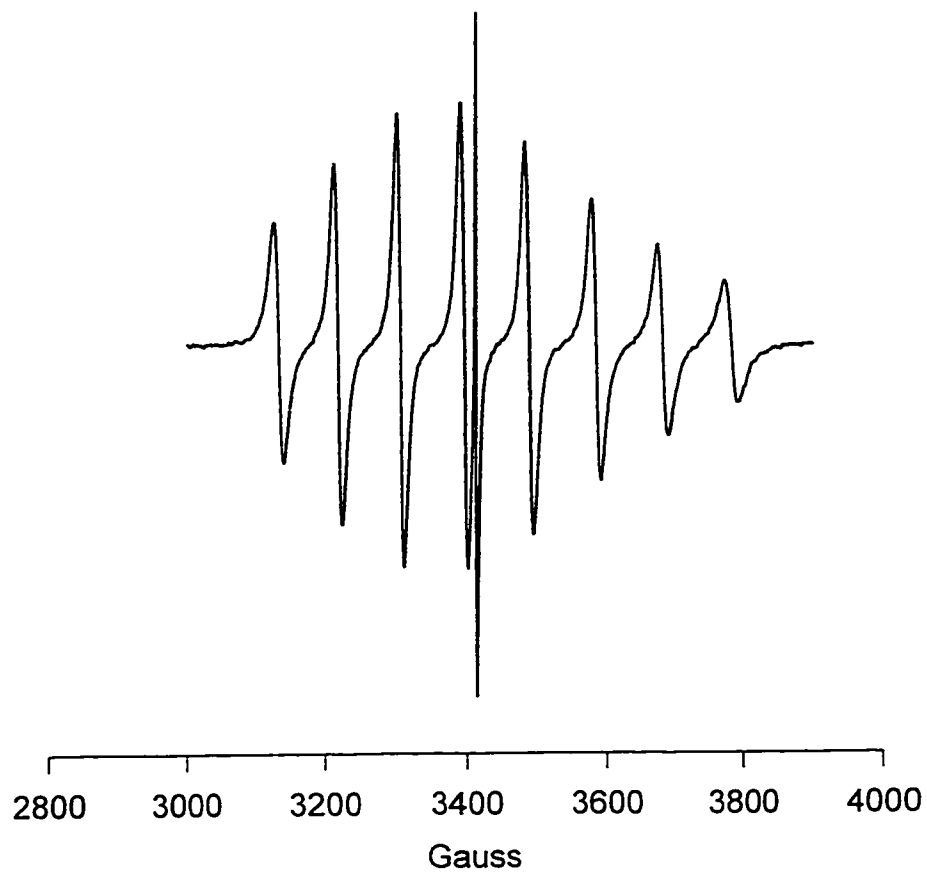


Figure 4.1.c: X-band spectrum of V3 in toluene at room temperature with DPPH as internal standard.

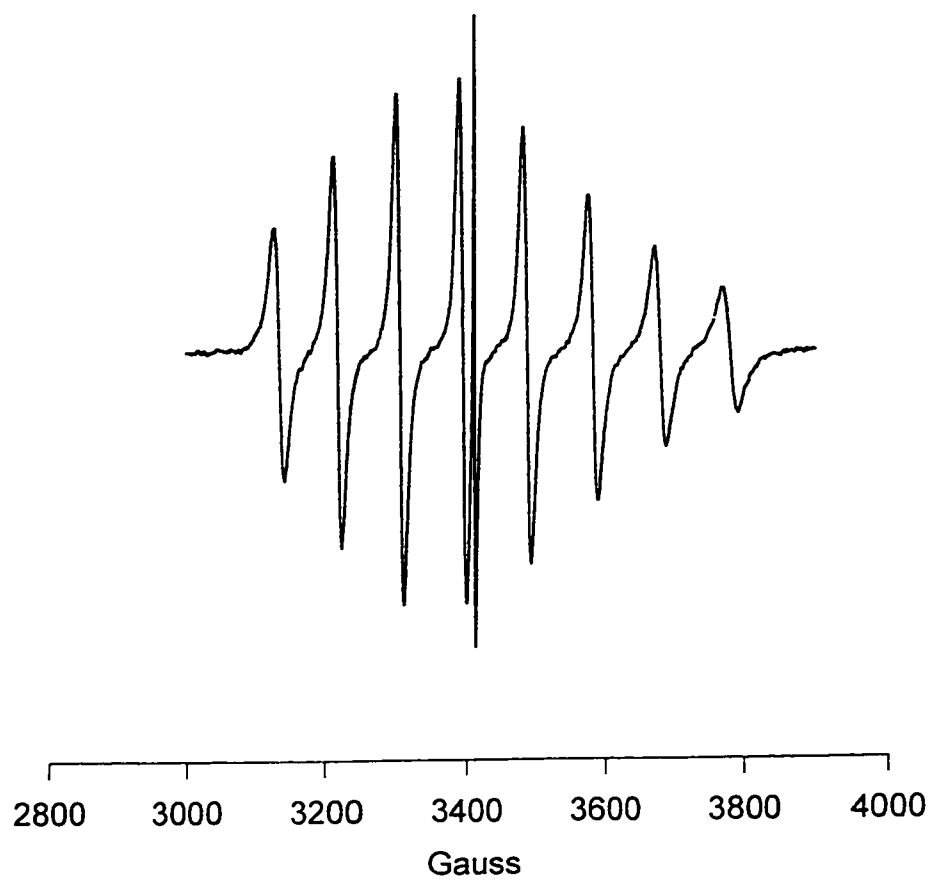


Figure 4.1.d: X-band spectrum of V4 in toluene at room temperature with DPPH as internal standard.

$$g_0 = g_s + g_s \left\{ \left[B_s - \frac{1}{2}(B_M - B_{-M}) \right] / \frac{1}{2}(B_M + B_{-M}) \right\} - g_0^2 (B_M + B_{-M})^2 \left[I(I-1) - M^2 \right] / 2g_s M^2 (B_M + B_{-M})^2 \quad (4.1)$$

$$A_0 = -g_0 \beta_c (B_M - B_{-M}) / 2M\hbar \quad (4.2)$$

In fact eq. (4.1) is obtained from eq. (2.8) and (2.9) and the last term is giving the second order effects. A_0 and g_0 were determined for each pair of M and $-M$ lines and averaged over all pairs for these four systems and are given in table 4.1.

4.1.2 Anisotropic Magnetic Parameters

The most important requirement in analyzing the variable temperature spectra is to have accurate values of magnetic tensors, A and g , determined from the rigid limit spectra.

The rigid limit spectra of V1 and V2 in toluene and V3 and V4 in methylene chloride at 9 GHZ are shown in figure 4.2. The anisotropic tensors were determined from these rigid limit spectra using second-order perturbation theory. These magnetic tensors are obtained from simulation. The rigid limit simulation was performed using the general method of Lefebvre and Maruani ⁷ adapted to oxovanadium (IV) systems. The simulation employs simpson's numerical integration over θ in 45 intervals and ϕ in 25 intervals.

Table 4.1 : Isotropic Magnetic Parameters:

Complex	Solvent	g_o	A_o (G)
V1	Toluene	1.9779	-88.53
V2	Toluene	1.9777	-88.69
V3	CH₂Cl₂	1.9774	-92.20
V4	CH₂Cl₂	1.9773	-91.97

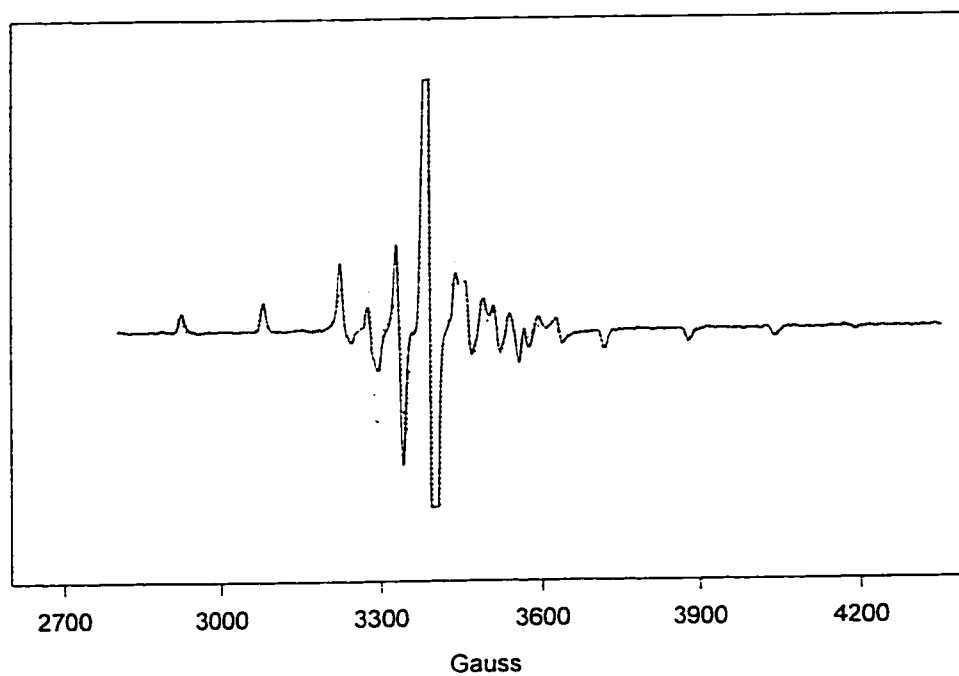


Figure 4.2.a: Rigid limit spectrum of V1 in toluene, experimental (solid line) and simulation (dashed line).

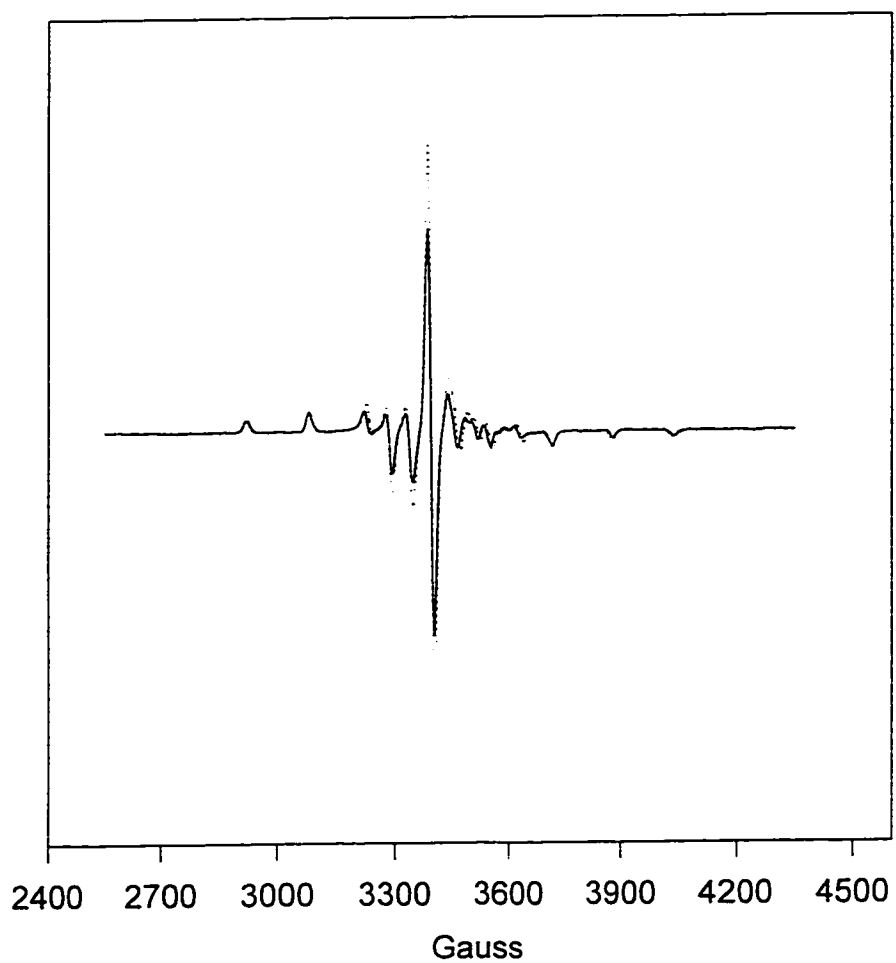


Figure 4.2.b: Rigid limit spectrum of V2 in toluene, experimental (solid line) and simulation (dashed line).

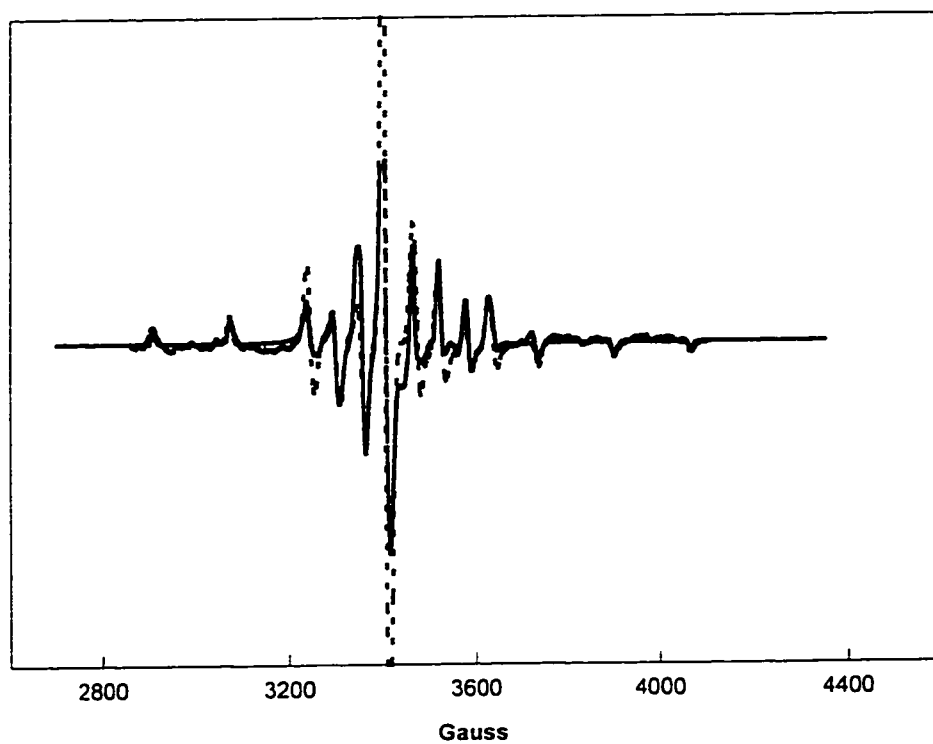


Figure 4.2.c: Rigid limit spectrum of V3 in CH_2Cl_2 , experimental (solid line) and simulation (dashed line).

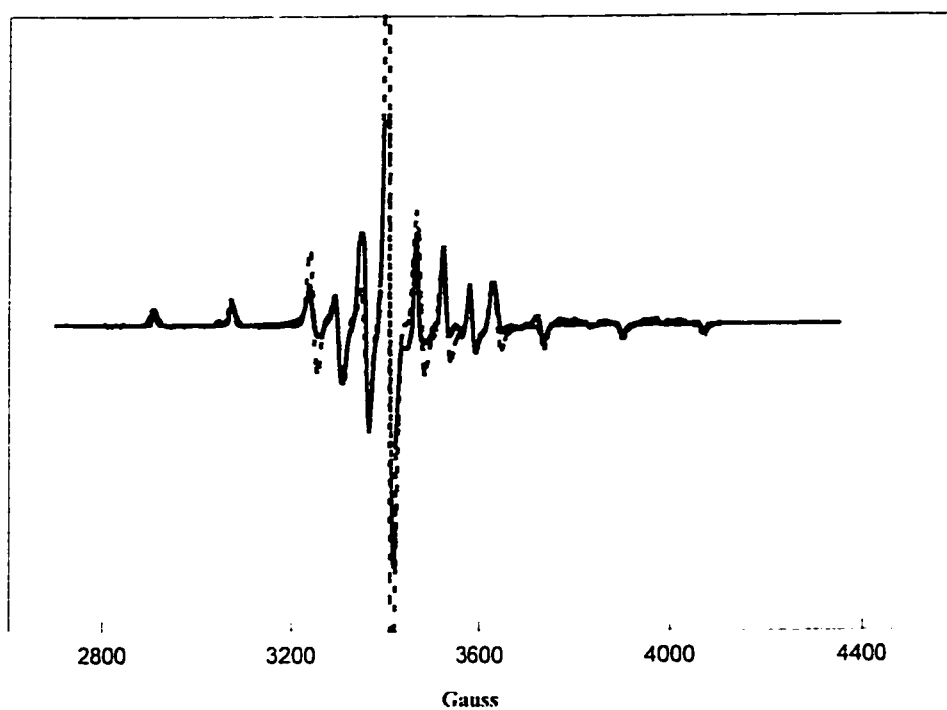


Figure 4.2.d: Rigid limit spectrum of V4 in CH_2Cl_2 , experimental (solid line) and simulation (dashed line).

In Lefebvre and Maruani original program the values of the magnetic tensors A and g were fed into the program until a good match was obtained between the experimental and the simulated rigid limit spectra.

First, the rigid limit program has been transformed into Microsoft power station (Version 4.0) to perform the calculation on a personal computer.

In our simulation, rather than feeding the g and A tensors, each time, as it is time consuming procedure, we wrote a small program which will vary the g and A tensors with predetermined increments simultaneously giving up to 1000 output files. Also this program (i.e. subroutine) will run the executable rigid limit program. Initial values for the magnetic tensors could be obtained by Kivelson's method ⁶. The simulation for the four systems is shown in Figure 4.2 with the experimental spectra and corresponding magnetic parameters are given in table 4.2.

The magnetic parameters for V1 and V2 are identical. This is reasonable since the only difference between the V1 and V2 rigid spectra is that the line widths of V2 are larger than those for V1 a behavior which will be further studied on the motional analysis study. Most probably this is due to the larger size of V2. In fact this equivalence of V1 & V2 magnetic parameters is expected since the ligands type is the same, both having $(NS)_2$.

Also V3 and V4 are having the same magnetic parameters, and the rigid limit spectra of V3 and V4 are almost identical. This is expected since the only difference between the two compounds is a methoxy group which is far away from and well separated from the unpaired electron. The differences in line widths of these systems will be discussed later.

Table 4.2 : Anisotropic Magnetic Parameters:

Parameter	V1	V2	V3	V4
Solvent	Toluene	Toluene	CH₂Cl₂	CH₂Cl₂
g_x	1.9945	1.9945	1.9915	1.9915
g_y	1.9826	1.9826	1.9835	1.9835
g_z	1.9556	1.9556	1.9573	1.9573
A_x	-49.76	-49.76	-54.76	-54.76
A_y	-56.48	-56.48	-54.76	-54.76
A_z	-159.96	-159.96	-166.62	-166.62

4.2 ELECTRONIC AND STRUCTURAL STUDY

4.2.1 Crystal Field Approximation:

The most studied d^1 ion is V^{4+} which appears in numerous complexes as VO^{2+} ^{6,4,37}. The complexes are close to square planar and so it is appropriate to develop their electronic energy level scheme by considering a strong tetragonal compression of an octahedral field. The level scheme is depicted in Fig. 4.3, from which we see that the singly occupied orbital should be d_{xy} ; for which³⁸

$$g_{||} = g_e - \frac{8\lambda}{E_{x^2+y^2} - E_{xy}} \quad (4.3)$$

$$g_{\perp} = g_e - \frac{2\lambda}{E_{xz} - E_{xy}} \quad (4.4)$$

Thus for D_{4h} and C_{4v} symmetry the g values sequence is $g_e > g_{\perp} > g_{||}$ which is our case. When there is lower symmetry due to more distortions

$$g_x = g_e - \frac{2\lambda}{E_{xz} - E_{xy}} \quad (4.5)$$

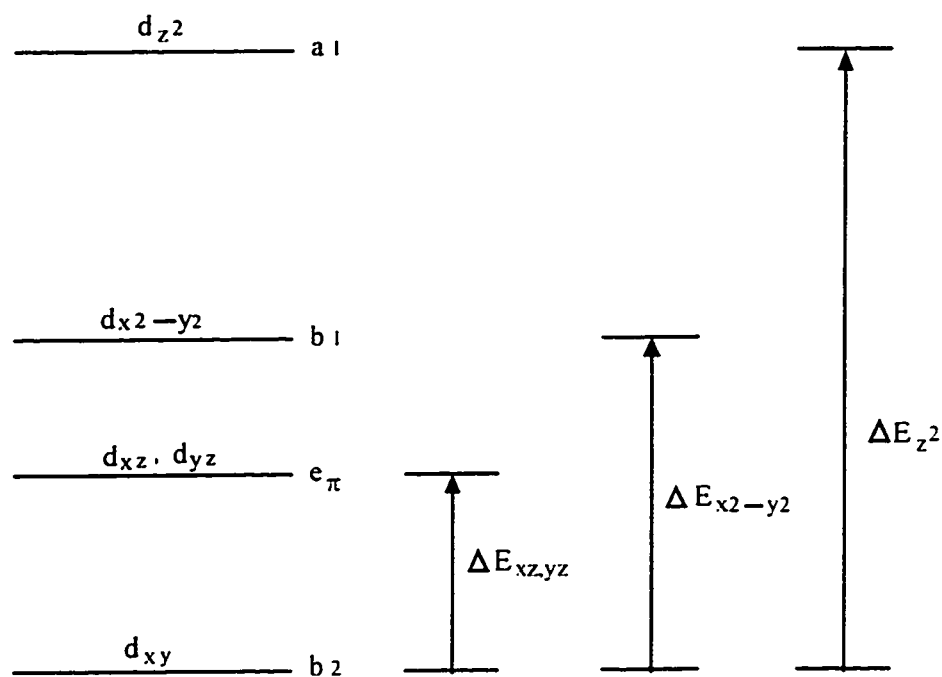


Figure 4.3: Splitting of the vanadium d-levels with C_{4v} symmetry .

$$g_y = g_e - \frac{2\lambda}{E_{yz} - E_{xy}} \quad (4.6)$$

$$\text{with} \quad g_e > g_x > g_y > g_z$$

Thus to get some information on the structure and the electronic structure, we have to investigate the g-values for these systems. For all our systems

$$g_e > g_x > g_y > g_z$$

which give support to five coordinated distorted square pyramidal structure. In case of distorted tetrahedral structure³⁸

$$g_z = g_e > g_x > g_y$$

For V1 (Group I) the complete lifting of the degeneracy d_{xz} and d_{yz} is confirmed by the electronic spectra.^{3b} The electronic transitions $d_{xy} \rightarrow d_{xz}$ and $d_{xy} \rightarrow d_{yz}$ are shown at 608nm and 612nm, respectively. Also $d_{xy} \rightarrow d_{x^2-y^2}$ transition is at 520nm.^{3b}

For V3 & V4 (group 2), all the three transitions are showing up as broad peak centered at 740nm,^{3b} which is in agreement with the obtained magnetic parameters. This is consistent with a decrease in the difference between g_x and g_y , i.e. there is no complete lifting of degeneracy. This is attributed due to the presence of 1,10-phenanthroline ligand which is rigid decreasing the possibility of the distortion.^{3b}

Electron Delocalization³⁹

In the crystal field approximation, it has been assumed that the unpaired electron is localized entirely on the metal atom. This is not usually the case since the formation of the molecular orbital results in the transfer of some of the unpaired electron density to the ligands. The effect is to reduce the orbital angular momentum i.e. further quench the orbital contribution and so make the magnetic parameters have values closer to the free electron g-value, i.e. $g = g_e = 2.0023$.

The orbital angular momentum, L , is reduced by factor of k to kL . Similarly the free ion spin-orbit coupling constant λ now becomes $\lambda_L = k\lambda$; where k is unity for no delocalization, and zero for complete delocalization. λ decreases with delocalization of the electrons. λ could be reduced from the free ion value as a result of shielding of the nucleus by the ligand bonding electrons. The spin-orbit coupling operator $\lambda \mathbf{L} \cdot \mathbf{S}$ now becomes $k\lambda \mathbf{L} \cdot \mathbf{S}$ and the equations for g are modified by a factor k^2 , thus $g_{||}$ for a d^1 ion in C_{4v} which is

$$g_e - \frac{8\lambda}{E_{x^2+y^2} - E_{xy}} \quad \text{becomes} \quad g_e - \frac{8\lambda k^2}{E_{x^2+y^2} - E_{xy}}$$

It is usually more convenient to use the molecular orbital coefficients rather than k .

4.2.2 Molecular Orbital Approach

The bonding in vanadyl complexes has been discussed by Ballhausen and Gray.^{37,40} The bonding molecular orbitals can be written as⁴⁰

$$\Psi^b = C_1 \phi \text{ (metal) } + C_2 \phi \text{ (ligand) } \quad (4.7)$$

and similarly the antibonding levels

$$\Psi^* = C_1^* \phi^* \text{ (metal) } + C_2^* \phi^* \text{ (ligand) } \quad (4.8)$$

with

$$C_1 C_1^* + C_2 C_2^* + C_1 C_2^* G_{ij} + C_1^* C_2 G_{ij} = 0$$

where ϕ (metal) and ϕ (ligand) refer to the proper combination of metal and ligand orbitals for the molecular orbital in question and G_{ij} are the usual group overlap integrals for each molecular orbital.

The complexes considered in this study are having C_{4v} effective symmetry and form coplanar bonds between the vanadium ion and each of the four ligands. The vanadyl oxygen is attached axially above the vanadium, i.e., along the z-axis (see Fig.4.4). A sixth ligand may lie opposite to the vanadyl oxygen, i.e., on the negative z-axis. V_1 and V_2 are fivefold coordinated complexes where as V_3 & V_4 are sixfold coordinated complexes.

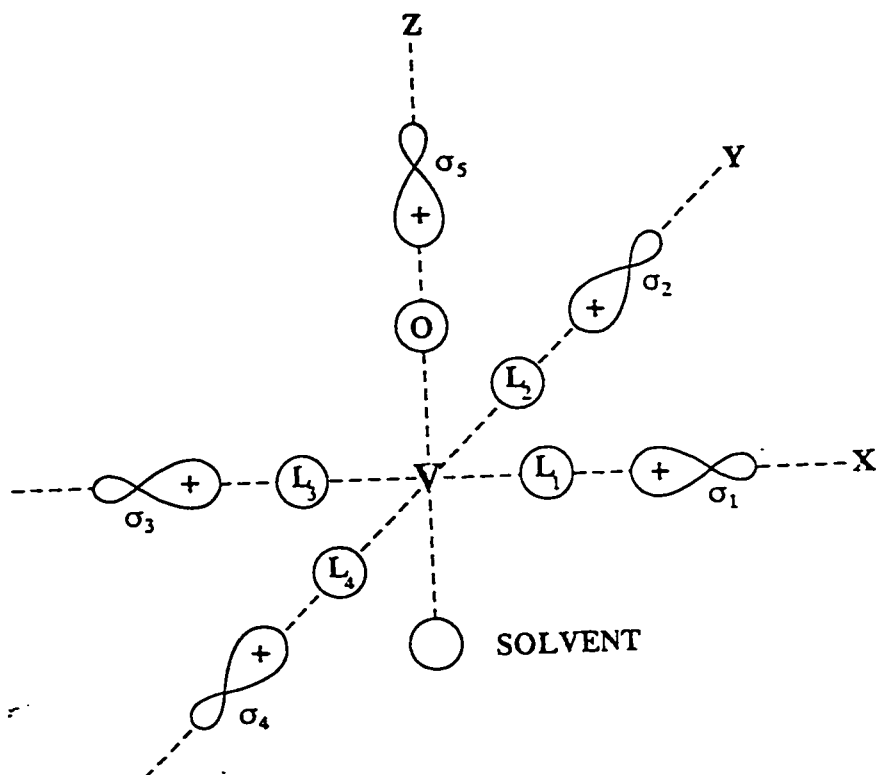


Figure 4.4: A typical oxovanadium(IV) general geometry
(σ -bonding)

The relevant molecular orbitals are essentially those given by Ballhausen and Gray ³⁷

$$\Psi (b_{2g}) = \beta_2 d_{xy} + \frac{1}{2} \beta'_2 (P_{y1} + P_{x2} - P_{y3} - P_{x4}) \quad (4.9)$$

$$\Psi (b_{1g}) = \beta_1 d_{x^2-y^2} + \frac{1}{2} \beta'_1 (+\sigma_1 - \sigma_2 + \sigma_3 - \sigma_4), \quad (4.10)$$

$$\Psi (e_{\pi x}) = \epsilon_{\pi} d_{xz} + \epsilon_{\pi}' P_{x5} + \frac{1}{2} \epsilon_{\pi}'' (P_{z1} - P_{z2}) \quad (4.11)$$

$$\Psi (a_1) = \alpha_1 (d_z^2 + S_0) + \alpha_1' \sigma_5 \quad (4.12)$$

$$\Psi (a_{11}) = \alpha_{11} (d_z^2 - S_0) - \frac{1}{2} \alpha_{11} + (\sigma_1 + \sigma_2 + \sigma_3 + \sigma_4) \quad (4.13)$$

The general geometry ³⁷ is indicated in Fig. 4.4. The d's represent vanadium 3d orbitals, S_0 the vanadium 4S orbital, σ_i refers to an sp^2 ligand orbital on the i th ligand directed towards the vanadium nucleus, the P_i 's are ligand 2p orbitals directed along the i th molecular axis, and the subscript 5 indicate the vanadyl oxygen. The β , α , and ϵ 's are coefficients of the ion wave functions whereas the β' , α' , ϵ' and ϵ'' are coefficients of the ligand wave functions. The molecular orbitals given above are bonding orbitals; the corresponding antibonding orbitals are given by replacing the coefficients by the starred quantities β^* , $-\beta'^*$, α^* , $-\alpha'^*$, ϵ^* , $-\epsilon'^*$, $-\epsilon''^*$. Ballhausen and Gray ³⁷ have set $\beta_2' = \beta_2'^* = \epsilon_{\pi}'' = \epsilon_{\pi}''^* = 0$, and they have given an energy level diagram in which the unpaired electron is in the

b_{2g}^* antibonding orbital and the first and second excited states are ϵ_{π}^* and b_{1g}^* , respectively.

$$g_{\parallel} - g_e = -\frac{8\lambda\beta_1^{*2}\beta_2^{*2}}{\Delta E_{x2-y2}} \left[1 - \frac{1}{2} \left(\frac{\beta_1'^*\beta_2'^*}{\beta_1^*\beta_2^*} \right) \cdot T(n) - \left(\frac{\beta_1'^*}{\beta_1^*} \right) \cdot S - \left(\frac{\beta_2'^*}{\beta_2^*} \right) \Pi \right], \quad (4.14)$$

$$g_{\perp} - 2.0023 = -\frac{2\lambda\beta_2^{*2}\epsilon_{\pi}^{*2}}{\Delta E_{xz}} \cdot X \left[1 - \left(\frac{\epsilon_{\pi}'''\beta_2'^*}{\epsilon_{\pi}^*\beta_2^*} \right) \left(\frac{1}{2} \right)^{\frac{1}{2}} - \left(\frac{\beta_2'^*}{\beta_2^*} \right) \Pi - \left(\frac{\epsilon_{\pi}'''}{\epsilon_{\pi}^*} \right) \frac{\Pi}{\sqrt{2}} - \left(\frac{\epsilon_{\pi}'''}{\epsilon_{\pi}^*} \right) \Pi_o \right] \quad (4.15)$$

$$A_{\parallel} = P \left[-\beta_2^{*2} \left(\frac{4}{7} + k \right) - \frac{8\lambda\beta_1^{*2}\beta_2^{*2}}{\Delta E_{x2-y2}} - \frac{\frac{6}{7}\lambda\beta_2^{*2}\epsilon_{\pi}^{*2}}{\Delta E_{xz}} \right] \quad (4.16)$$

$$A_{\perp} = P \left[\beta_2^{*2} \left(\frac{2}{7} - k \right) - \frac{11}{7}\lambda\beta_2^{*2}\epsilon_{\pi}^{*2} / \Delta E_{xz} \right] \quad (5.17)$$

λ is the spin-orbit coupling constant for the free ion in the appropriate valence state, K is Fermi contact term for the vanadium; ΔE_{x2-y2} and ΔE_{xz} are the transition energies from the b_{2g}^* state to b_{1g}^* and ϵ_{π}^* states, respectively; P is the direct dipolar interaction which gives direct

information about electron delocalization and covalency; S and π are the overlap integrals

$$S = \langle d_{x^2-y^2} | \sigma_N \rangle + \langle d_{x^2-y^2} | \sigma_S \rangle \quad \text{for } N_2S_2 \text{ systems}$$

$$S = 3 \langle d_{x^2-y^2} | \sigma_N \rangle / 2 + \langle d_{x^2-y^2} | \sigma_S \rangle / 2 \quad \text{for } N_3S \text{ systems}$$

$$\pi = 2 \langle d_{xy} | P_{y1} \rangle = 2 \langle d_{xz} | P_{z1} \rangle ;$$

$$\pi_o = \langle d_{xz} | p_{x5} \rangle$$

$$T = n - \frac{1}{3} \frac{1}{2} \left(1 - n^2 \right) \frac{1}{2} \int_0^\infty r^2 R_{21}(r) \frac{d}{dr} (R_{20}) dr,$$

Where R is the vanadium-ligand distance and $R_{21}(r)$ and $R_{20}(r)$ are normalized radial 2p and 2s functions, respectively, and $n^2 / (1 - n^2)$ is the ratio of 2p to 2s character in the ligand orbital, i.e., 2 for sp^2 orbital.

The overlap integrals S & π depend upon R, the distance between the vanadium ion and the equatorial ligands, and the axial oxygen. R is estimated by DTMM as⁵⁸

Axial	$R(V - O) = 1.59 \text{ \AA}$
Equatorial	$R(V - N) = 1.90 \text{ \AA}$
Equatorial	$R(V - S) = 2.01 \text{ \AA}$
Equatorial	$R(V - O) = 1.97 \text{ \AA}$

The overlap integrals can then be estimated with the help of Jaffe's tables ^{41,42} and the following effective nuclear charges obtained from Roothaan-Hartree-Fock calculation ^{37,43}

$$Z(V^+, 3d) = 2.93 \qquad Z(O^{2-}, 2p) = 1.70$$

$$Z(N, 2s) = 1.61 \qquad Z(N, 2p) = 1.72$$

$$Z(S^-, 3s) = 2.56 \qquad Z(S^-, 3p) = 1.66$$

The V^+ ion has been used because the calculations of Ballhausen ⁴⁰ and Gray indicate that the apparent charge on vanadium is approximately +1.

$$\text{For } V1 \text{ \& } V2 \qquad S = 0.186 \text{ (N}_2\text{,S}_2 \text{ Systems)}$$

$$\text{For } V3 \text{ \& } V4 \qquad S = 0.195 \text{ (N}_3\text{S Systems)}$$

$$\pi_o = 0.189$$

Kivelson & Lee ³⁷ obtained more understandable M.O. calculation by setting $\lambda = 170 \text{ cm}^{-1}$. In order to interpret the magnetic data in terms of the orbitals given in equations (4.14-4.17), it is important to have spin orbit constant, λ , for the vanadium ion in the appropriate valence state. We set $\lambda = 170 \text{ cm}^{-1}$ based on Kivelson and Lee work on VO^{2+} systems ³⁷.

The molecular orbital coefficient β_1^* and β_2^* can be obtained from equation (4.14) combined with the normalization relationship

$$\beta_1^{*2} + \beta_1'^{*2} - \beta_1^* \beta_1'^* S = 1 \quad (4.18)$$

Similarly ϵ_π^* and $\epsilon_\pi'^*$ can be obtained from equation (4.15) and the normalization relationship

$$\epsilon_\pi^{*2} + \epsilon_\pi'^{*2} - \epsilon_\pi^* \epsilon_\pi'^* S = 1 \quad (4.19)$$

The Excitation energies ΔE_{x2-y2} & $\Delta E_{x,2}$, needed for this calculations, for the studied systems are in table 4.3. The obtained values for β_1^* , $\beta_1'^*$, ϵ_π^* and $\epsilon_\pi'^*$ are listed in table (4.3).

The orbital coefficients β_1^{*2} , $\beta_1'^{*2}$, ϵ_π^{*2} and $\epsilon_\pi'^{*2}$ allow us to make fruitful comparisons between these complexes as does the anisotropic hyperfine parameter (P) which gives direct information about electron delocalization and covalency^{37-40,44-49}.

K and P were obtained using equations (4.16) and (4.17) and they are presented in table (4.4). Increasing delocalization of the unpaired electron on to the ligands (increasing covalent bonding) is expected to lead to a reduction in the P value, since this depends on the spin population of the 3d orbitals. The value of P will show the % of the unpaired electron localized on the metal. Closer inspection both of our results and those of

Table 4.3 : Molecular orbitals coefficients

	$\Delta E_{x^2-y^2}$ (cm ⁻¹)*	ΔE_{xz} (cm ⁻¹)*	$\beta_1 \cdot^2$	$\beta_1'^* \cdot^2$	$\epsilon^* \cdot^2$	$\epsilon'^* \cdot^2$
V1	15655**	19200	0.770	0.67	0.949	0.475
V2	14700	20,000	0.794	0.649	0.905	0.537
V3&V4	13500	18500 [#]	0.731	0.712	0.703	0.726

* are taken from refrence 3b.

** = (14970 + 16340)/2

[#] The value for 4-MeO(SalSB)VO(Phen) complex is used ^{3b}.

Table 4.4 : P and K values

	$\Delta E_{x_2-y_2} (\text{cm}^{-1})^*$	$\Delta E_{xz} (\text{cm}^{-1})$	$P\beta_2^2 (10^{-4} \text{cm}^{-1})$	K
V1	15700	19200	107.2	0.745
V2	14700	20,000	107.2	0.744
V3 & V4	13500	18500	114.2	0.715

others show that there is a good correlation between P and the nature of the coordinating atom. The larger value of P for N_3S systems (V3 & V4) compared with N_2S_2 systems (V1&V2) studied, 114×10^{-4} and $107 \times 10^{-4} \text{cm}^{-1}$ respectively, indicates less delocalization of the unpaired electron onto the smaller p_π orbitals on N. Generally P for sulfur coordinating complexes, is much smaller indicating significant delocalization of the electron into the relatively larger empty π -orbitals (d-orbitals) on the sulfur ligand ⁴⁴. While the complexes bonding via N and O have large P values (less delocalization) since involve smaller orbitals. Also, for these negatively charged sulfur atoms, orbital expansion due to the negative charge and consequent greater delocalization of the electron is expected. The isotropic contact term, K , which is related to the amount of the unpaired electron density at the vanadium nucleus varies considerably from complex to complex ^{2,45}. Since the orbital that contains the unpaired electron, d_{xy} , has zero electron density at the vanadium nucleus and does not mix with the metal 4s orbital (in C_{4v} symmetry), there is no direct way of putting unpaired electron density on the nucleus. The nonzero value of K must then arise from an indirect mechanism. McGarvey ² suggested that the variation can be explained by invoking a spin polarization mechanism. The unpaired electron in the d_{xy} orbital formally creates unpaired electron density in filled 2s and 3s orbitals of vanadium. In the absence of covalent bonding and 4s mixing, spin polarization should remain constant for all vanadium complexes and be equal to the free ion value, K_0 . Taking into account covalent bonding, K should depend on the d-orbital population for the unpaired electron:

$$K \approx (\beta_2^*)^2 K_0$$

i.e., K should increase with covalency. Since K increases with covalency, it is not surprising that N_2S_2 systems, as far as sulfur ligands are extensively covalently bonded relative to nitrogen ligands. In fact the values of $(\beta_2^*)^2$ follow the general π -bonding order of ligand donor atom, $S > C > N > Cl \geq O$.

The in-plane σ bonding represented by β_1^{*2} varies from compound to compound and decrease as the covalency of the bond increases ³⁷. The larger value of β_1^{*2} for N_2S_2 (V1&V2) systems compared to N_3S (V3 & V4) systems reflecting more in-plane σ bonding in N_2S_2 systems. Most probably this is due to the extreme polarizable electrons on the negatively charged sulfur are capable of forming strong σ bonding with the empty $d_{x^2-y^2}$ orbital on the vanadium which is of high electron deficiency.

The out-of-plane π -bonding represented by ϵ_π^{*2} is very sensitive to solvent basicity and sixth ligand attached on the z-axis *trans* to V=O unique bond ². The decrease in ϵ_π^{*2} for N_3S systems compared to N_2S_2 systems is due to the oxygen coordinated at the sixth position along z-axis *trans* to the oxovanadium oxygen. The decrease in the V=O bond strength is also reflected in a decrease in the V=O bond vibrational frequency of N_3S systems ($\nu = 950 \text{ cm}^{-1}$) compared to N_2S_2 systems ($\nu = 975 \text{ cm}^{-1}$) ^{3b}.

4.3 APPLICATION TO NON-PORPHYRIN VANADIUM SPECIES IN ASPHALTENS

Yen ^{2,50} found a linear relationship between A_0 and g_0 for VO^{2+} complexes for ligands made of varying compositions. In our model compounds, the vanadyl complexes has equatorial donor atoms of the type $VO(N_2S_2)$ and $VO(N_3S)$. Their A_0 and g_0 are in table 4.1. The g_0 and A_0 values for our model compounds of the type $VO(S_4)$ and $VO(N_4)$ are plotted in figure 4.5. In comparing hyperfine coupling constants of different complexes, it is important that the solvents used be the same nature (non-coordinating) since the solvent effects on A_0 can be moderately large ($\sim 5G$) ⁵¹⁻⁵⁴. This is because, due to the geometry of the vanadyl complex, a sixth ligand molecule or solvent can be added to the vanadium complex at the position *trans* to the axial oxygen, conversely g_0 value are less sensitive to solvents effects and any variations in g_0 values are due to varying ligand types. Using the additivity relationship one can calculate A_0 for N_2S_2 systems $A_0 = (70.0G + 97.0G)/2 = 83.5G$, which compares favorably with the experimental value of 88.73G. For N_3S systems $A_0 = (70.0G + 3 \times 97.0 G)/4 = 92.25G$, which almost equal to the experimental value of 92.05G. The additivity rule is based on the well-known rule of average environment in ligand field theory ⁴⁶. The solvent used in literature ^{51,52} was chloroform, while we use toluene for N_2S_2 systems (V1 and V2) and methylene chloride for N_3S systems (V3 and V3).

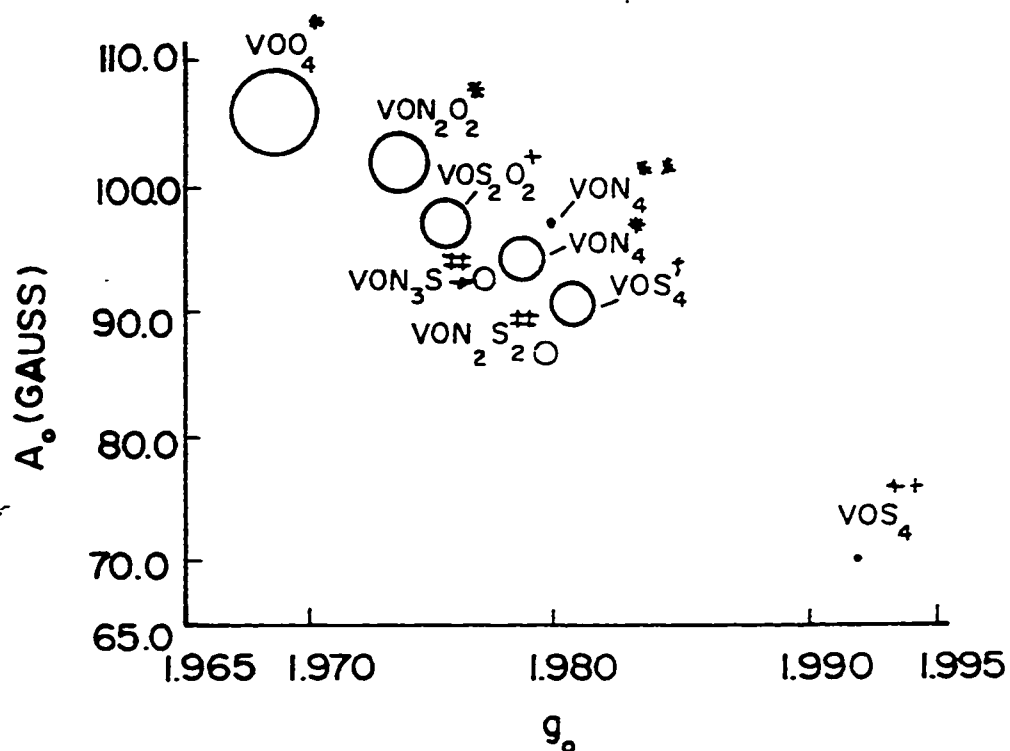


Figure 4.5: Correlation between A_0 and g_0 values for a variety of square pyramidal vanadyl (IV) complexes with equatorial ligand fields of the type $VO(O_4)$, $VO(N_2O_2)$, $VO(S_2O_2)$, $VO(N_4)$, $VO(N_3S)$, $VO(N_2S_2)$, and $VO(S_4)$.

(*)Boucher, L.J.; Tynan, E. C.; Yen, T. F. In *Electron Spin Resonance of Metal Complexes*; Yen, T. F. Ed., Plenum press: NewYork, 1969, pp 111-130.

(**) Assour, j. M. J. Chem. Phys. 1965,43,2477.

(+) Bozis, R. A.; McCormick, B.J. Inorg. Chem. 1970,9,1514.

(†) Dickson, F. E.; Kunesh, C. J.; McGinnis, E. L.; Petrakis, L. Anal. Chem. 1972,44,978.

(++) Atherton, N. M.; Locke, J.; McCleverty, J.A. Chem. Ind. 1965,29,11300.

(#) This work.

This may explain the better agreement for N_3S systems. Moreover in N_3S systems the sixth position is protected by the coordinated oxygen. The additivity rule must be used with caution as it does not take into account the size of the chelate ring, the chelate geometry or the effect of axial ligand. Figure 4.5 shows that while the correlation between g_0 and A_0 value is quite good for a variety of square pyramidal vanadyl (IV) complexes with equatorial ligand fields of the type $VO(O_4)$, $VO(N_2O_2)$, $VO(S_2O_2)$ and $VO(N_4)$, the correlation is not quite as good for the vanadyl complexes with equatorial ligand field of the type $VO(N_4)$, $VO(N_2S_2)$, $VO(N_3S)$ and $VO(S_4)$. Holyk ^{14,15} has shown that the correlation between $g_{||}$ and $A_{||}$ is perhaps more useful because $g_{||}$ depends directly on the in-plane ligand field and the range of the values for $g_{||}$ and $A_{||}$ is about twice that of g_0 and A_0 . The correlation between $g_{||}$ and $A_{||}$ is plotted in figure 4.6. One sees that there is a linear relationship between $g_{||}$ and $A_{||}$ for VO^{2+} complexes for ligands made of varying compositions, and the correlation is good for the vanadyl (IV) complexes with equatorial ligand field of the type $VO(N_4)$, $VO(N_3S)$, $VO(N_2S_2)$ and $VO(S_4)$ which is not so good for g_0 and A_0 plot. The chemistry and structure of the non-porphyrin species of vanadium in asphaltenes are poorly understood and few studies have dealt with the characterization of the vanadyl compounds present. In a study of vanadyl compounds in heavy crude petroleum from Boscan, Cerro Negro, Wilmington, and Prudhoe Bay ⁵⁵, it was found that vanadyl compounds associated with the large molecular weight asphaltenes can be extracted with aqueous pyridine and these compounds have apparent molecular weights greater than 2000 actually have molecular weights less than 400. This strongly implies that a considerable percentage (60-80%) of

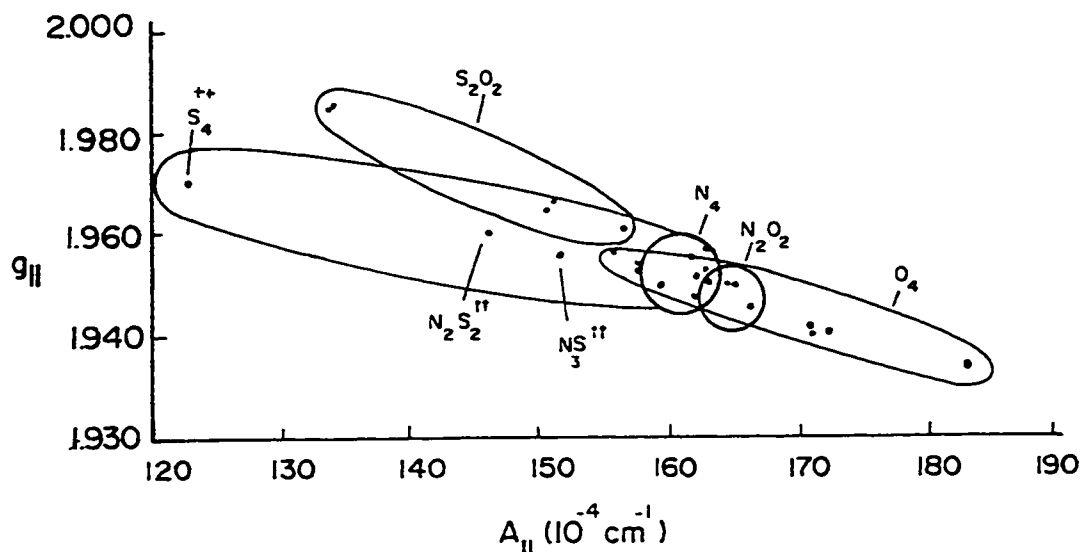


Figure 4.6: Correlation between $g_{||}$ and $A_{||}$ values for a variety of square pyramidal vanadyl (IV) complexes with equatorial ligand fields of the type $VO(O_4)$, $VO(N_2O_2)$, $VO(S_2O_2)$, $VO(N_4)$, $VO(N_3S)$, $VO(N_2S_2)$, and $VO(S_4)$. [The data for were reprinted from Plenum Press ⁵⁴].

(++) Atherton, N. M.; Locke, J.; McCleverty, J. A. *Chem. Ind.* **1965**, 1300.

(#) This work.

vanadyl non-porphyrin compounds are complexed to the large molecular weight asphaltenic component of the heavy crude petroleum and could be removed by solvent selection extraction techniques. If one uses sequential elution solvent chromatography to obtain fractions for asphaltenes based on functionality, then one can use the correlation diagram between $g_{||}$ and $A_{||}$ to determine more explicitly, the nature of the square planar complexes responsible for the characteristic spectrum, particularly with regard to nitrogen and sulfur heteroatoms.

CHAPTER 5

5. TRANSLATIONAL DIFFUSION STUDY

The translational diffusion constant can be determined at room temperature (22 ± 1 °C) by a capillary diffusion cell. The translational diffusion processes were monitored by electron spin resonance spectral intensities as a function of time. In this study, the translational diffusion constant of V1 and V2 in toluene, and V3 and V4 in methylene chloride were measured at room temperature (22 ± 1 °C) by the capillary diffusion method. From the measurement of the translational diffusion coefficient (in cm^2/sec) one can determine the hydrodynamic radius of solvated molecules in solution from the Stokes-Einstein equation for translational diffusion under the stick boundary condition ¹⁰

$$D = \frac{k_B T}{6 \pi \eta r_o} \quad (5.1)$$

where r_0 is the hydrodynamic radius of the solvated molecules in Å, k_B is the Boltzmann constant, T is the absolute temperature, η is the shear viscosity in pa. s (pa = 0.1 poise).

The intensity was monitored as a function of time with EPR spectroscopy because of the high sensitivity of an EPR spectrometer. The EPR capillary diffusion experiment measurement technique is advantageous because it allows simultaneous measurement of translational and reorientational diffusion coefficients for a given sample.

5.1 THE DIFFUSION CONSTANT

5.1.1 V1 in Toluene

The capillary diffusion experiment for V1 in toluene is followed by EPR technique. Spectra were collected over about three weeks and for each spectrum the time is recorded. Selected spectra obtained at different time intervals in the translational diffusion experiment of V1 in toluene are shown in figure 5.1, where the intensities of the spectra were normalized with respect to the intensity of the spectrum acquired at zero time. Each spectrum is analyzed and the intensity of each of the eight lines were found. The obtained data is introduced to the program "diff.fortran" (A copy of this program is found in reference 10.b). This program calculate the diffusion coefficient using equation 2.26 from these data. The basic logic behind this program is to fit the total intensity versus

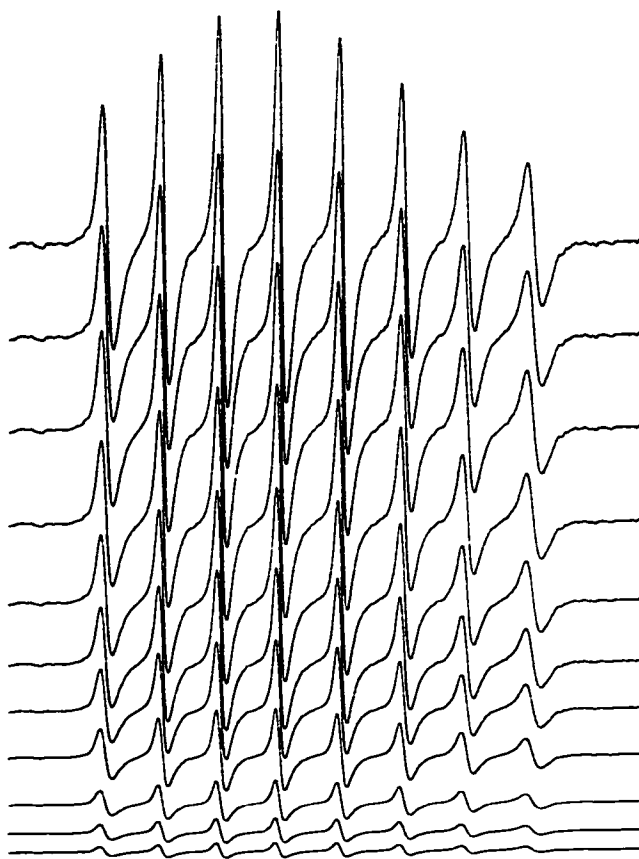


Figure 5.1: EPR experimental spectra at different time intervals during the diffusion process of V1 in toluene.

time data by a polynomial regression. A data point is located at which the best match is achieved between theoretically generated data and experimental data. This data point is then used to calculate the translational constant, D , from equation 2.26. The obtained D value obtained is then used in equation 2.26 to calculate a theoretical curve which is compared with the experimental curve. In figure 5.2 experimental and calculated total EPR intensities as a function of time for V1 in toluene are plotted.

The diffusion constant calculated for V1 in toluene is $0.680 \times 10^{-5} \text{ cm}^2/\text{sec}$. The value of $R (=I_s/I_t)$ calculated ($R_{\text{calc}}=0.677$) is within experimental error of $R_{\text{expt}} (0.677_4)$.

5.1.2 For V2 in toluene

Spectra were collected for V2 in toluene during the diffusion experiment. Selected spectra obtained at different time intervals are shown in figure 5.3. A plot of time versus experimental and calculated total EPR intensities as a function of time for V2 in toluene are shown in figure 5.4. The diffusion constant obtained for V2 in toluene is $0.642 \times 10^{-5} \text{ cm}^2 / \text{sec}$. The experimental and calculated R values are 0.688 and 0.678, respectively.

5.1.3 For V3 in methylene chloride:

The diffusion experiment for V3 were carried out in methylene chloride. Selected spectra obtained at different time intervals are shown in figure 5.5. A plot of experimental and calculated time versus total EPR

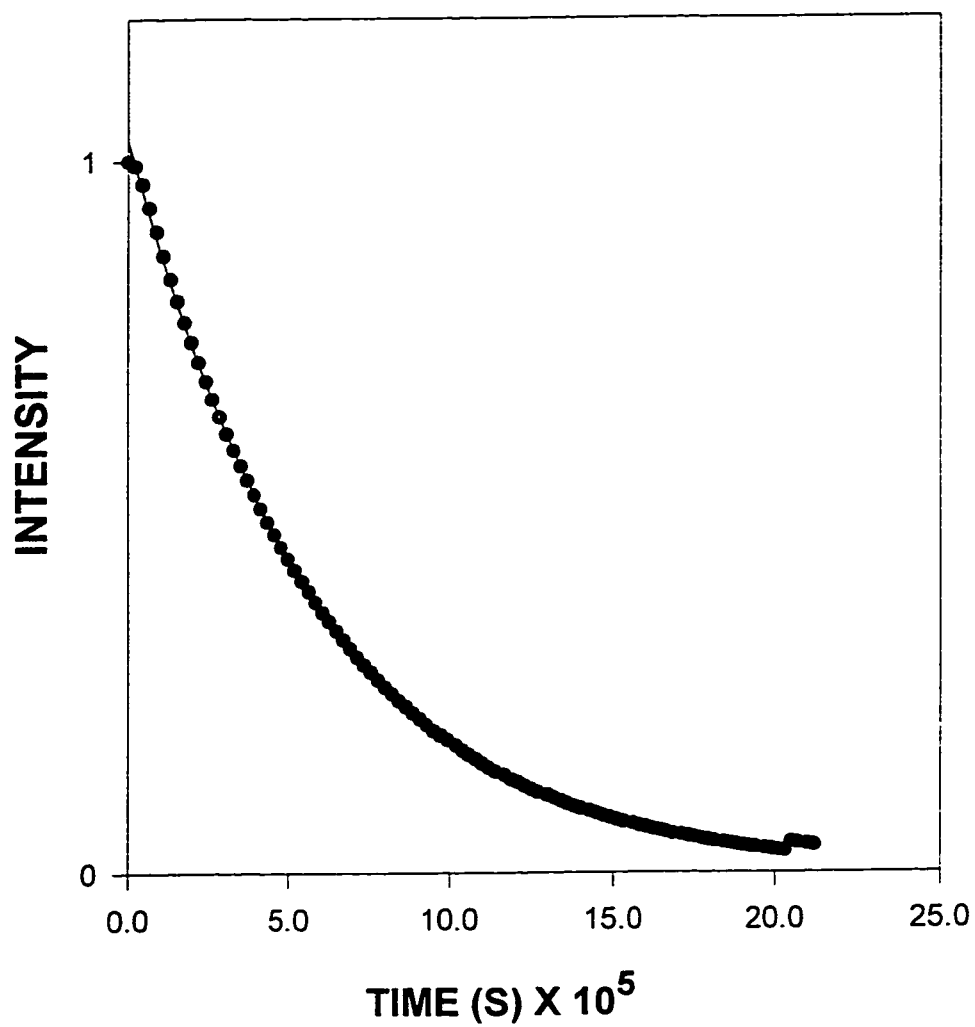


Figure 5.2: Total ESR intensities as a function of time for V1 in toluene during the diffusion experiment.

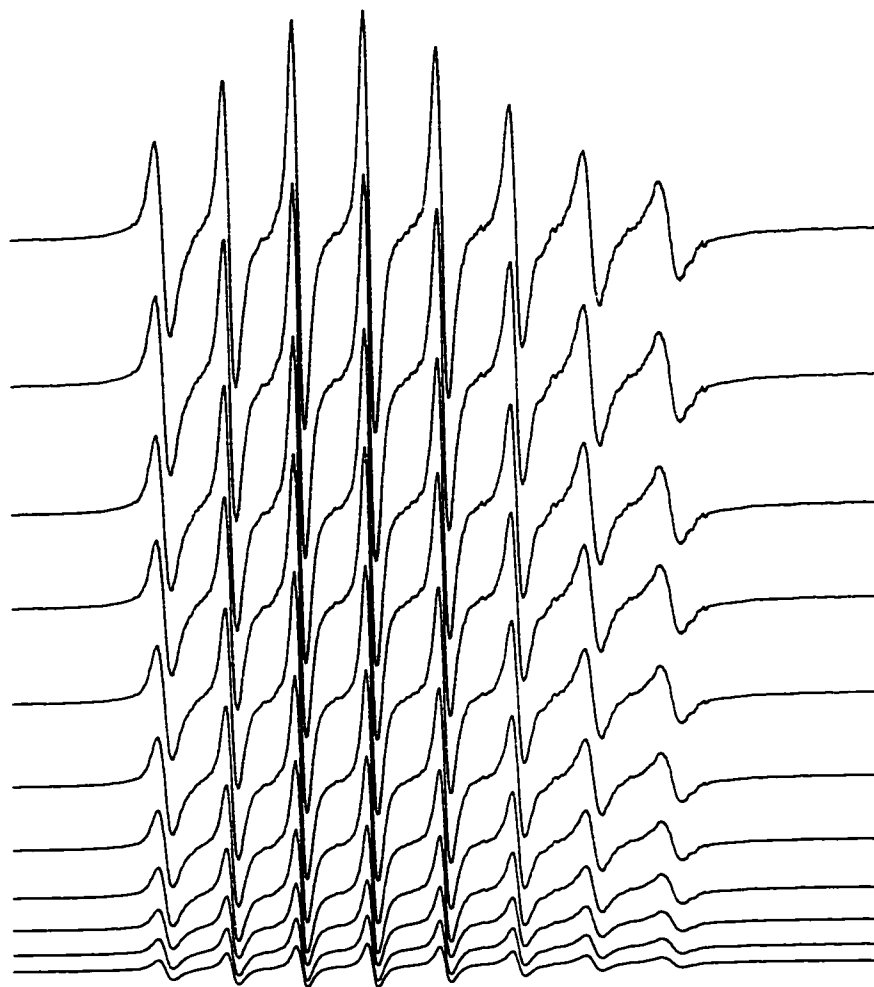


Figure 5.3: EPR experimental spectra at different time intervals during the diffusion process of V2 in toluene.

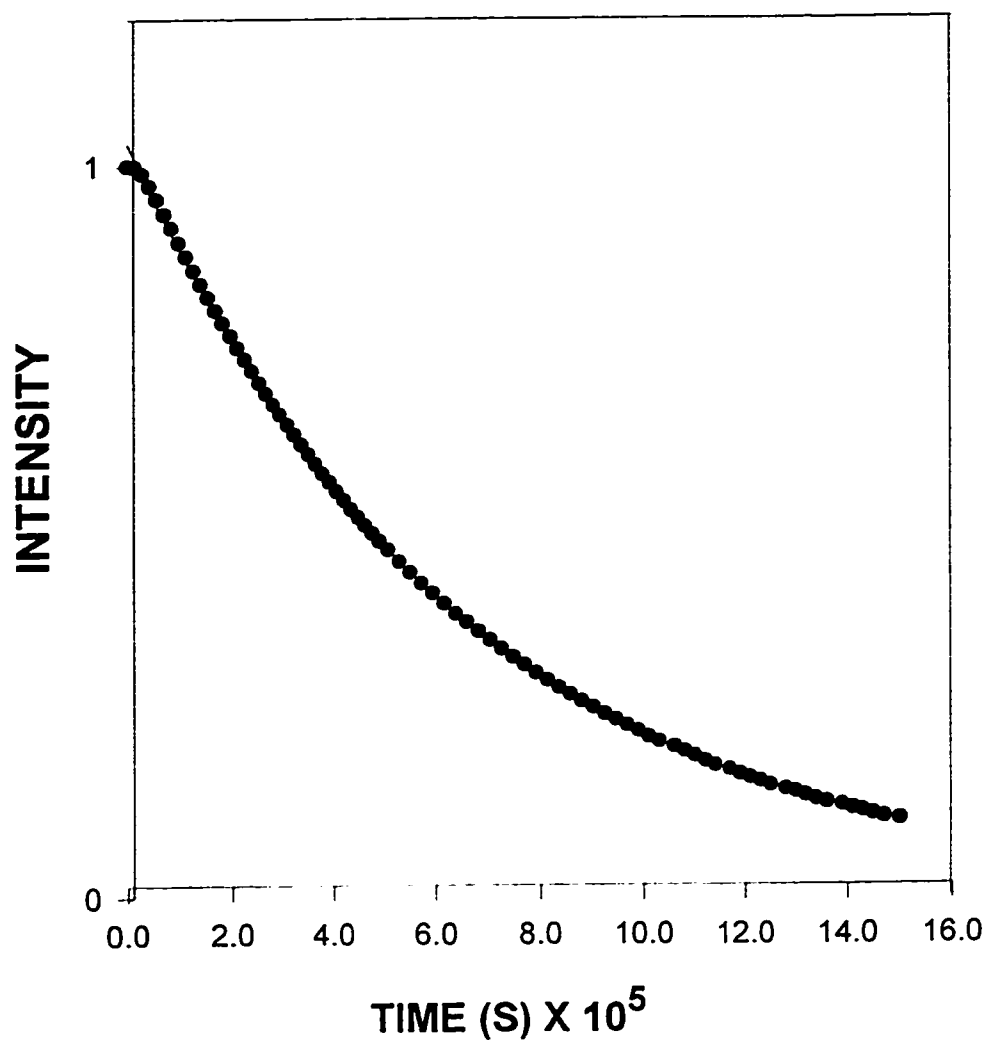


Figure 5.4: Total ESR intensities as a function of time for V2 in toluene during the diffusion experiment.

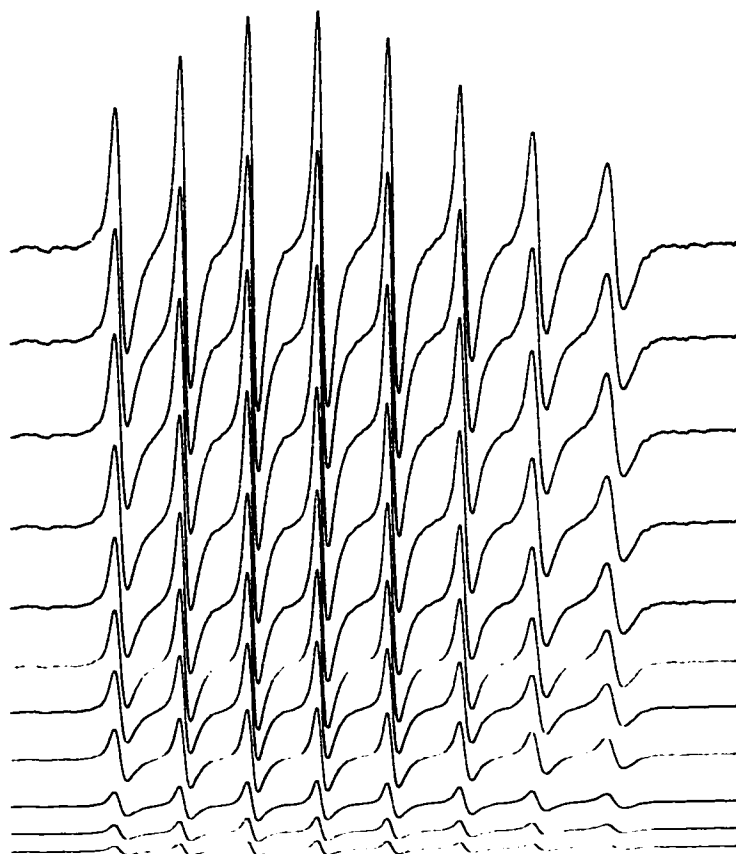


Figure 5.5: EPR experimental spectra at different time intervals during the diffusion process of V3 in CH_2Cl_2 .

intensities for V3 in methylene chloride is shown in figure 5.6. The diffusion constant obtained for V3 in methylene chloride is 0.712×10^{-5} cm² / sec. The experimental and calculated R values are 0.667 and 0.670, respectively.

5.1.4 For V4 in methylene chloride:

For V4 in methylene chloride about 100 spectra were collected during the diffusion experiment. Selected spectra obtained at different time intervals are shown in figure 5.7. A plot of experimental and calculated time versus total EPR intensities for V4 in methylene chloride is shown in figure 5.8. The diffusion constant obtained for V4 in methylene chloride is 0.661×10^{-5} cm² / sec. The experimental and calculated R values are 0.656 and 0.660, respectively.

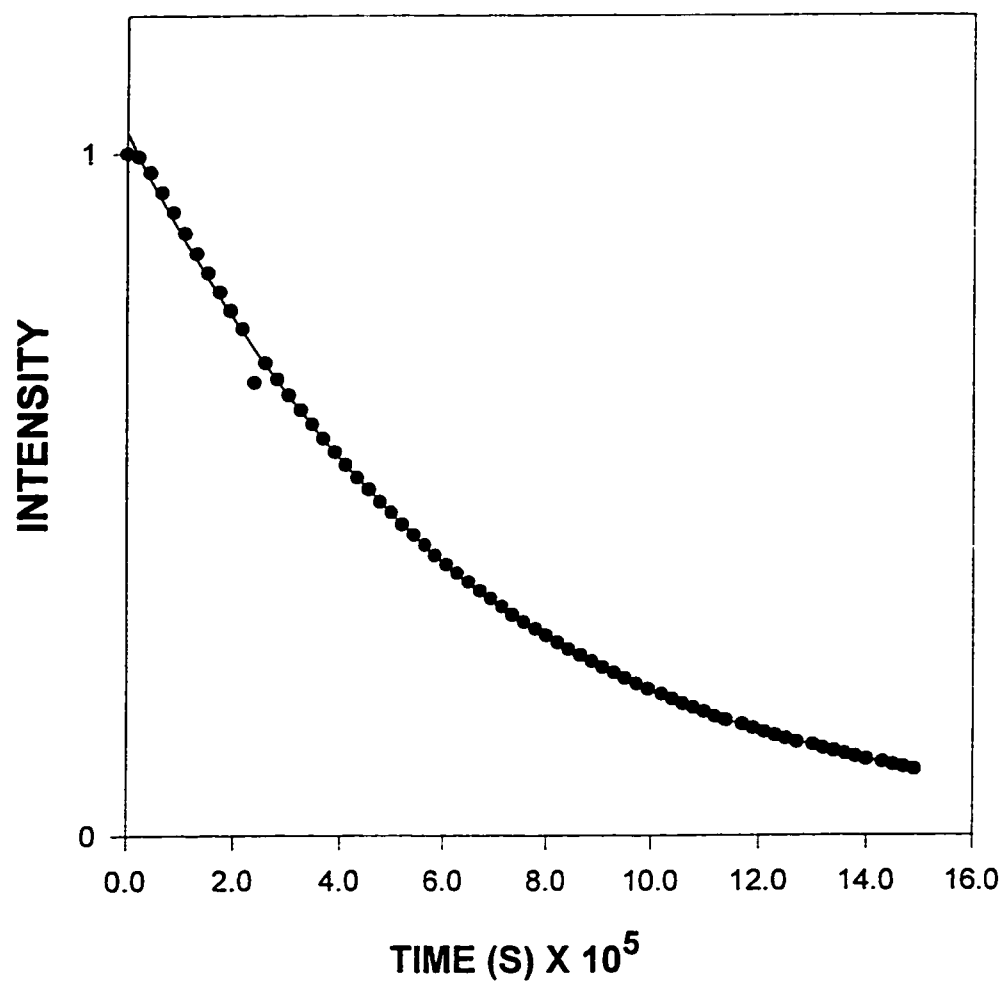


Figure 5.6: Total ESR intensities as a function of time for V3 in CH_2Cl_2 during the diffusion experiment.

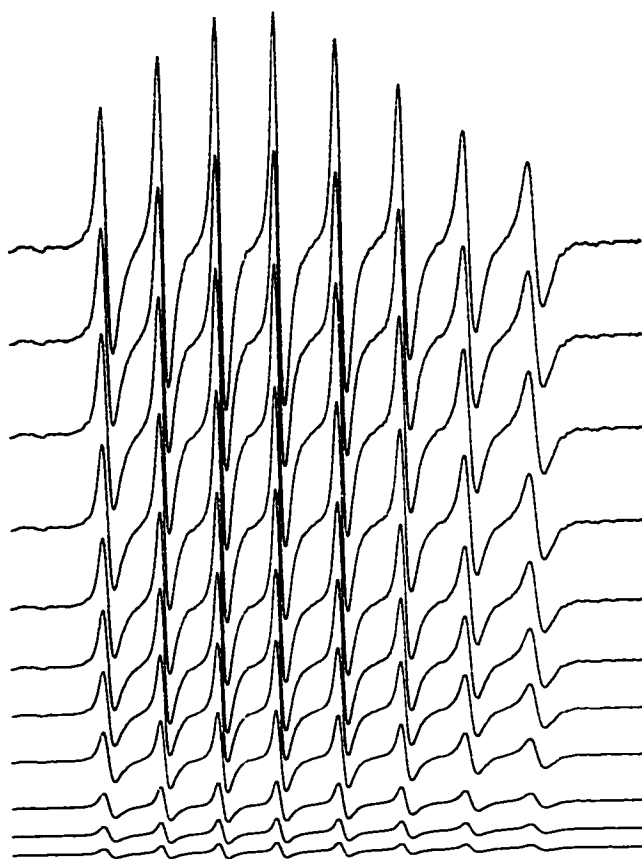


Figure 5.7: EPR experimental spectra at different time intervals during the diffusion process of V4 in CH_2Cl_2 .

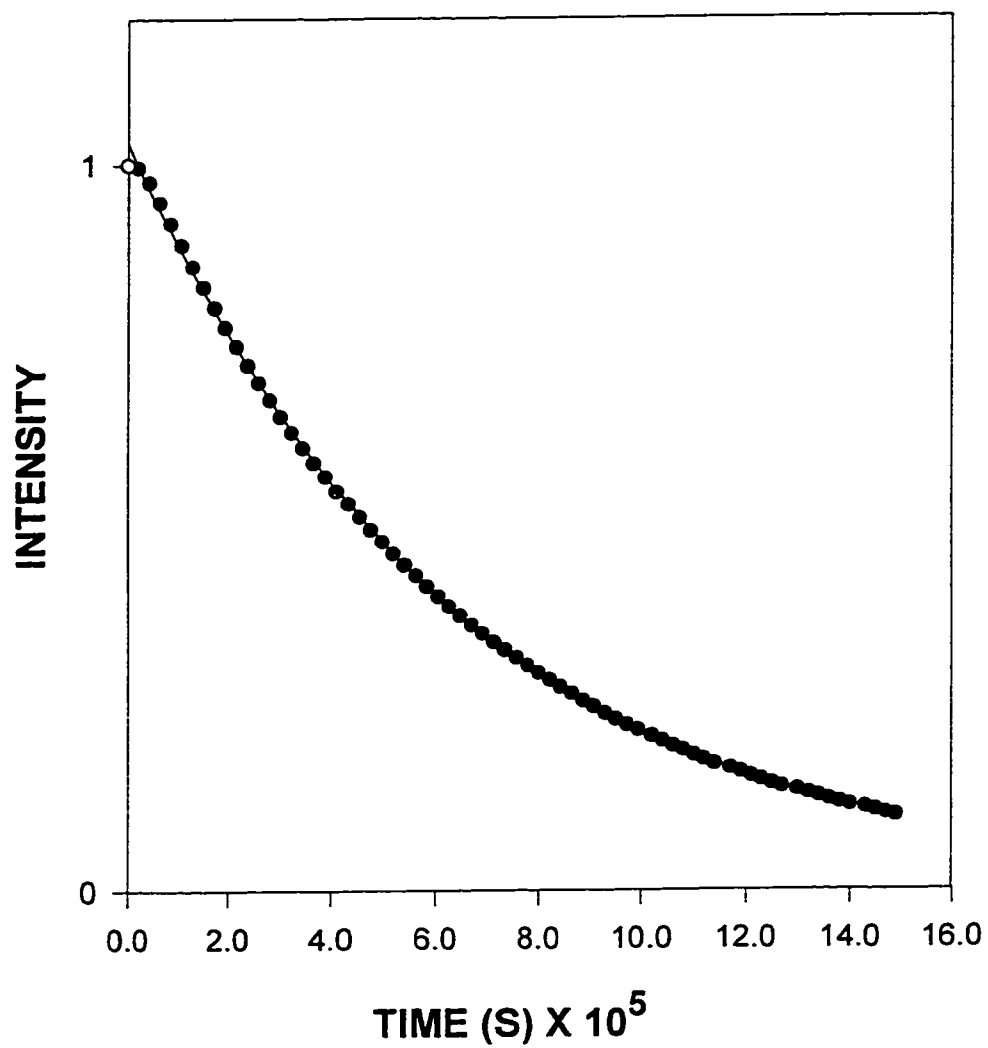


Figure 5.8: Total ESR intensities as a function of time for V4 in CH_2Cl_2 during the diffusion experiment.

5.2 THE HYDRODYNAMIC RADIUS:

Using the Stokes-Einstein equation for translational diffusion (equation 5.1), the hydrodynamic radius r_0 was calculated. The viscosity were obtained from literature⁵⁶. The experimental results were summarized in the Table 5.1.

Table 5.1. Results from Translational Diffusion Experiment:

COMPOUND	D (cm ² /s)	η (in pa)	r_0 (Å)	VOLUME (Å ³)
V1	6.80x10 ⁻⁶	5.903x10 ⁻⁴	5.39	656
V2	6.42x10 ⁻⁶	5.903x10 ⁻⁴	5.70	776
V3	7.12x10 ⁻⁶	4.267x10 ⁻⁴	7.12	1510
V4	6.61x10 ⁻⁶	4.267x10 ⁻⁴	7.67	1890

CHAPTER VI

6. MOTIONAL ANALYSIS

6.1 MOTIONAL NARROWING ANALYSIS :

The spectra in figures 6.1 & 6.2 are the motional narrowing spectra for V_1 & V_2 in toluene, respectively. The EPR spectra for V_1 were recorded at 9.5394GHz over a temperature range (294-234K). The EPR spectra for V_2 were recorded at 9.5440GHz over a temperature range (293-248K). Each EPR spectrum consists of eight lines which is consistent with a free radical of a single unpaired electron spin ($S=1/2$) which interacts with the vanadyl nucleus, which has spin $I=7/2$. Each EPR line is corresponding to a nuclear spin magnetic number M .

$$M=I, I-, \dots, -I.$$

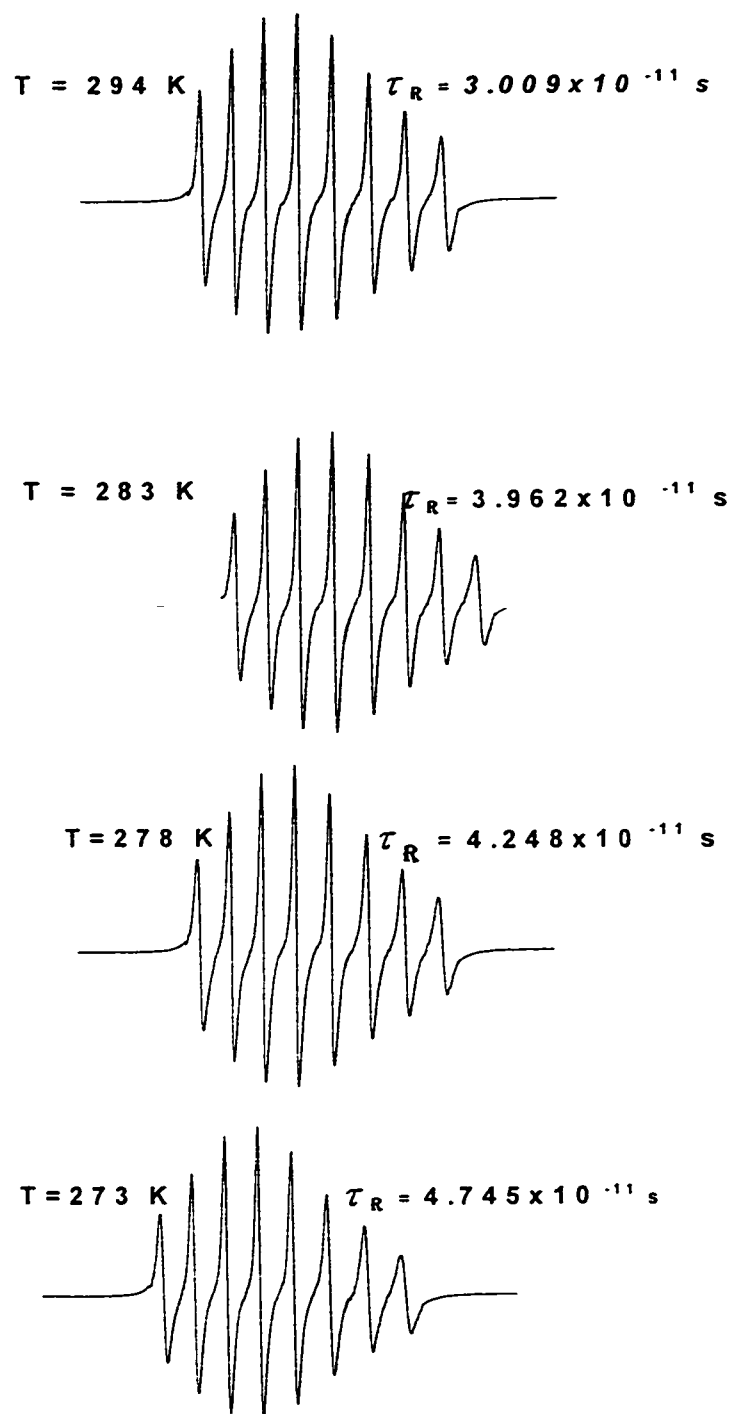


Figure 6.1: Variable temperature spectra of V1 in toluene at 9GHz.

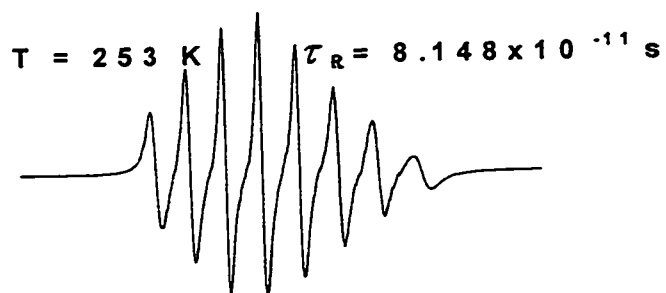
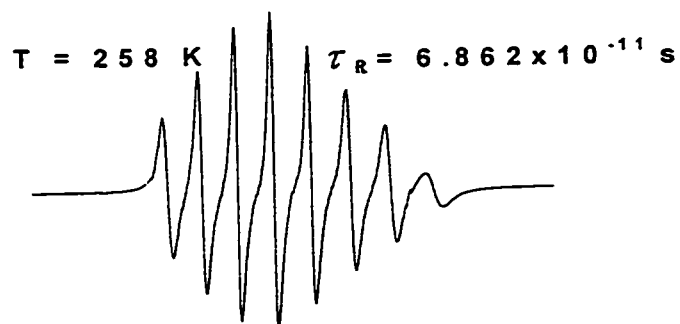
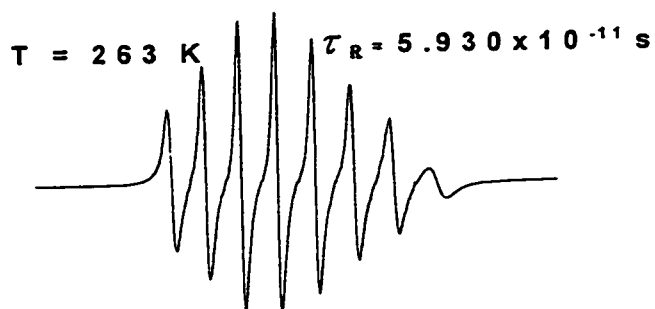
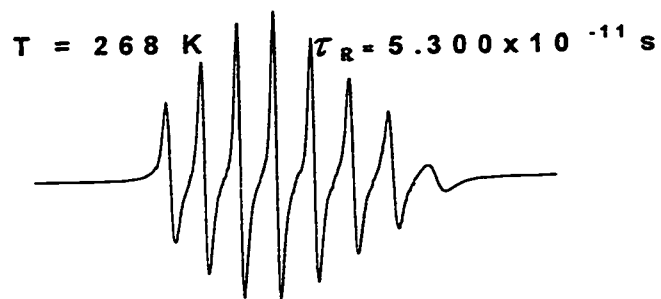


Figure 6.1: Variable temperature spectra of V1 in toluene at 9GHz.

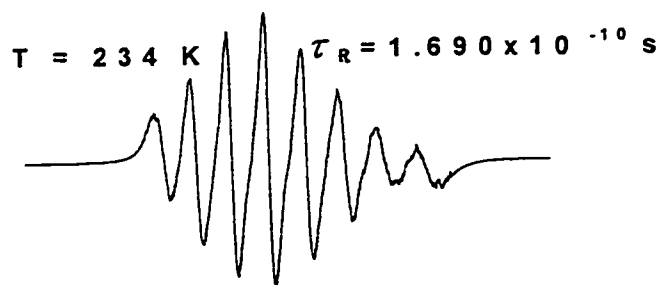
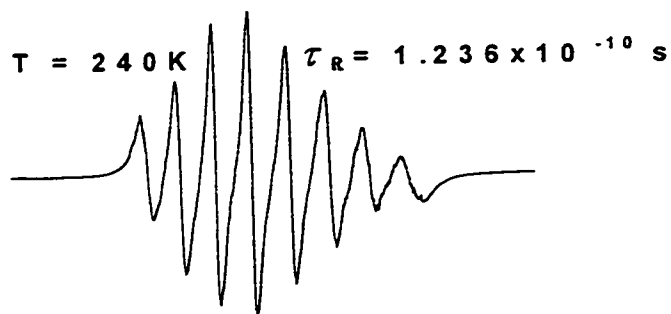
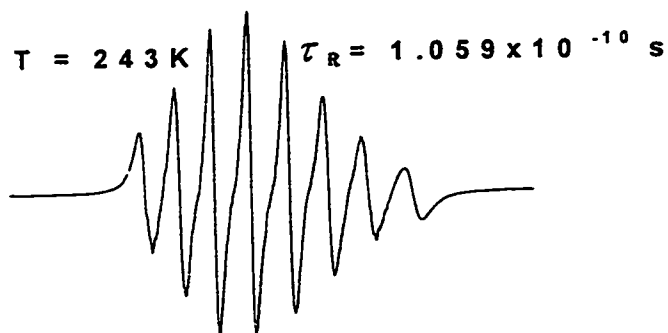
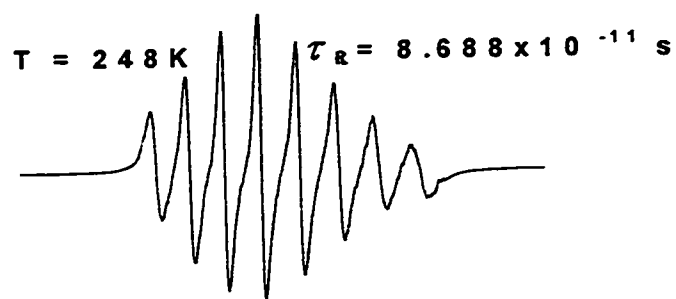


Figure 6.1: Variable temperature spectra of V1 in toluene at 9GHz.

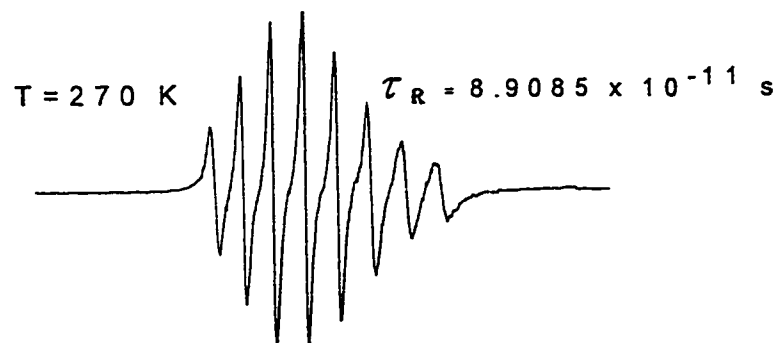
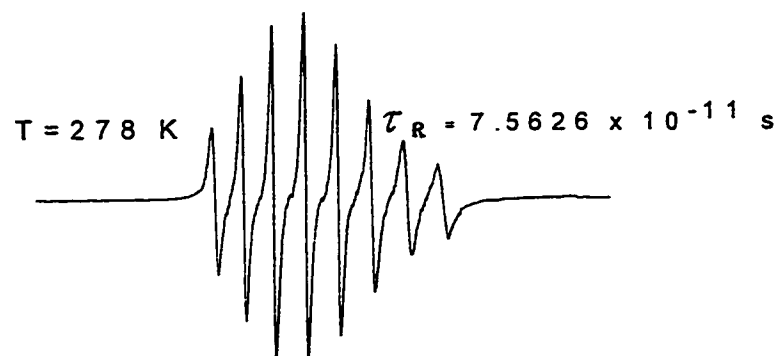
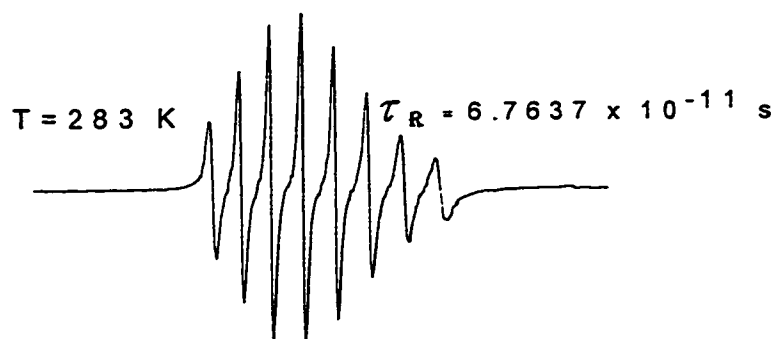
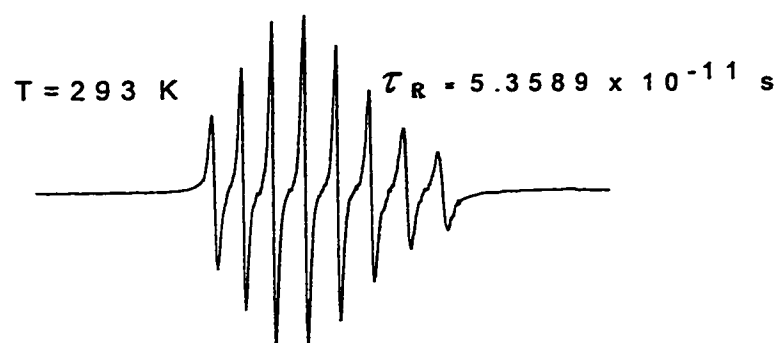


Figure 6.2: Variable temperature spectra of V2 in toluene at 9GHz

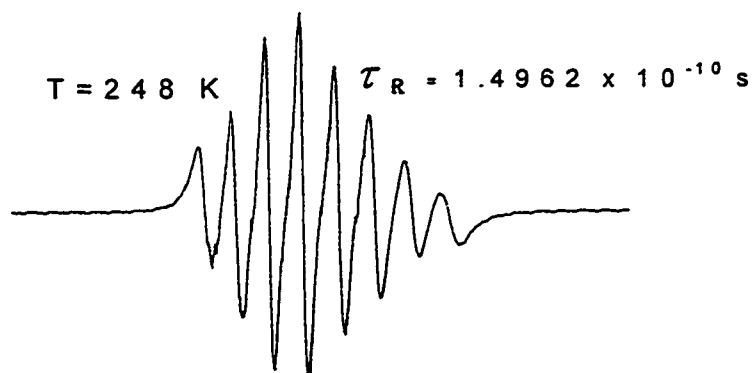
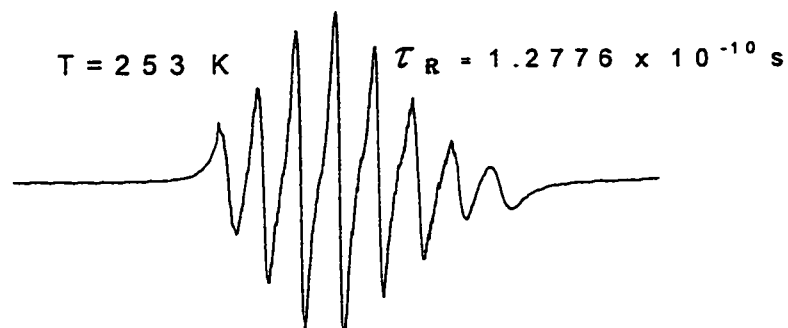
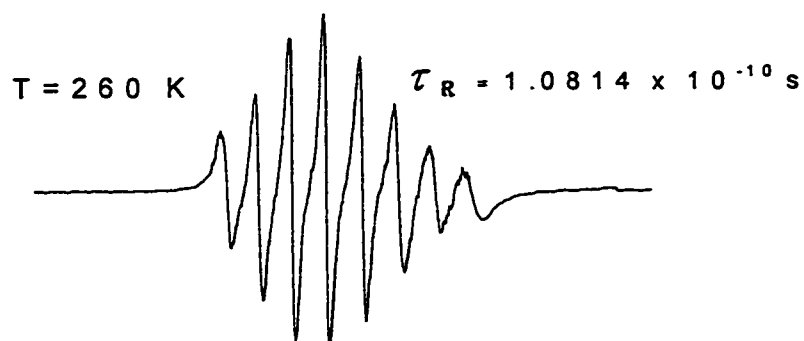
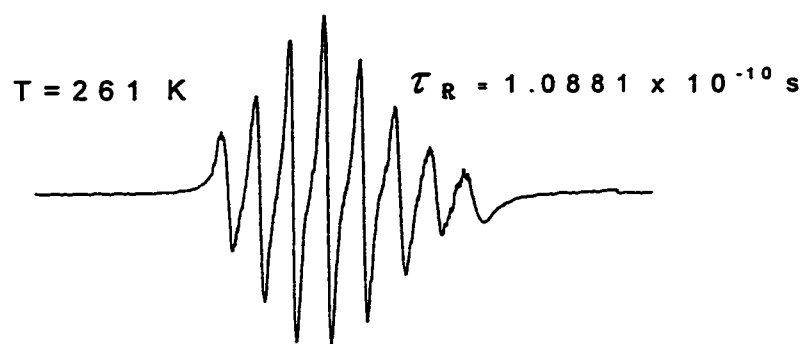


Figure 6.2 : Variable temperature spectra of V2 in toluene at 9GHz

Since we did not wish to measure intermolecular spin-spin exchange effects the concentration of the sample was lowered until no further narrowing was observed as a function of concentration. Concentration ($5 \times 10^{-4} \text{M}$) well below the critical concentration was used. The separation of the hyperfine components is not equal but this effect can easily be accounted for by a second order treatment of the hyperfine splitting. This second -order effect enters because the hyperfine splitting is very large. The individual lines are not completely symmetric. The asymmetry probably arises from incomplete motional narrowing, and the asymmetry is increasing as the temperature is lowered while at high temperatures the asymmetry tends to vanish. The line widths were determined by measuring the line width of the narrowest line ($M = -1/2$) and the peak heights of the eight lines assuming that the eight lines are well separated and lorentzian. As a matter of fact to have more reliable data the narrowest lines have been recorded separately. The peak-to-peak height varies as the inverse line width squared. The line widths in the motional narrowed region can be described by an expansion in M , the component of the nuclear spin along the direction of the applied magnetic field given by equation (2.19)

$$\Delta H(M) = A + BM + CM^2 + DM^3$$

The line widths were fitted to the above equation and the line width coefficients A, B, C and D were determined from a least-squares fit. The coefficients B and C, and the ratio C/B for different temperatures are shown in table 6.1 and 6.2 for V_1 and V_2 respectively.

When nonsecular terms are unimportant, the ratio of the line width coefficients C/B can yield information on the anisotropy (N) and the axis of rotation. In order to determine N, the axis of rotation, and τ_R values, the theoretical calculations of B and C coefficients given by equations (2.22 to 2.27) are used.

The magnetic parameters g's and A's for V_1 and V_2 necessary for the simulation of B and C are taken from table 4.2. Based on the experimental B and C values, the reorientational correlation times, τ_R , for the spectra at different temperature, and the corresponding theoretical B and C values were calculated using ABC programs written for equations (2.22 to 2.27). The parameters used in these simulation (after experimenting with $Z' = x, y$ or z , $N = 1$ to 7) are $Z' = y$, $N = 2.5$ and 1.7 for V_1 and V_2 respectively. The correlation times, τ_R values, were then calculated by the ABC program by matching experimental B and C with those calculated by different correlation times. The obtained τ_R value for each temperature is presented

Table 6.1: Experimental Values of Temperature, B and C for V1.

T (K)	B	C	C/B
294	0.690	0.362	0.525
283	0.836	0.478	0.572
278	0.893	0.512	0.573
273	0.997	0.572	0.574
268	1.11	0.639	0.577
263	1.22	0.715	0.586
258	1.38	0.828	0.600
253	1.60	0.984	0.615
248	1.68	1.05	0.625
243	2.05	1.28	0.624
240	2.36	1.50	.613
234	3.21	2.15	0.636

Table 6.2: Experimental Values of Temperature, B and C for V2.

T (K)	B	C	C/B
293	1.17	0.661	0.565
283	1.44	0.857	0.595
273	1.60	0.944	0.590
268	1.89	1.10	0.582
263	2.25	1.37	0.609
258	2.24	1.35	0.603
253	2.63	1.60	0.608
248	3.07	1.86	0.606

with the corresponding experimental spectrum in figures 6.1 and 6.2 for v1 and v2, respectively. Curves of experimental and theoretical B and C values are shown in figure 6.3 for v1 and those for v2 are in figure 6.4.

Thus it is determined from simulation that V1 in toluene experiences anisotropic rotational diffusion at axis $Z' = y$ with $N = 2.5 \pm 0.4$ while for V2 $Z' = y$ with $N = 1.7 \pm 0.4$.

The variable temperature spectra for V3 and V4 in methylene chloride are shown in figures 6.5 and 6.6 respectively. The EPR spectra for V3 were recorded at 9.5350GHz over the temperature range (294-235K). The EPR spectra for V4 were recorded at 9.5370GHz over the temperature range (340-250K). These compounds shown eight lines spectra as expected. The line widths of these compounds were determined by measuring the line width of the narrowest line ($M = -1/2$), from a separate scan, and the peak-to-peak heights of the eight lines. The values of B, C were obtained by fitting these line widths to equation (2.19). The values of B, C and C/B ratio obtained for V3 and V4 in methylene chloride are presented in tables 6.3 and 6.4 for V3 and V4 in methylene chloride, respectively.

The magnetic parameters needed for the line shape analysis is taken from table 4.2. The theoretical B and C values, the anisotropy of rotation,

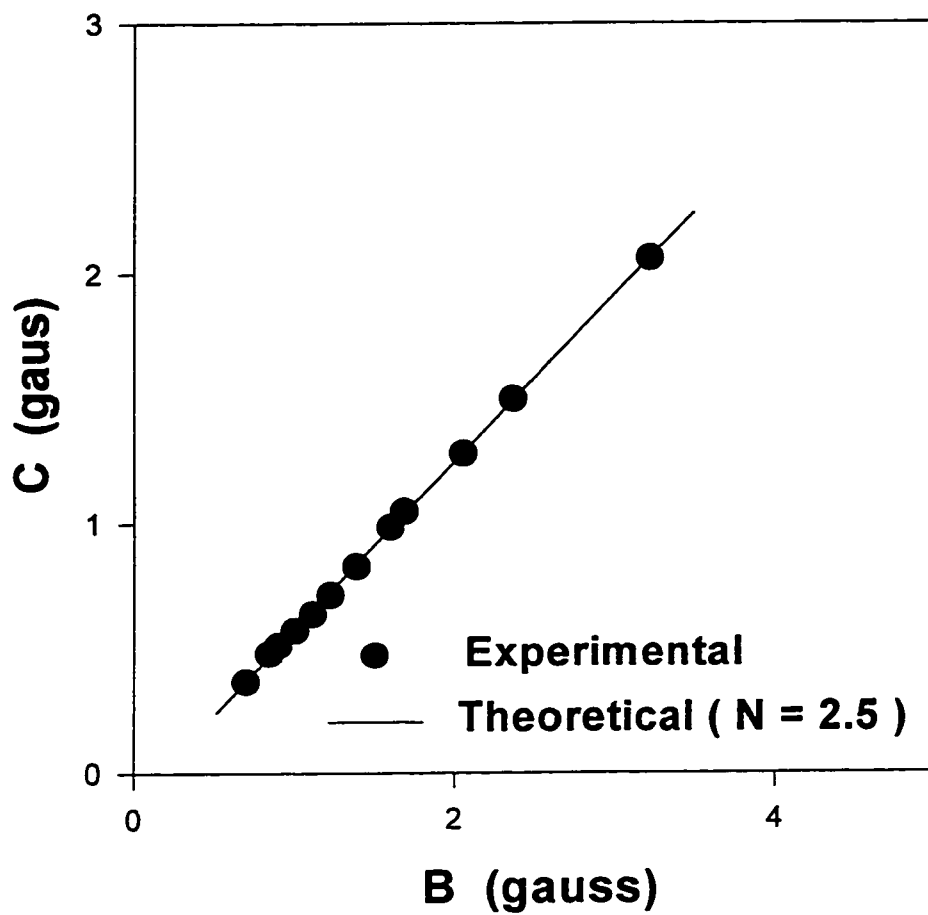


Figure 6.3: B vs C for ν_1 in toluene at different temperature.

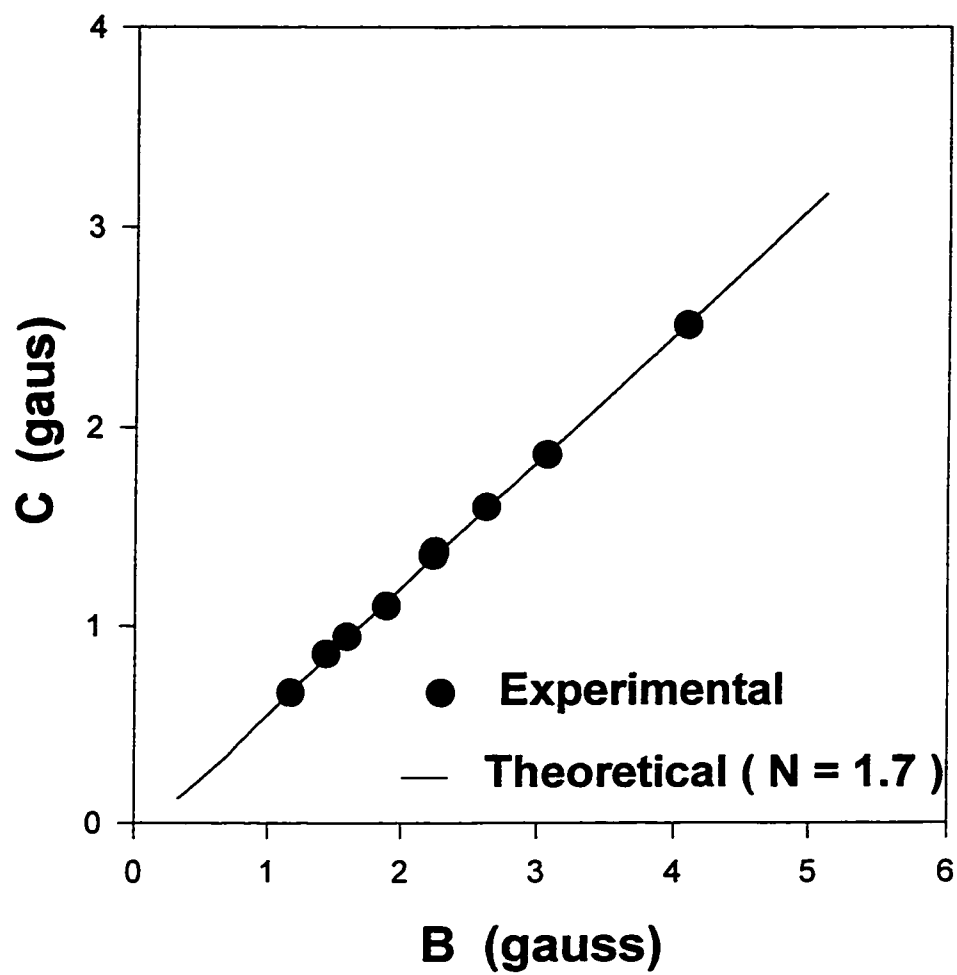


Figure 6.4: B vs C for V2 in toluene at different temperature.

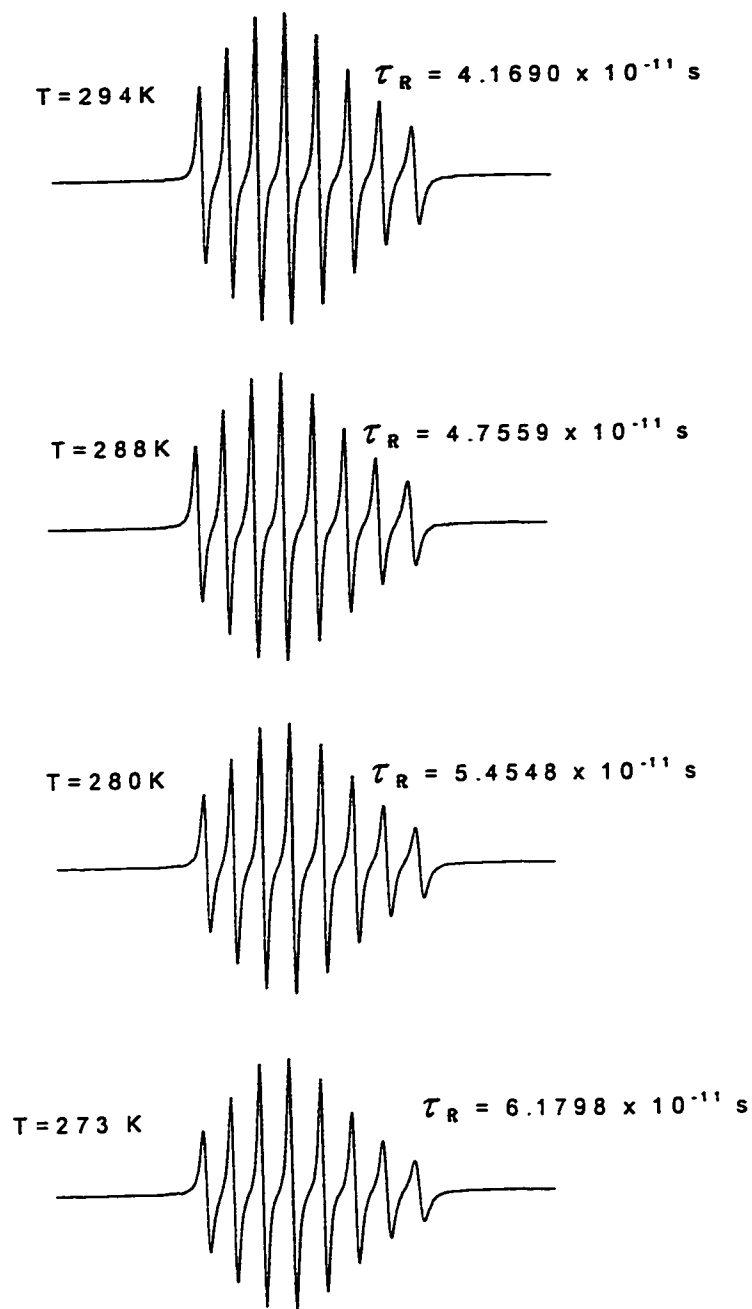


Figure 6.5: Variable temperature spectra of V3 in methylene chloride at 9GHz.

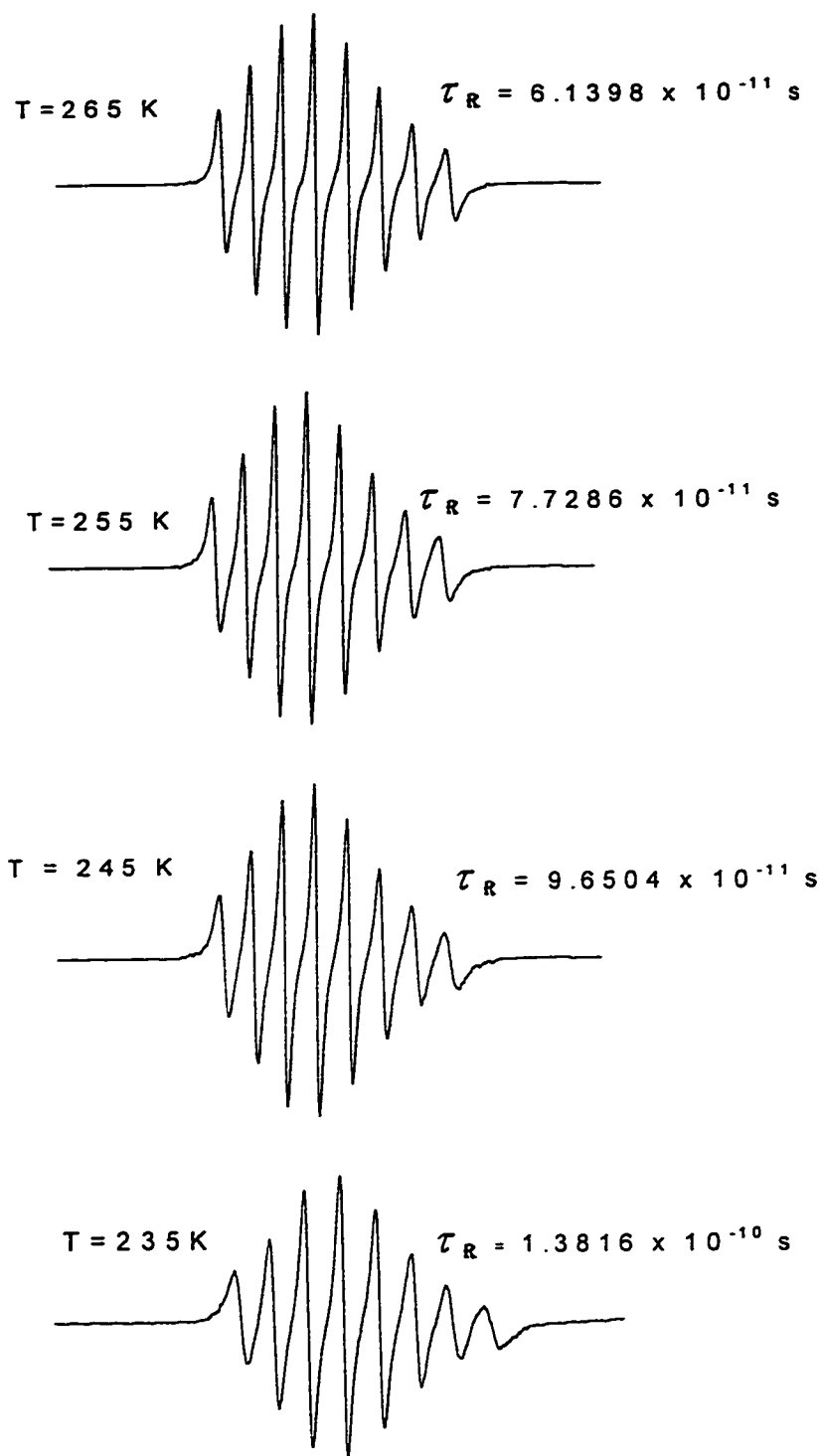


Figure 6.5: Variable temperature spectra of V3 in methylene chloride at 9GHz

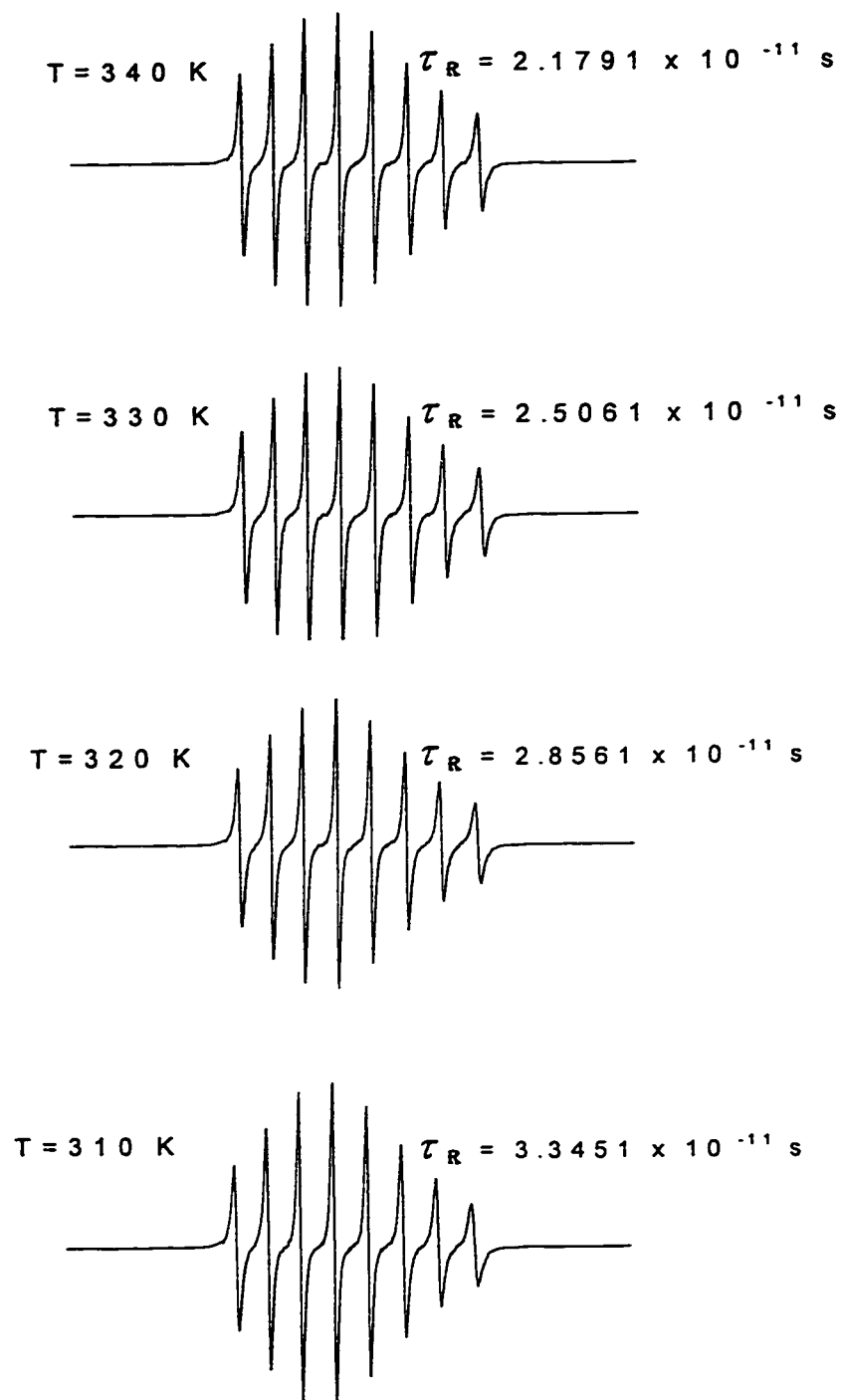


Figure 6.6 : Variable temperature spectra of V4 in methylene chloride at 9GHz.

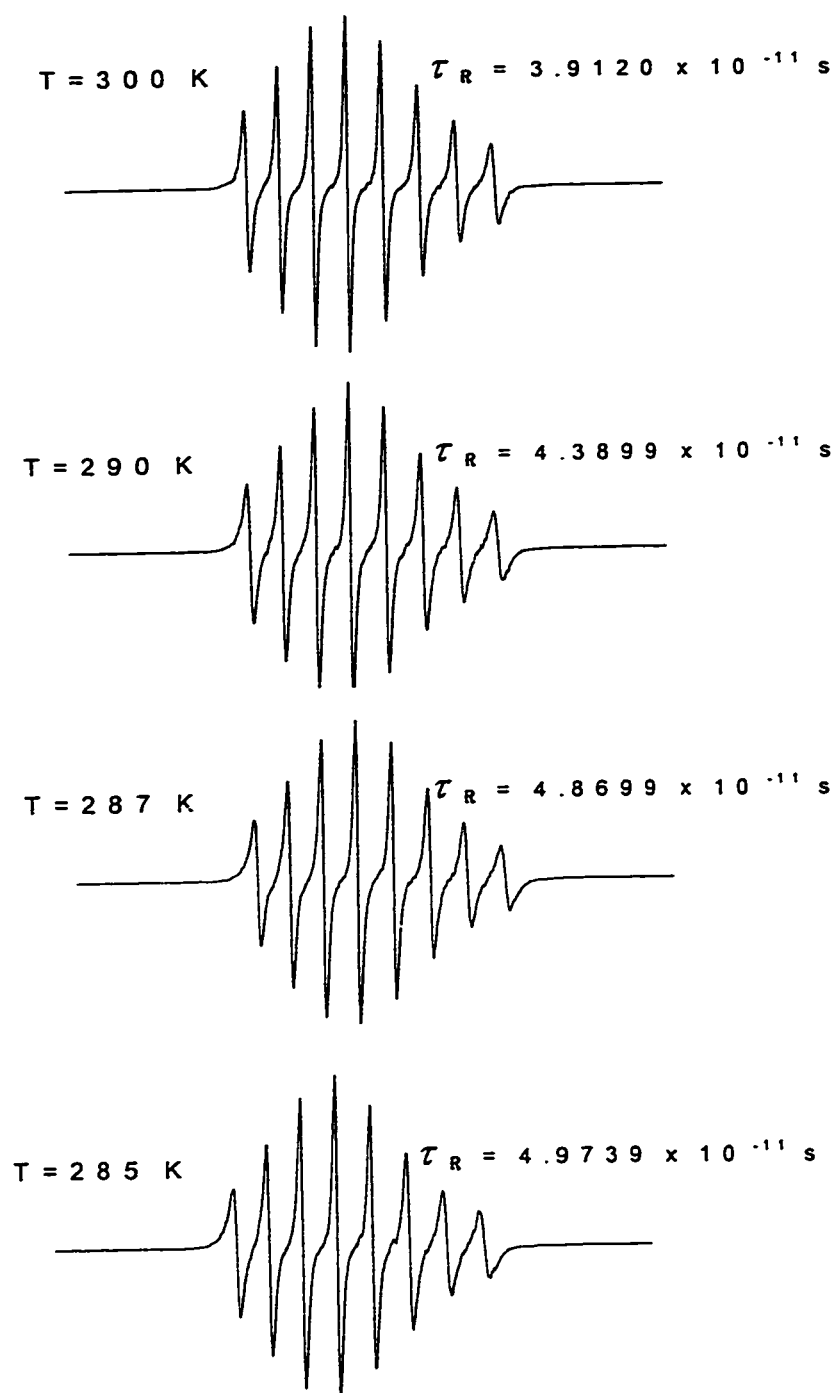


Figure 6.6: Variable temperature spectra of V4 in methylene chloride at 9GHz.

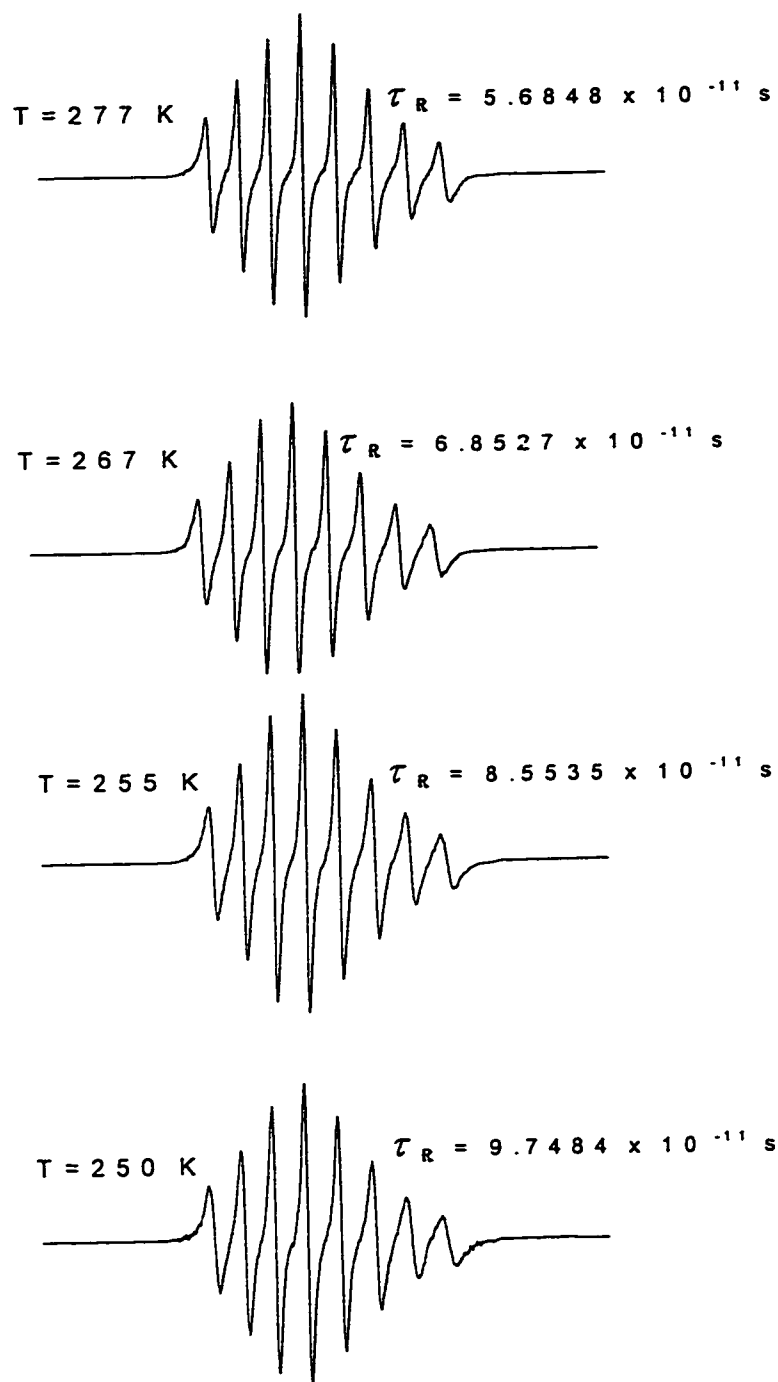


Figure 6.6: Variable temperature spectra of V4 in methylene chloride at 9GHz.

Table 6.3: Experimental Values of Temperature, B and C for V3.

T (K)	B	C	C/B
294	0.961	0.574	0.597
288	1.05	0.655	0.624
280	1.18	0.751	0.636
273	1.29	0.868	0.673
265	1.33	0.846	0.636
255	1.62	1.07	0.660
245	1.99	1.33	0.668
235	2.77	1.94	0.699

Table 6.4: Experimental Values of Temperature, B and C for V4.

T (K)	B	C	C/B
340	0.562	0.300	0.534
330	0.612	0.344	0.562
322	0.681	0.388	0.570
320	0.692	0.392	0.566
310	0.760	0.460	0.605
300	0.890	0.540	0.607
290	0.990	0.651	0.658
287	1.08	0.698	0.646
285	1.08	0.710	0.657
277	1.21	0.814	0.673
267	1.48	1.01	0.682
255	1.75	1.19	0.680

the axis of rotation and τ_R values were obtained by simulation following the same procedures of v1 and v2. The experimental and simulated B and C values for v3 and v4 are plotted in figures 6.7 and 6.8, respectively. The determined axis of rotation is $Z' = y$ for both, while the anisotropy of rotation, N, is 1.5 ± 0.4 for V3 and 1.7 ± 0.4 for V4. The reorientational correlation times, τ_R , obtained are presented with the experimental spectra for different temperatures in figures 6.5 and 6.6, respectively. The axis of rotation and N values obtained for these systems are summarized in table 6.5.

In the absence of external influence, an ellipsoid would always prefer to rotate along its longest axis, since the energy barrier for rotation along the longest axis is less than those for the other two axes. This is actually what we observed. The four studied systems have a preferential rotation along the longest axis, which is the y-axis. V1 rotates along the y-axis 2.5 times faster than along the other two axes. V2 rotates along the y-axis 1.7 times faster than along the other two axes. V3 rotates along the y-axis 1.5 times faster than along the other two axes. V4 rotates along the y-axis 1.7 times faster than along the other two axes. These values can be understood on bases of the dimensions of these molecules. In fact the anisotropy of rotation can be calculated from the dimensions of the molecule using Stokes-Einstein model ^{21,34}. This calculation will be performed in the fourth section of this chapter.

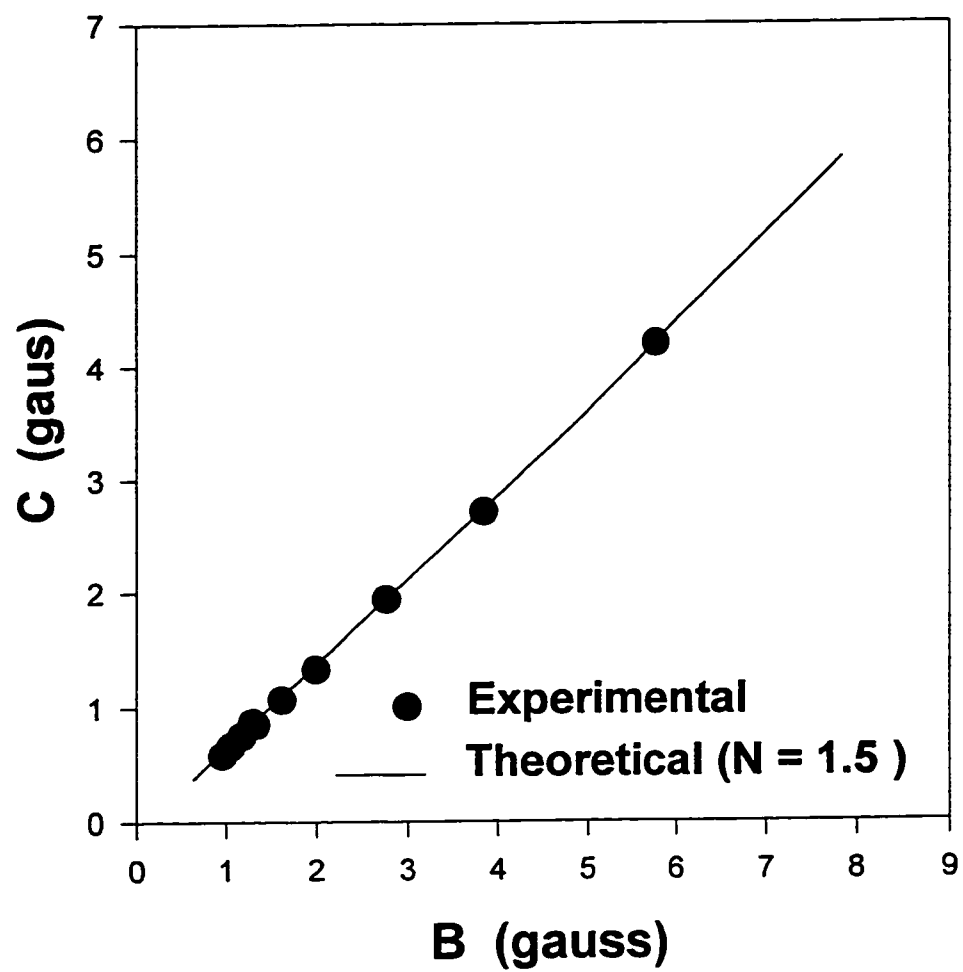


Figure 6.7: B vs C for ν_3 in CH_2Cl_2 at different temperature.

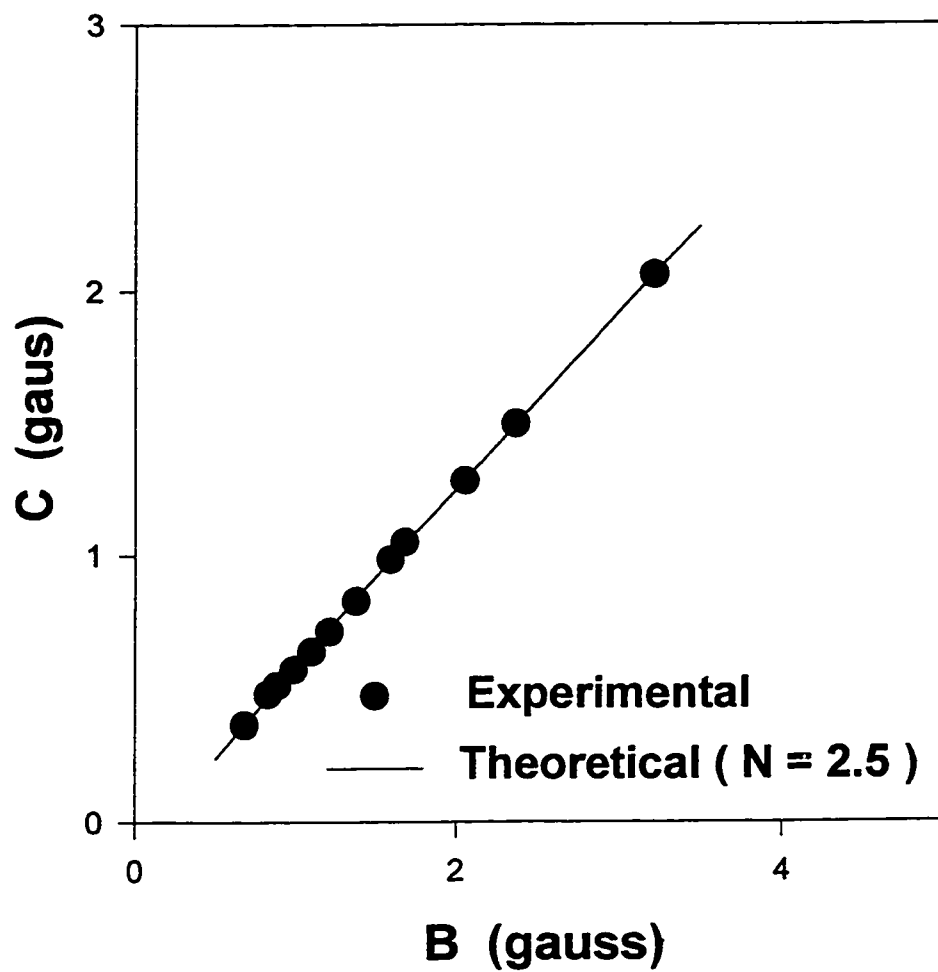


Figure 6.8: B vs C for v4 in CH_2Cl_2 at different temperature.

Table 6.5 The Axis and the Anisotropy of Rotation of the Studied Systems

COMPOUND	Solvent	Z'	N \pm 0.4
V1	toluene	y-axis	2.5
V2	toluene	y-axis	1.7
V3	CH₂CL₂	y-axis	1.7
V4	CH₂CL₂	y-axis	1.5

Alternatively, when nonsecular terms are unimportant the anisotropy of rotation can be calculated from the magnetic parameters, and the line widths coefficients B and C by the Allowed Values Equation. This calculations will be carried out in the third section of this chapter ⁵⁷.

6.2 SLOW TUMBLING

The experimental spectra at the slow tumbling regions for the studied systems together with the simulated theoretical spectra are shown in figures 6.9, 6.10, 6.11 and 6.12. Inspection of these spectra revealed that at the slow tumbling region there are three types of spectra:

- (1) The incipient slow tumbling type which is similar to the motional narrowed region, with the line width for the $m=7/2$ hyperfine line begins to deviate significantly from the motional narrowed region analysis result.
- (2) The typical slow tumbling type.
- (3) The rigid limit type.

The theoretical simulation of these spectra were performed using stochastic Liouville theory of slow motional effects in EPR spectra for $S=1/2$ and $I = 7/2$ for vanadyl systems. The magnetic parameters used in the simulation were those listed in table 4.2.

The slow tumbling region refers to the region where the rotational motion is slow compared to the anisotropy of the intramolecular magnetic interactions. The resulting EPR line shape is no longer a superposition of

Lorentzian lines. Because vanadyl complexes have a more orientation - dependent spin Hamiltonian than nitroxides, the slow tumbling region for vanadyl probes occurs at shorter rotational correlation times, τ_R . For typical vanadyl complexes, slow tumbling occurs in the region $\tau = 8 \times 10^{-11}$ to 10^{-7} s/rad. Longer τ yields essentially the rigid limit EPR spectrum. The axis and the anisotropy of rotation needed for slow tumbling simulation are taken from the motional narrowed region analysis, table 6.5. For the slow tumbling simulation, as the τ_R is increased the n & L values must be increased. Typical n and L values used are listed in Table 6.6.

Anisotropy of rotation N is defined as the ratio of R_{\parallel}/R_{\perp} where R_{\parallel} is the rotational diffusion constant along Z' - axis and R_{\perp} is the rotational diffusion constant perpendicular to the Z' -axis. In fact R_{\parallel} and R_{\perp} is what we feed in the program, keeping the ratio R_{\parallel}/R_{\perp} constantly equal to the N value, which in turns determine the τ_R value depending on the model.

There can be three models of rotation: Brownian, free diffusion or moderate jump and strong jump. The following equations are used to find R_{\perp} for all the three models.

$$\text{Brownian Model, } R_{\perp} = \frac{1}{\sqrt{N} \times 6\tau_R},$$

Table 6.6 Computational Data

spectrum type	typical τ_R, s	typical L, n
motionally narrowed	2.0×10^{-11}	2, 2
incipient slow motional	2.0×10^{-10}	8, 2
slow motional	5.0×10^{-10}	12, 2
slow motional	2.0×10^{-9}	12, 3

$$\text{Moderate Jump, } R_{\perp} = \frac{\sqrt{7}}{\sqrt{N} \times \tau_R}, \text{ and}$$

$$\text{Strong Jump, } R_{\perp} = \frac{1}{\sqrt{N} \times \tau_R}$$

The Brownian model is used for all these simulations. To find rotational correlation time (τ_R), the axis of rotation and the anisotropy of rotation were kept constant and the τ_R values were changed for different spectra until the simulated spectrum matches the experimental spectrum.

The experimental spectra for VI in toluene together with the simulated spectra are shown in figure 6.9. Spectrum obtained at $T = 228$ K is representative of the so-called “incipient slow-tumbling” region. It is characterized by asymmetric absorption line shapes that are shifted relative to their motional narrowed positions. Such spectra occur when $H_1(\Omega)\tau_R \approx 1$. Here $\tau_R = 1.81 \times 10^{-10}$ s and $\tau_R T_2^{-1} = 1.7$. The spectra obtained in the temperature range 228-213K are all falling in incipient slow-tumbling region. All the spectra obtained in this range (1.8×10^{-10} s to 4.1×10^{-10} s) are showing very good agreement between simulation and experimental

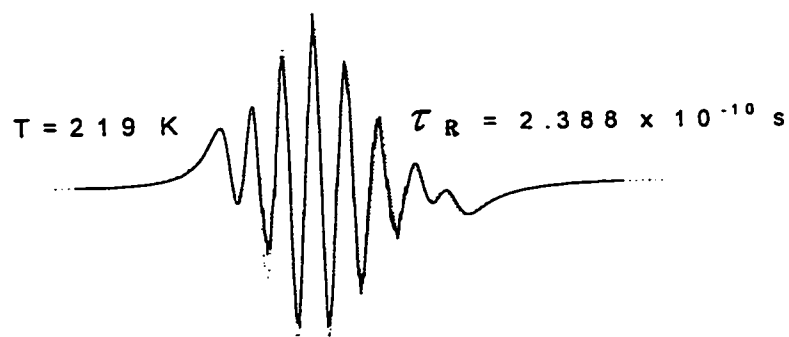
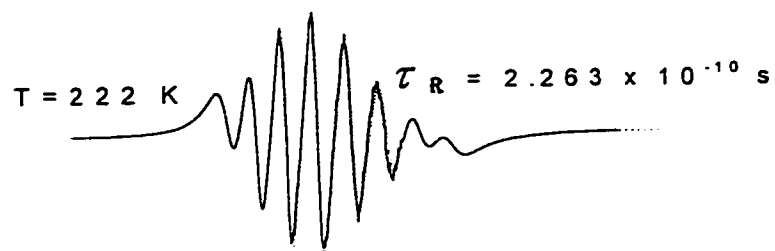
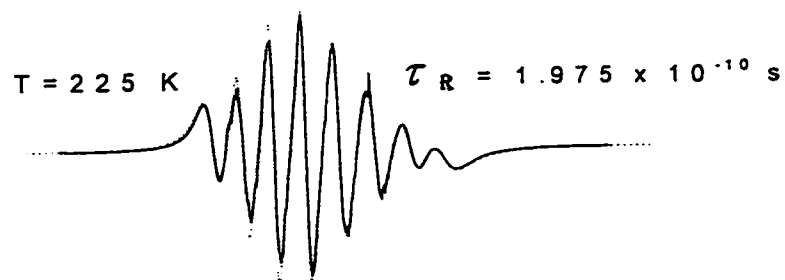
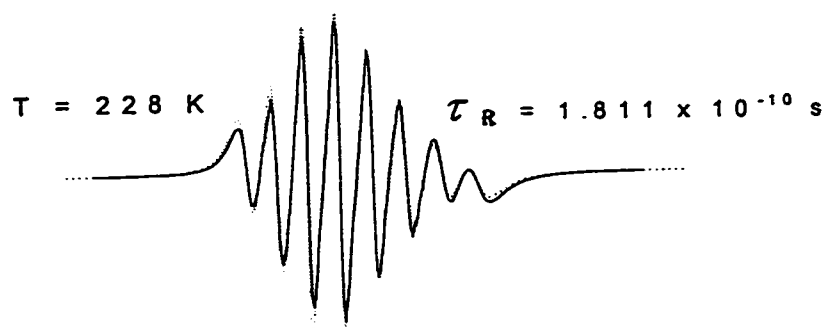


Figure 6.9: Variable temperature spectra of V1 in toluene at 9GHz.

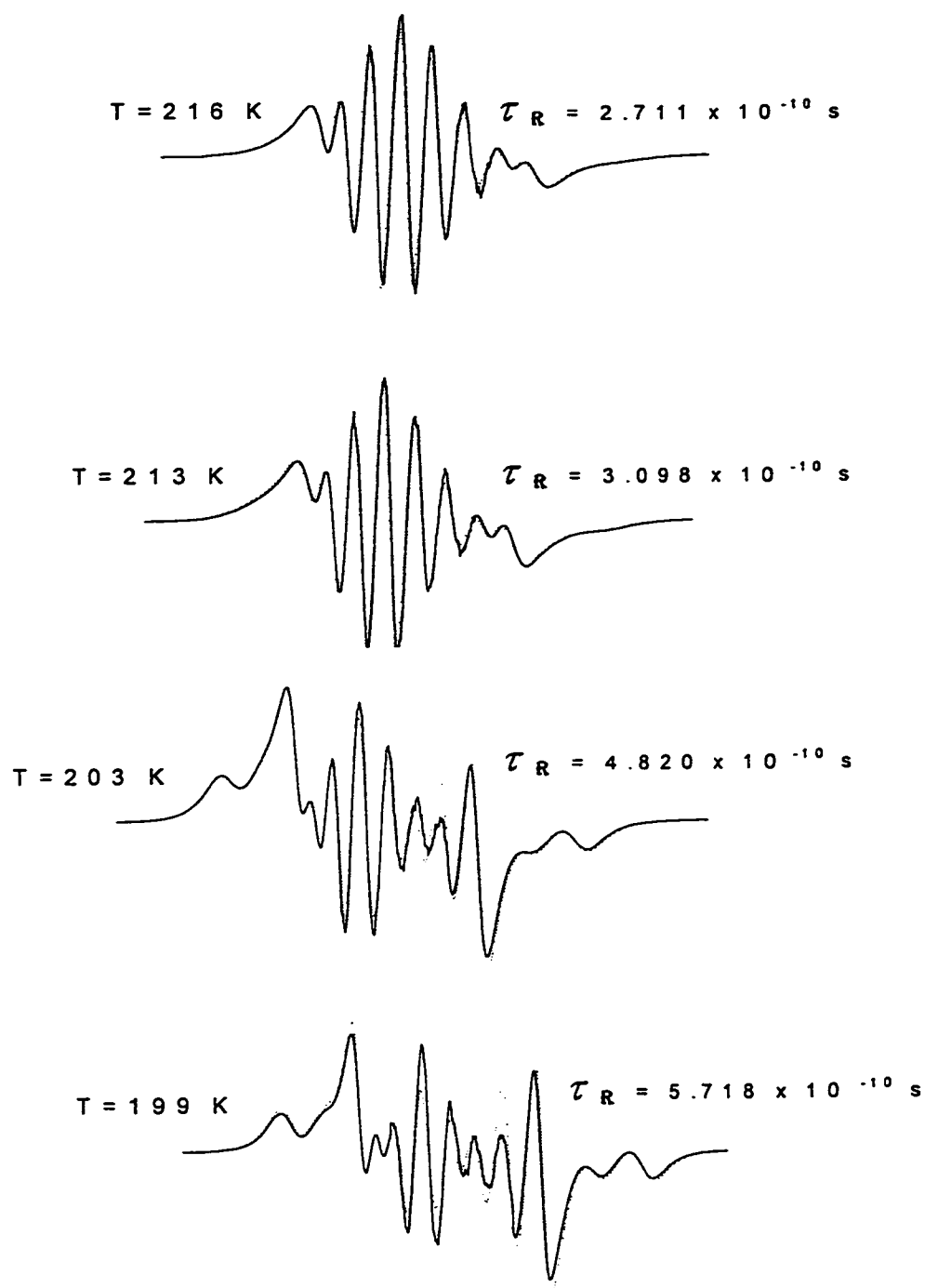


Figure 6.9: Variable temperature spectra of V1 in toluene at 9GHz.

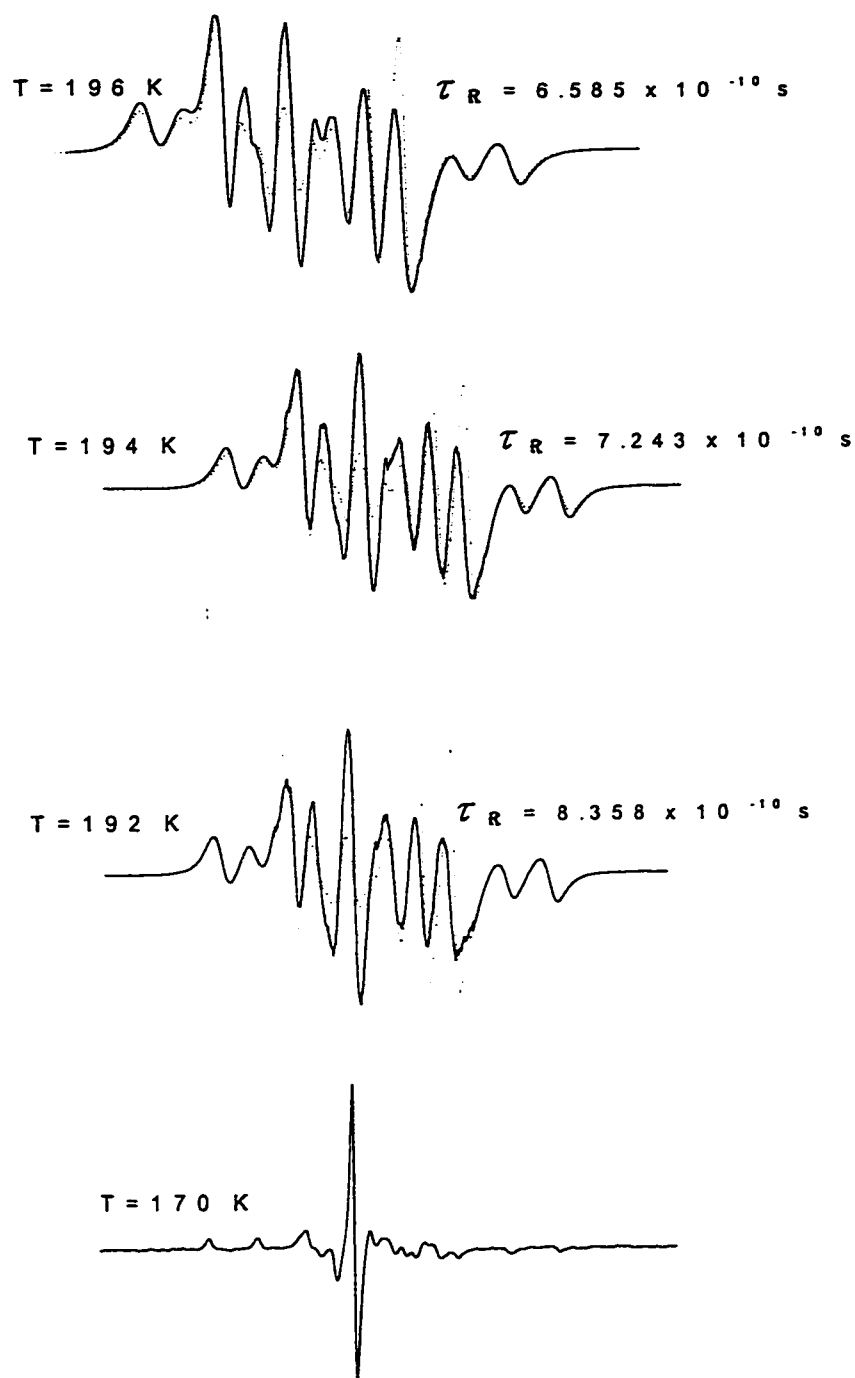


Figure 6.9: Variable temperature spectra of V1 in toluene at 9GHz.

spectra that are shown in figure 6.9. The obtained τ_R values are presented in the spectra. All these spectra in this region are simulated by $T_2^{-1} = 1.7$ G. For this range, the use of axially symmetric magnetic parameters is a good approximation.

In the temperature range of 203K-192K, the slow-tumbling spectra were obtained as the rotational correlation time becomes longer (i.e. $H_1(\Omega)\tau_R > 1$) at lower temperatures. This corresponds to τ_R in the range 4.8×10^{-10} s to 8.84×10^{-10} s with $T_2^{-1} = 2.0$ G. Molecular tumbling at this range is clearly characterized by anisotropic magnetic interactions. Although perfect agreement between experiment and simulation is not obtained, the overall spectral fit is still very good and clearly shows that the problems in fitting the central portion of slow tumbling observed earlier by Bruno et al. have been resolved. The use of axial magnetic parameters is a limiting factor in this work. Specially when the temperature is going beyond the freezing point of the solvent.

The great similarity between spectrum obtained at $T=170$ K and that of the rigid limit, Fig. 4.2a, identifies it to be of the so called “near rigid-limit” type. The experimental spectrum shows the distinctive low field “absorption” and high field “emission” line shapes that characterize frozen

spectral line shapes. Likewise, the highly asymmetric and overlapped central region is typical of spectrum in the rigid limit.

The experimental and the simulated spectra for V2 in toluene are shown in figure 6.10. The spectrum obtained at $T = 238$ K is representative of The incipient slow tumbling region. Here $\tau_R = 1.98 \times 10^{-10}$ s. The $T_2^{-1} = 1.7$ G for the simulation of all the spectra. The spectra in this region are collected in the temperature range 238K - 218K. All the spectra obtained in this range (1.98×10^{-10} s to 3.81×10^{-10} s) are showing excellent agreement between simulation and experimental spectra. The τ_R values obtained for different temperature spectra are presented in figure 6.10. One can notice that the slow tumbling for V2 occurs at higher temperature ($T = 238$ K) compared to VI ($T = 228$ K). This is due to the larger size of V2 compared to V1.

As the temperature is lowered the rotational motion is slowed down (i.e. larger τ_R values) by increasing viscosity of the solvent leading to the typical slow tumbling region. The spectra obtained in the temperature range 212 K to 190K are of this type, corresponding to correlation time range 4.83×10^{-10} s to 1.45×10^{-9} s. These spectra were simulated with $T_2^{-1} = 1.7$ G.

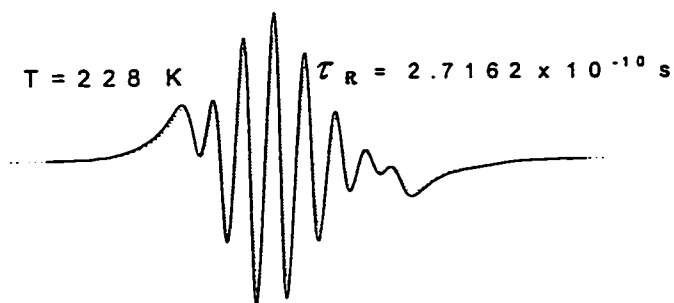
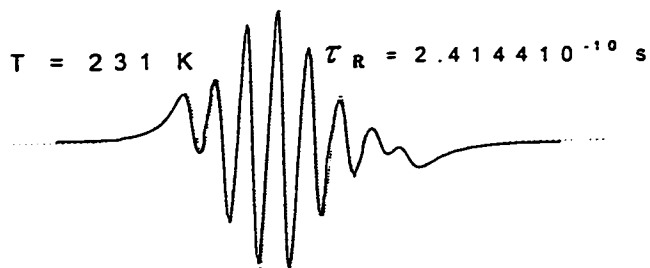
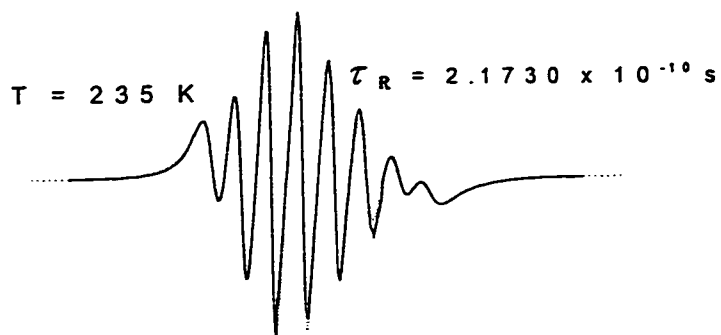
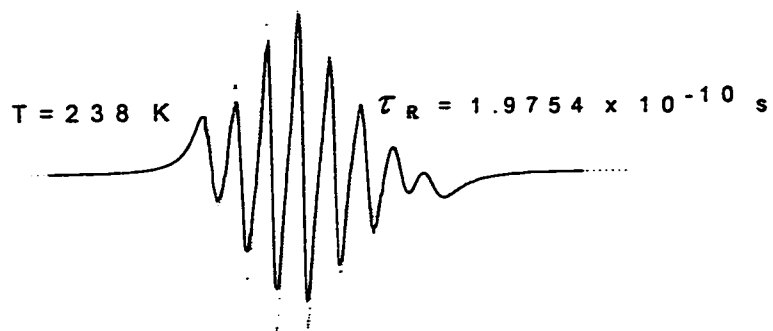


Figure 9.10: Variable temperature spectra of V2 in toluene at 9GHz.

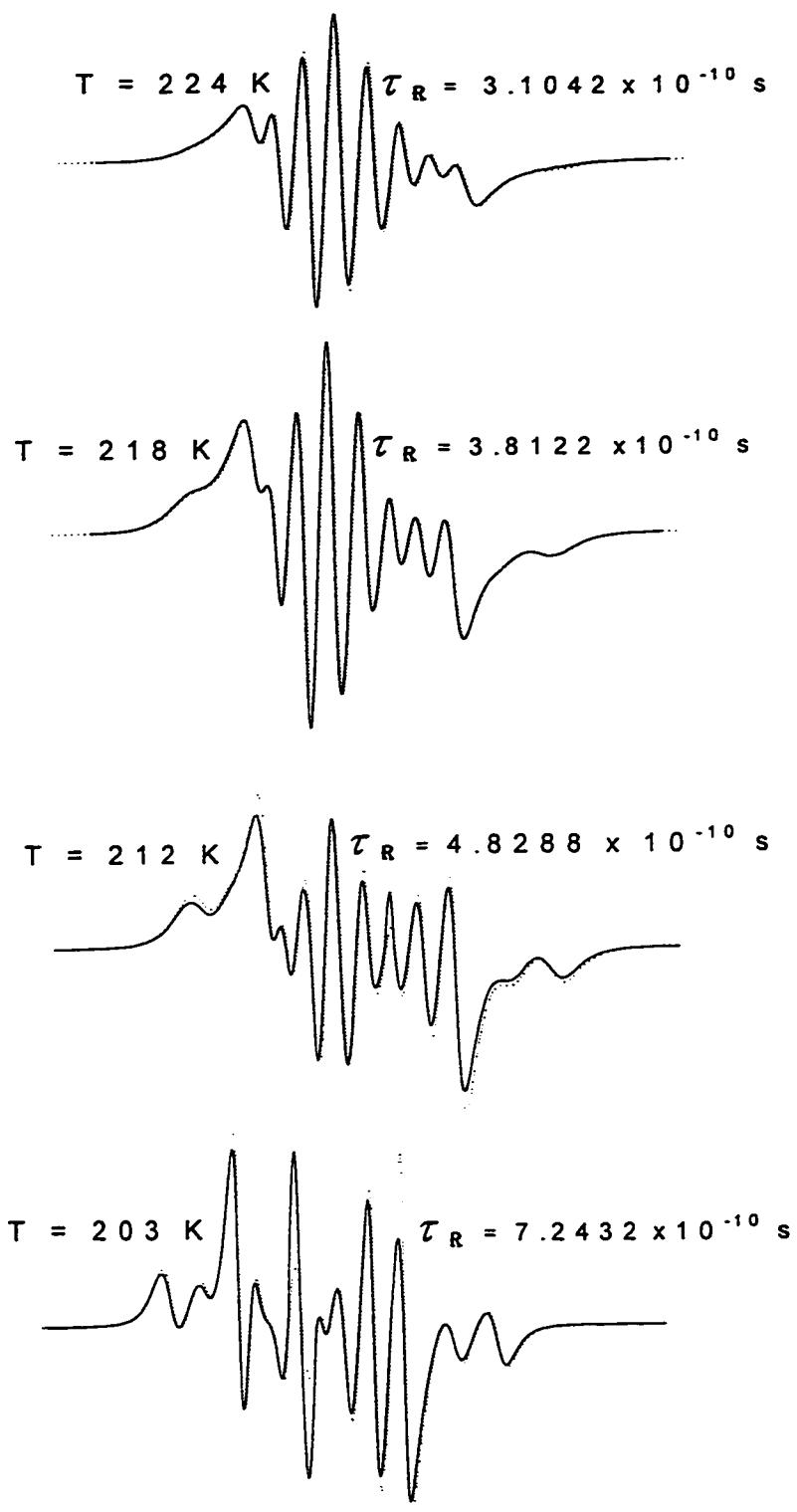


Figure 6.10: Variable temperature spectra of V2 in toluene at 9GHz.

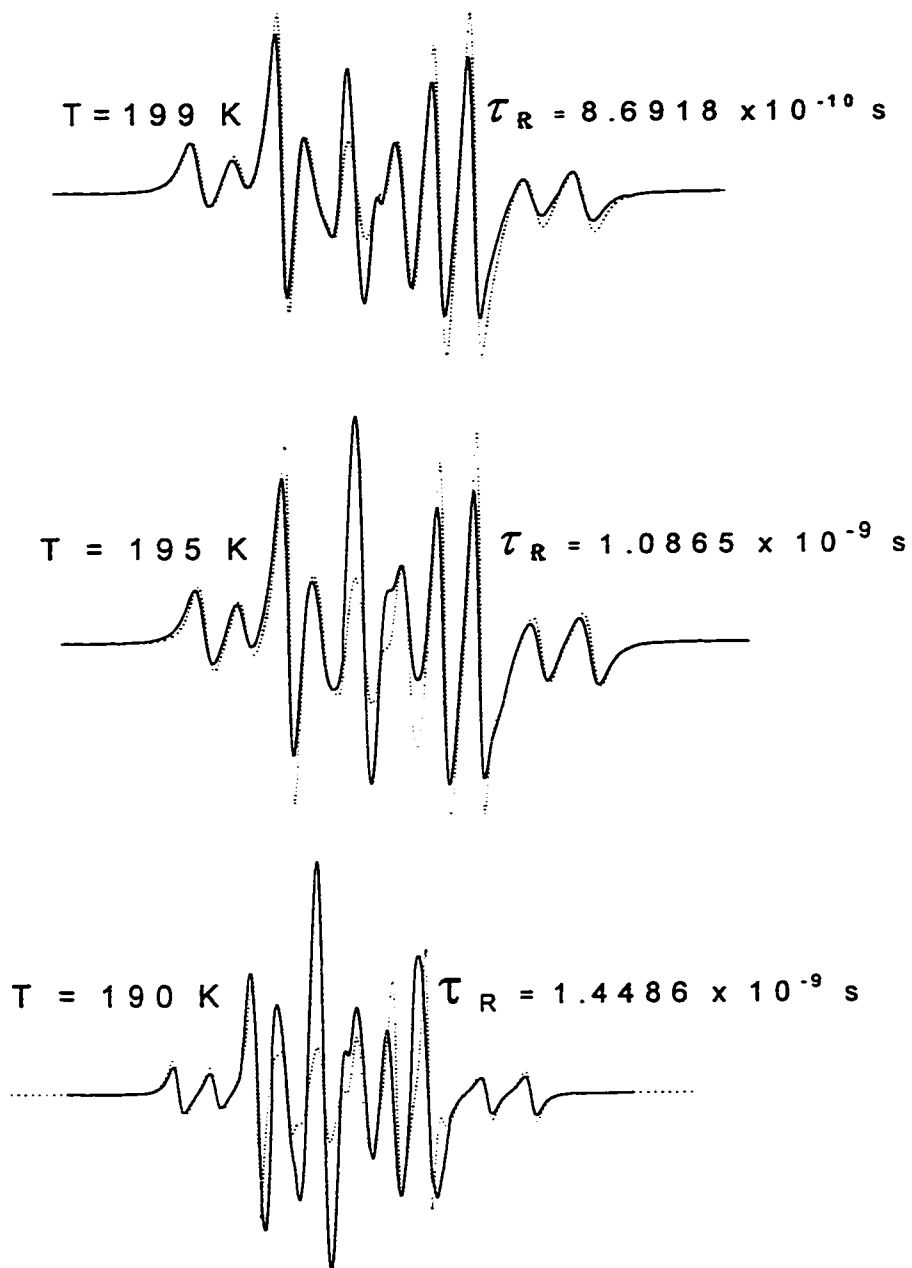


Figure 6.10: Variable temperature spectra of V2 in toluene at 9GHz.

The overall fit is very good, yet some variations in the intensities of the simulation and experimental spectra are existing. The use of fully anisotropic magnetic parameters (g_x, g_y, g_z , A_x, A_y and A_z) rather than the axial sets would further improve this simulation. Comparing the correlation times for V1 & V2, it is noticed that V2 rotates slower than V1 at identical temperatures, e.g. at 203K V2 rotates at $\tau_R = 7.24 \times 10^{-10}$ s while V1 rotates at 4.82×10^{-10} s, $\tau_R(V2)/\tau_R(V1) = 1.50$. Also at 199K V2 rotates at 8.69×10^{-10} s while V1 rotates at 5.72×10^{-10} s, with $\tau_R(V2)/\tau_R(V1) = 1.51$. Since the solvent and the magnetic parameters are the same, this is due to differences in size more specifically, due to the dimensions of these compounds. These differences in dimensions already reflected in the anisotropy, $N(V2)/N(V1) = 2.5/1.5 = 1.5$.

The experimental spectra and the simulated spectra for V3 in methylene chloride are shown in figure 6.11. The experimental spectra are collected over the temperature range 224K to 180K. The simulated spectra were obtained with τ_R values ranging from 1.93×10^{-10} s to 8.29×10^{-10} s and they are presented in figure 6.11. The incipient slow tumbling spectra were obtained in the temperature range 224K to 205K ($\tau_R = 1.93 \times 10^{-10}$ s to 3.09×10^{-10} s). In this region there is a very good agreement between simulated

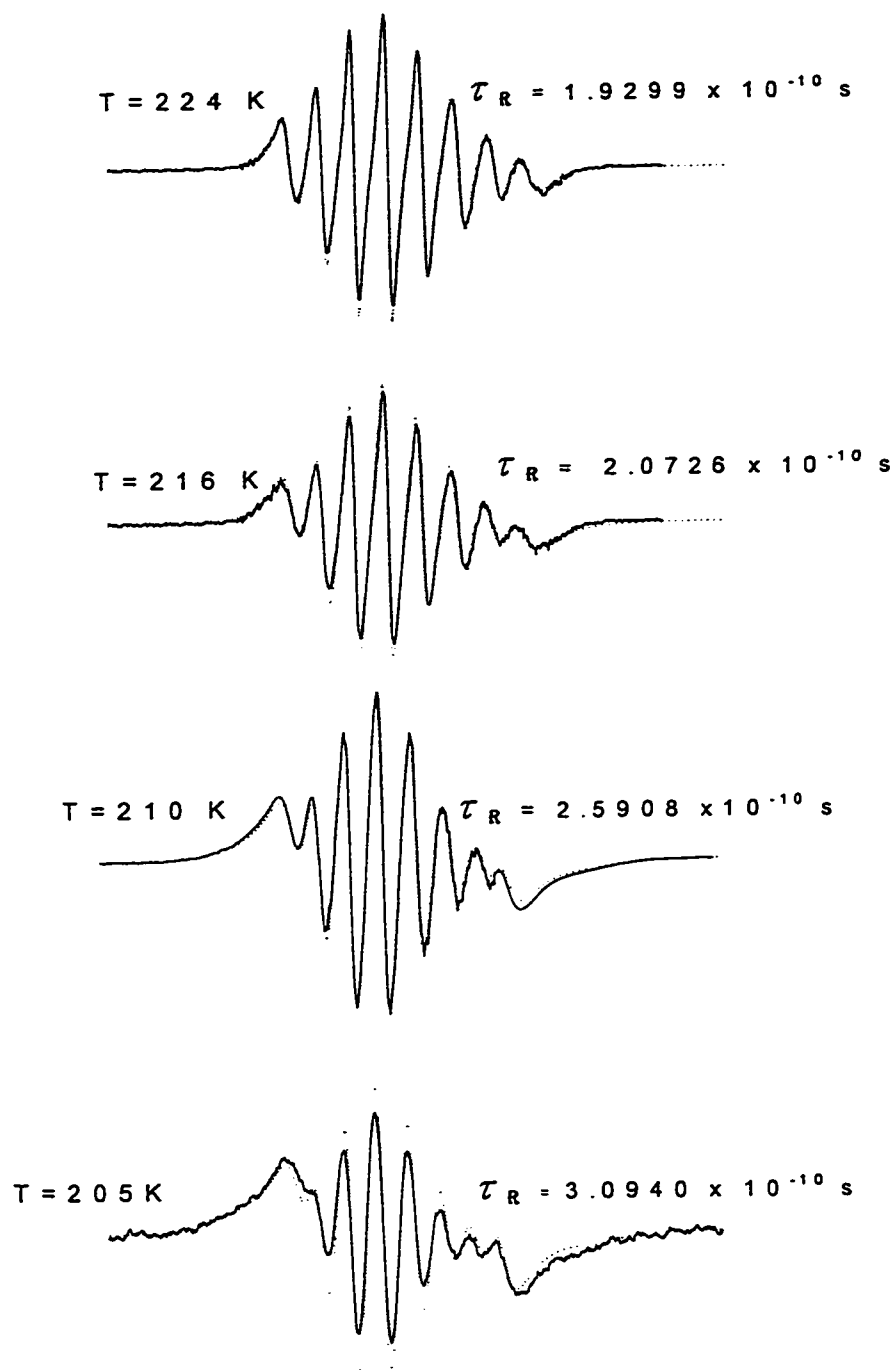


Figure 6.11: Variable temperature spectra of V3 in methylene chloride at 9GHz.

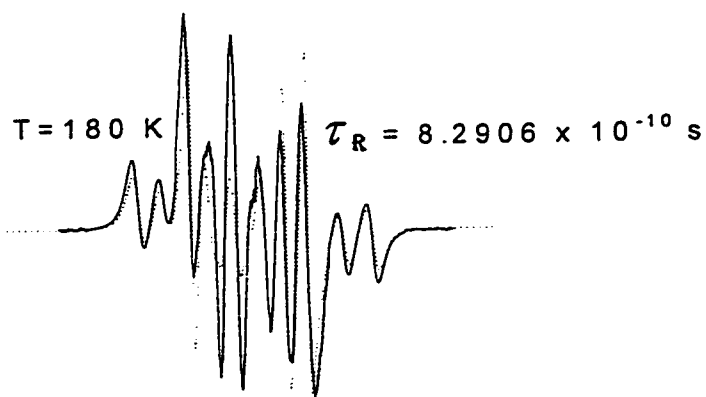
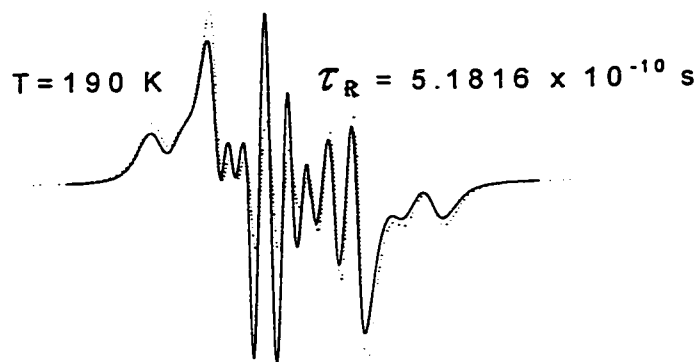
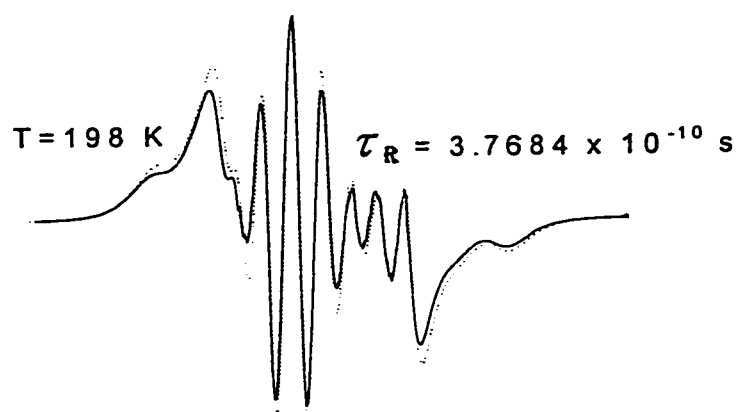


Figure 6.11: Variable temperature spectra of V3 in methylene chloride at 9GHz..

and experimental spectra. T_2^{-1} value used for simulation is 2.0G. The spectra obtained at lower temperature are the slow tumbling spectra. Although some intensity variations is observed between experimental and simulated spectra, the overall spectral fit is still very good and it is even better than that for V1 & V2 spectra.

The experimental and simulated spectra for V4 in methylene chloride are shown in figure 6.12. These spectra are obtained in the temperature range 240K to 171K extending over both the incipient slow tumbling and the typical slow tumbling regions. The correlation time range 1.14×10^{-10} s to 1.09×10^{-9} s. The spectra are simulated with $T_2^{-1} = 2.0$ G. The correlation times obtained are presented on the spectra in figure 6.12. Excellent spectral fit is obtained at higher temperatures in the incipient slow tumbling region. As the temperature is further lowered the intensity variation is monitored nevertheless the overall spectral fit is good.

Comparing the fitting of V3 and V4 to that of V1 and V2, we see that the fitting for V3 & V4 is much better and extending to much lower temperatures. This can be explained based on the magnetic parameters. The magnetic parameters for V3 & V4 are closer to axial symmetry than the magnetic parameters for V1 & V2.

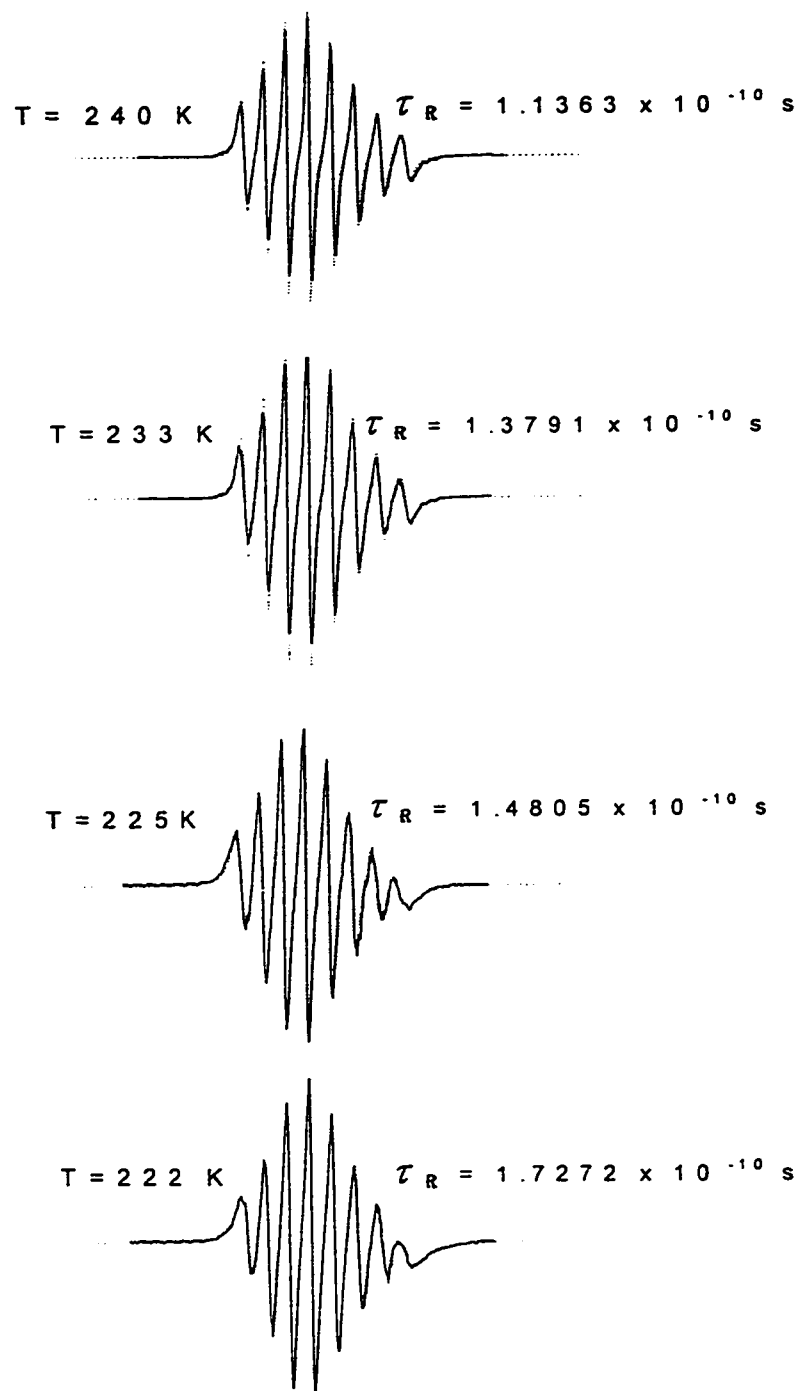


Figure 6.12: Variable temperature spectra of V4 in methylene chloride at 9GHz.

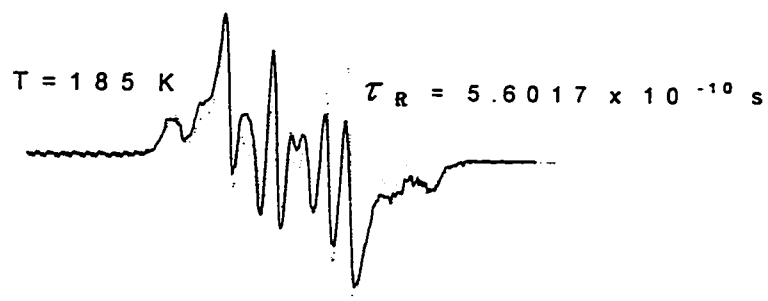
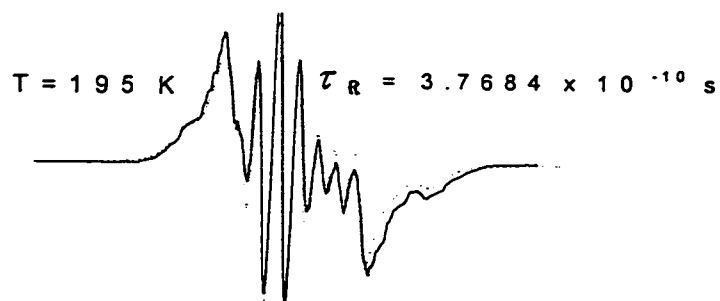
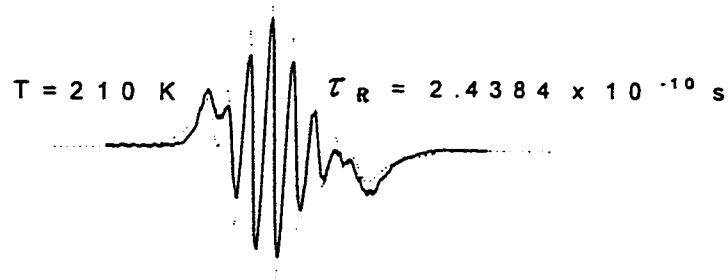
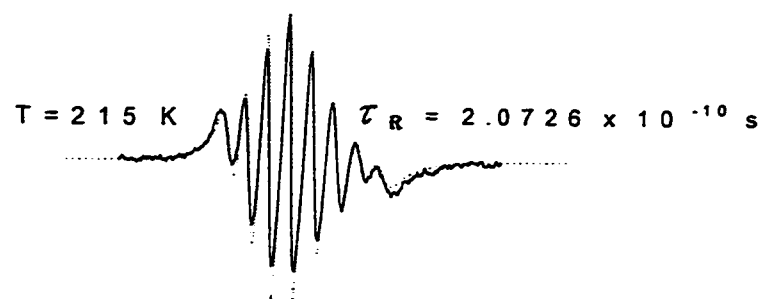


Figure 6.12 Variable temperature spectra of V4 in methylene chloride at 9GHz.

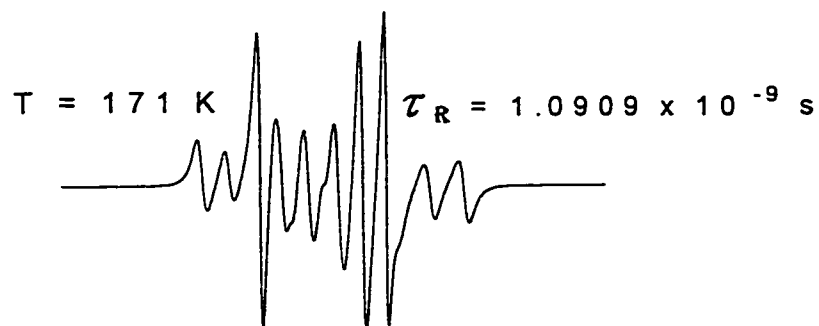
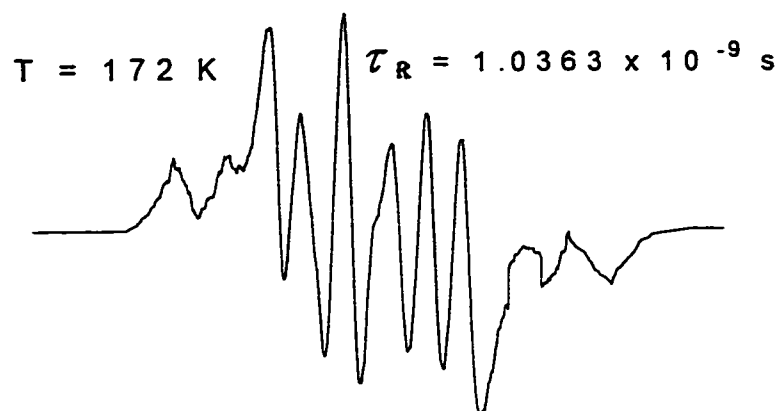


Figure 6.12: Variable temperature spectra of V4 in methylene chloride at 9GHz.

V3 & V4 are having the same magnetic tensors and have been studied in the same solvent thus any variation in motional behavior will reflect the shape and dimensions of the molecule. As can be seen from figure 6.11 and 6.12, V3 is showing slower tumbling behavior as compared to V4.

6.3 ALLOWED-VALUES EQUATION (AVE)

N can also be determined by using the allowed-values equation, AVE⁵⁷,

$$a \rho_x = b \rho_y + c \quad (6.1)$$

where

$$a = (\Delta A - 3\delta A)[(C/B)(\Delta g - 3\delta g) - (5/16)(\Delta A - 3\delta A)] \quad (6.2a)$$

$$b = (\Delta A + 3\delta A)[(5/16)(\Delta A + 3\delta A) - (C/B)(\Delta g + 3\delta g)] \quad (6.2b)$$

$$c = 4\Delta A[(5/16)\Delta A - (C/B)\Delta g] \quad (6.2c)$$

with

$$\Delta A = A_z - (1/2)(A_x + A_y) \quad (6.3a)$$

$$\delta A = (1/2)(A_x - A_y) \quad (6.3b)$$

$$\Delta g = [g_z - (1/2)(g_x + g_y)][\beta H_0/(h/2\pi)] \quad (6.3c)$$

$$\delta g = (1/2)(g_x - g_y)[\beta H_0/(h/2\pi)] \quad (6.3d)$$

$$\text{and} \quad \rho_x = R_x/R_z \quad (6.4a)$$

$$\rho_y = R_y/R_z \quad (6.4b)$$

The g_i , A_i and R_i are the principal values of the hyperfine, Zeeman, and rotational diffusion tensors, respectively. B and C are the experimental line width coefficients when nonsecular terms are unimportant.

The AVE shows that the g_i and A_i derived from single crystal or glass spectra can be combined with the experimental C/B ratio to yield ρ_x as a linear function of ρ_y . Although this relation does not permit us to determine the ratios of the diffusion tensor components ρ_x and ρ_y it does show that for a given value of ρ_x only one ρ_y is compatible with experiment. Hence refer to as “allowed-values equation” or AVE. It can be used to check whether the rotational diffusion is possibly isotropic or axially symmetric. For the former $\rho_x = \rho_y = 1$, while for the latter three possibilities exist: $\rho_x = 1$, $\rho_y = 1$, or $\rho_x = \rho_y$; for a given radical-solvent system we can check if any of these more symmetric results are compatible with the experiment.

The AVE indicates that only one value of $\rho_x = R_x/R_z$ is consistent with a ratio C/B obtained from experiment for a given $\rho_y = R_y/R_z$.

The values of the various expressions in equation 6.1 for v1 using the magnetic parameters g's and A's taken from table 4.2; and using C/B value of 0.601 ± 0.004 determined experimentally at 9.5394GHz are listed as follows (in Hz),

$$A = 6.08 \times 10^{17}$$

$$B = 3.99 \times 10^{17}$$

$$C = -2.33 \times 10^{17}$$

the allowed-values equation is

$$6.08 \times 10^{17} \rho_x = 3.99 \times 10^{17} \rho_y - 2.33 \times 10^{17} \quad (6.5a)$$

Dividing the equation by 6.08×10^{17} gives

$$\rho_x = 0.656 \rho_y - 0.383 \quad (6.5b)$$

Equation (6.5b) is not consistent with isotropic reorientation and only consistent with axial symmetry if $\rho_x = 1$, $\rho_y = 2.11$. The allowed-values equation is very sensitive to variation in the C/B value. We have estimated the error in N to be ± 0.11 for a C/B value of 0.601 ± 0.004 . Thus N obtained by using the allowed-values equation should be 2.11 ± 0.11 . This result is consistent with $N = 2.5 \pm 0.4$ determined from motional narrowing analysis.

Similar analysis was carried out for V2, V3 and V4. The magnetic parameters g 's and A 's were taken from table 4.2. The C/B values and the corresponding frequency were taken from the motional narrowing analysis; and are listed together with the results obtained from AVE calculations. The results obtained from AVE calculations for all the systems are consistent with that obtained from the motional narrowing analysis.

Table 6.7 : AVE Parameters and Results :

	V1	V2	V3	V4
Solvent	Toluene	Toluene	CH₂Cl₂	CH₂Cl₂
ν (in GHz)	9.5394	9.5440	9.5350	9.5370
C/B	0.601 ± 0.004	0.597 ± 0.012	0.663 ± 0.012	0.665 ± 0.021
a (in Hz)	6.08×10^{17}	5.95×10^{17}	4.82×10^{17}	4.89×10^{17}
b (in Hz)	3.99×10^{17}	4.02×10^{17}	4.47×10^{17}	4.44×10^{17}
c (in Hz)	-2.33×10^{17}	-2.03×10^{17}	-7.58×10^{16}	-9.51×10^{16}
ρ_y (at $\rho_x=1$)	2.11	1.99	1.25	1.32
N (AVE)	2.11 ± 0.11	1.99 ± 0.40	1.25 ± 0.30	1.32 ± 0.40
N (expt)	2.5 ± 0.4	1.7 ± 0.4	1.5 ± 0.4	1.7 ± 0.4

6.4 STOKES-EINSTEIN MODEL

The anisotropy for rotation (N), defined as $N = R_{\parallel}/R_{\perp}$ is related to the geometric structure factor by means of the Stokes-Einstein equation^{21,34},

$$R_i = \frac{k_B T}{(8 \pi \eta r_i^3 \sigma_i)}, \quad i = \parallel \text{ or } \perp \quad (6.6)$$

where,

$$N = \frac{R_{\parallel}}{R_{\perp}} = \frac{\sigma_{\perp}}{\sigma_{\parallel}} \quad (6.7)$$

$$\sigma_{\parallel} = \frac{2}{3} \lambda^2 (1 - \lambda^2) [1 - (1 - \lambda^2) \lambda^{-1} \ln \frac{1 + \lambda}{(1 - \lambda^2)^{1/2}}]^{-1} \quad (6.8)$$

$$\sigma_{\perp} = \frac{2}{3} \lambda^2 (2 - \lambda^2) [(1 + \lambda^2) \lambda^{-1} \ln \frac{1 + \lambda}{(1 - \lambda^2)^{1/2}} - 1]^{-1} \quad (6.9)$$

and λ is a dimensionless structure factor,

$$\lambda = \frac{(r_{\perp}^2 - r_{\parallel}^2)^{\frac{1}{2}}}{r_{\parallel}} \quad \text{and } 0 < \lambda \leq 1 \quad (6.10)$$

Using Desktop Molecular Modeler [DTMM] program⁵⁸, the length of the axes of V1 estimated to be, $r_{\parallel} = 5.40 \text{ \AA}$, $r_{\perp} = 2.20 \text{ \AA}$, then $\lambda = 0.913$, $\sigma_{\parallel} = 0.128$, $\sigma_{\perp} = 0.308$, and $N = 2.39$, which is consistent, within experimental error, with our observation that is $N = 2.5 \pm 0.4$. Similar analysis is carried for V2, V3 and V4 and the results are presented in table 6.8.

Table 6.8 : Stokes-Einstein Model Results :

Parameter	V1	V2	V3	V4
$2 \times r_{\parallel} (A^0)$	10.80	11.22	11.50	13.50
$2 \times r_{\perp} (A^0)$	4.40	6.67	6.40	6.40
λ	0.913	0.804	0.831	0.880
ρ_{\parallel}	0.129	0.298	0.256	0.180
ρ_{\perp}	0.308	0.458	0.423	0.357
N	2.39	1.54	1.65	1.98
N (AVE)	2.11 ± 0.11	1.99 ± 0.40	1.25 ± 0.30	1.32 ± 0.40
N (expt)	2.5 ± 0.4	1.7 ± 0.4	1.5 ± 0.4	1.7 ± 0.4

The results obtained are consistent, within experimental error, with our motional narrowed results and the Allowed Values Equation results. Furthermore, this Stokes-Einstein results describe quantitatively the dependence of the anisotropy of rotation on the dimensions of the molecule thus explain the N values obtained from motional narrowed study.

6.5 Anisotropic Interaction Parameter (κ):

Molecular reorientation of paramagnetic species in solution as a function of temperature has been recently analyzed taking into account the effect of anisotropic rotational diffusion¹¹. The rotational correlation time, τ_R , plotted as a function of temperature was found to be linear in η/T , as indicated by equation(1.1). The anisotropic interaction parameter can be determined from the slope of rotational correlation time, τ_R , plotted as a function of η/T which is

$$\text{Slope} = (4 / 3)(\pi r_0^3 / k_B)\kappa \quad (6.11)$$

where k_B is the Boltzmann constant, T the absolute temperature, η the coefficient of shear viscosity of the solvent, $4\pi r_0^3/3$ a molecular hydrodynamic volume, and κ is an experimentally determined dimensionless coupling parameter called the anisotropic interaction parameter^{11,12}. The viscosity values for the used solvents at different temperatures were calculated using the following equations⁵⁶,

$$\eta = \exp \left[-7.266 + \frac{409.6K}{T-103.1 K} \right] \quad \text{for toluene} \quad (6.12)$$

and

$$\eta = \frac{5.8768}{(128.88 + t)^{1.4408}} \quad \text{for methylene chloride} \quad (6.13)$$

where T in Kelvin and t in degree centigrade. The results are shown in tables 6.9 to 6.12. together with τ_R values.

The plot of τ_R as a function of η/T for V1 in toluene, c.f. figure 6.13. τ_R was found to be linear in η/T , and the slope was found to be $2.32 \times 10^{-6} \text{ s K P}^{-1}$. The molecular hydrodynamic radius for V1 is determined from the measurement of translational diffusion constant using the capillary diffusion cell, in chapter 5, and found to be 5.39 \AA . From the slope of τ_R vs η/T , value of the anisotropic interaction parameter, κ , can be calculated as follows:

$$\kappa = \frac{2.32 \times 10^{-6} \times 1.381 \times 10^{-16}}{\frac{4}{3} \pi \times (5.39 \times 10^{-8})^3} = 0.488.$$

The curve of τ_R versus η/T for V2 in toluene, shown in figure 6.14, was found to be linear. The slope for this plot is $3.58 \times 10^{-6} \text{ s K P}^{-1}$. The molecular hydrodynamic radius for V2, is determined by the capillary diffusion cell method, in chapter 5, to be 5.70 \AA . This gives $\kappa = 0.637$.

Table 6.9 : η , η/T and τ_R Values for V1 in toluene

T (K)	η (P)	η /T (P K⁻¹)	τ_R (sec)
294	0.005974	2.03E-05	3.0091e11
283	0.006811	2.41E-05	3.9620e11
278	0.007269	2.61E-05	4.2480e11
273	0.007788	2.85E-05	4.7450e11
268	0.008379	3.13E-05	5.2999e11
263	0.009055	3.44E-05	5.9298e11
258	0.009836	3.81E-05	6.8617e11
253	0.010743	4.25E-05	8.1476e11
248	0.011805	4.76E-05	8.6885e11
243	0.01306	5.37E-05	1.0588e11
240	0.013925	5.8E-05	1.2359e10
234	0.015972	6.83E-05	1.6898e10
228	0.018563	8.142E-05	1.8110e10
225	0.020123	8.944E-05	1.9754e10
222	0.021904	9.867E-05	2.2635e10
219	0.023947	1.093E-04	2.3879e10

216	0.026305	1.218E-04	2.7110e10
213	0.029043	1.364E-04	3.0983e10
209	0.033433	1.600E-04	3.6147e10
203	0.042176	2.078E-04	4.8196e10
199	0.050042	2.515E-04	5.7183e10
198	0.052346	2.644E-04	6.5847e10
196	0.057443	2.931E-04	6.5847e10
194	0.063295	3.263E-04	7.2432e10
192	0.070048	3.648E-04	8.3575e10
190	0.077884	4.099E-04	9.0540e10

Table 6.10 : η , η/T and τ_R Values for V2 in toluene

T (K)	η (P)	η/T (P K ⁻¹)	τ_R
293	0.006042	2.06E-05	5.3589e-11
283	0.006811	2.41E-05	6.7637e-11
278	0.007269	2.61E-05	7.5627e-11
270	0.008133	3.01E-05	8.9085e-11
261	0.009354	3.58E-05	1.0881e-10
260	0.00951	3.66E-05	1.0814e-10
253	0.010743	4.25E-05	1.2776e-10
248	0.011805	4.76E-05	1.4962e-10
238	0.014557	6.12E-05	1.9754e-10
235	0.015598	6.64E-05	2.1730e-10
231	0.017189	7.44E-05	2.4144e-10
228	0.018563	8.14E-05	2.7162e-10
224	0.020691	9.24E-05	3.1042e-10
218	0.024695	1.13E-04	3.8122e-10
212	0.030054	1.42E-04	4.8288e-10
203	0.042176	2.08E-04	7.2432e-10

199	0.050042	2.51E-04	8.6918e-10
195	0.060266	3.09E-04	1.0865e-9
190	0.077884	4.10E-04	1.4486e-9

Table 6.11 : η , η/T and τ_R Values for ν_3 in CH_2Cl_2

T (K)	η (P)	η/T (P K ⁻¹)	τ_R
294	0.004304	1.46E-05	4.1690e-11
288	0.004577	1.59E-05	4.7559e-11
280	0.00497	1.78E-05	5.4548e-11
273	0.005364	1.96E-05	6.1798e-11
265	0.005884	2.22E-05	6.1398e-11
255	0.006664	2.61E-05	7.7286e-11
245	0.007638	3.12E-05	9.6504e-11
235	0.00888	3.78E-05	1.3036e-10
225	0.010507	4.67E-05	1.4805e-10
215	0.012713	5.91E-05	2.0726e-10
205	0.015835	7.72E-05	2.5900e-10
195	0.020521	0.000105	3.0940e-10
198	0.018891	9.54E-05	3.7680e-10
190	0.02383	0.000125	5.1816e-10
180	0.034004	0.000189	8.2900e-10

Table 6.12 : η , η/T and τ_R Values for V4 in CH_2Cl_2

T (K)	η (P)	η/T (PK ⁻¹)	τ_R
340	0.002933	8.63E-06	3.0091e11
330	0.003163	9.59E-06	3.9620e11
322	0.00337	1.05E-05	4.2480e11
320	0.003426	1.07E-05	4.7450e11
310	0.003728	1.2E-05	5.2999e11
300	0.004077	1.36E-05	5.9298e11
288	0.004486	1.55E-05	6.8617e11
285	0.004623	1.61E-05	8.1476e11
280	0.004718	1.66E-05	8.6885e11
275	0.005133	1.85E-05	1.0588e11
260	0.005746	2.15E-05	1.2359e10
255	0.006664	2.61E-05	1.6898e10
250	0.007123	2.85E-05	1.8110e10
235	0.00917	3.94E-05	1.9754e10
230	0.010507	4.67E-05	2.2635e10
225	0.011096	5E-05	2.3879e10

215	0.012713	5.91E-05	2.7110e10
205	0.014129	6.73E-05	3.0983e10
195	0.020521	0.000105	3.6147e10
183	0.028156	0.000152	4.8196e10
175	0.048994	0.000285	5.7183e10
170	0.051656	0.000302	6.5847e10

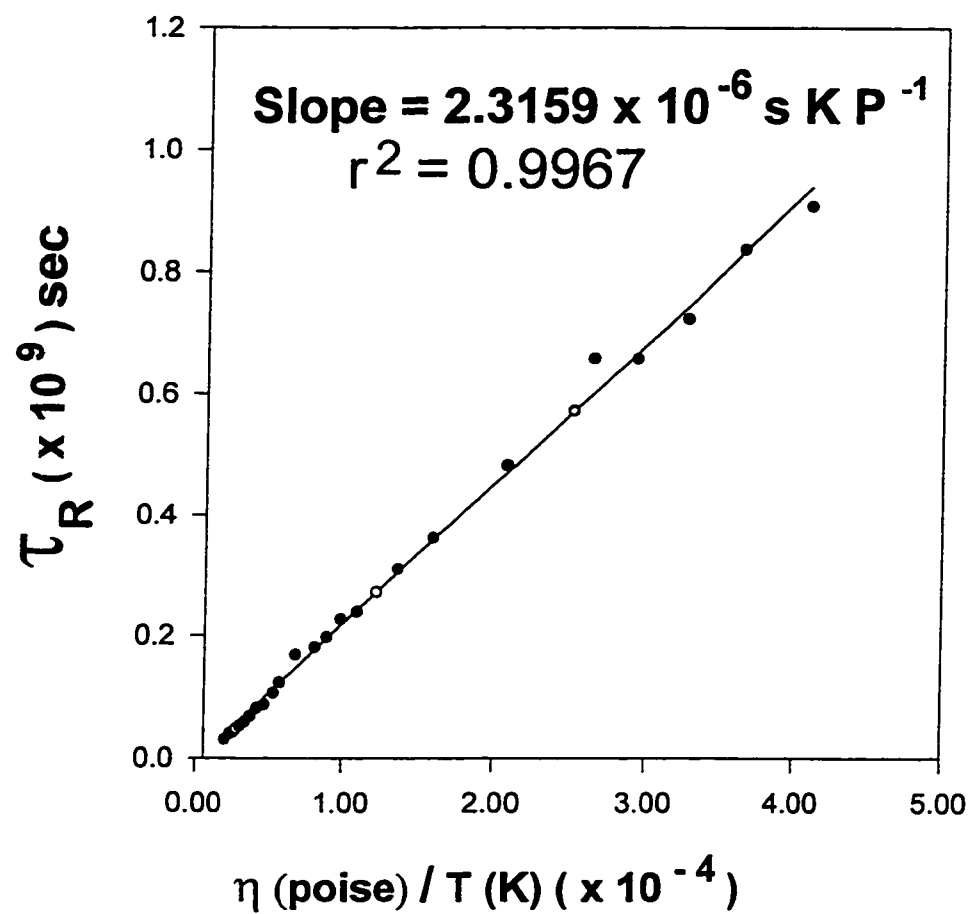


Figure 6.13: $\eta \text{ (poise)} / T \text{ (K)} \text{ vs } \tau_R$ for V1 in toluene at 9GHz.

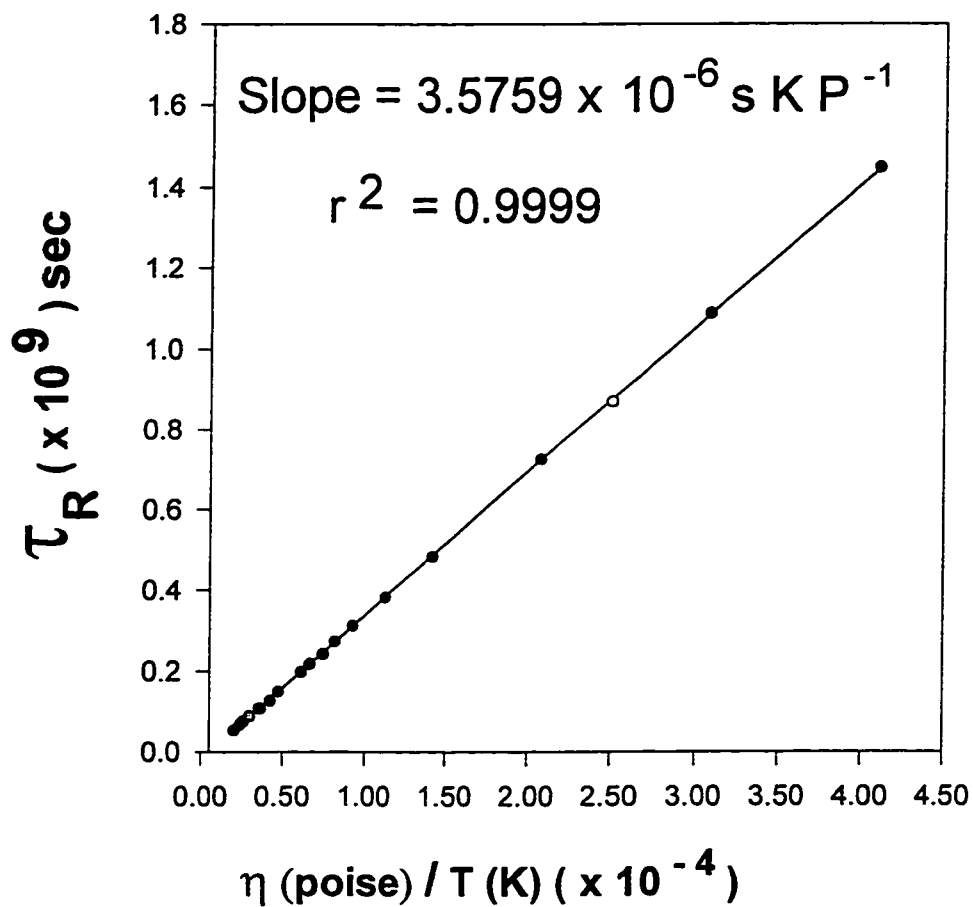


Figure 6.14: $\eta \text{ (poise)} / T \text{ (K)}$ vs τ_R for V2 in toluene at 9GHz.

The rotational correlation time, τ_R , of V3 in methylene chloride plotted as a function of η/T , c.f. figure 6.15, was found to be linear, and the slope was found to be $4.47 \times 10^{-6} \text{ s K P}^{-1}$. The molecular hydrodynamic radius for V3, in methylene chloride, is determined in chapter 5, from the measurement of translational diffusion constant using the capillary diffusion cell to be 7.12Å. From the slope of τ_R versus η/T , the value of the anisotropic interaction parameter, κ , is determined to be 0.408.

Similarly, the curve of τ_R versus η/T for V4 in methylene chloride, presented in figure 6.16, was found to be linear. The slope for this plot is $3.67 \times 10^{-6} \text{ s K P}^{-1}$. The molecular hydrodynamic radius for V4 in methylene chloride, needed to calculate κ , is 7.67Å obtained by the capillary diffusion experiment, and discussed in chapter 5. The κ value obtained for V4 in methylene chloride is 0.268.

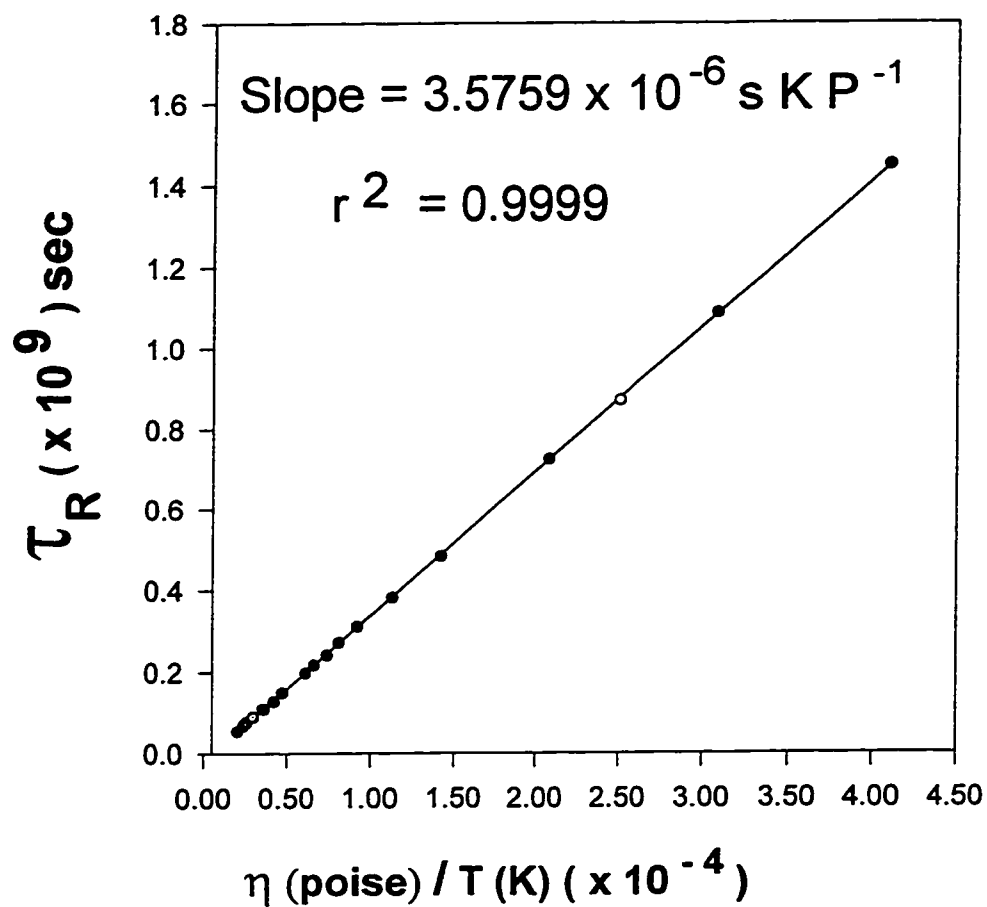


Figure 6.15: $\eta \text{ (poise)} / T \text{ (K)}$ vs τ_R for V3 in t methylene chloride at 9GHz.

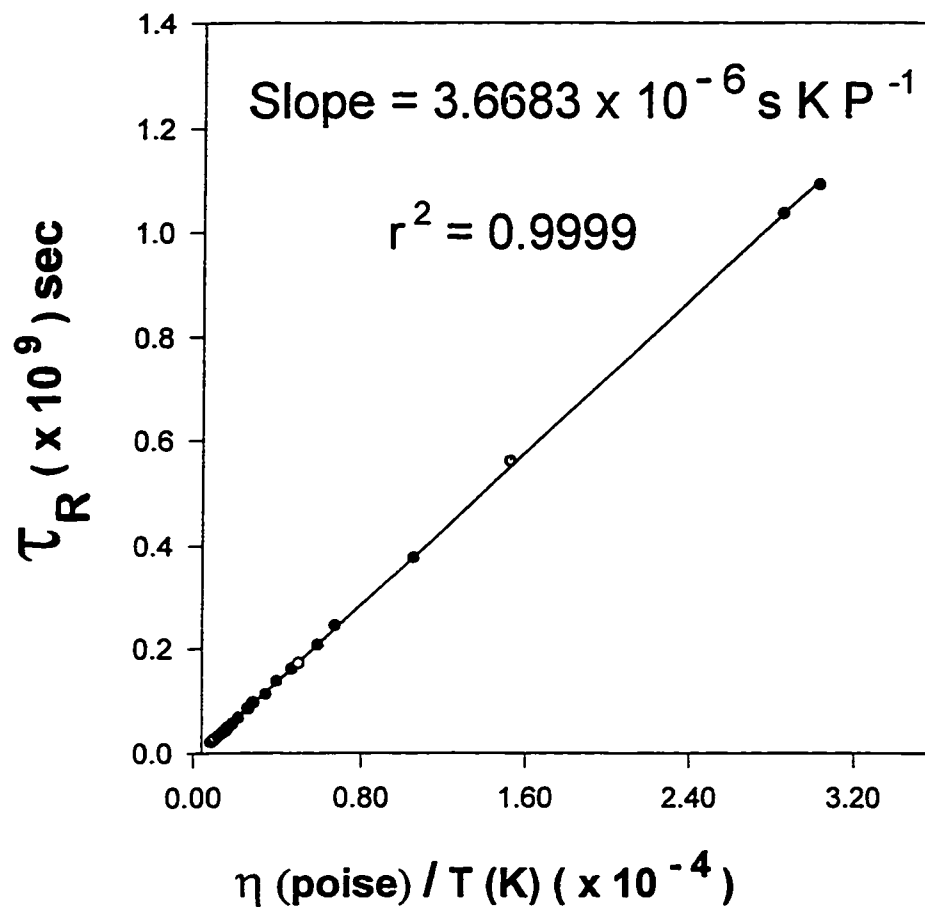


Figure 6.16: $\eta (\text{poise}) / T (\text{K})$ vs τ_R for V4 in methylene chloride at 9GHz.

6.6 STICKINESS FACTOR (S)

The stickiness factor, S is independent of molecular geometry and is zero in the slip limit and 1 in the stick limit. For truly hydrodynamic situation $0 \leq S \leq 1$. It could be calculated from the relationship ⁵⁹

$$S = \frac{\kappa - C_{\text{slip}}^{\text{hyd}}}{1 - C_{\text{slip}}^{\text{hyd}}} \quad (6.14)$$

The data obtained can be analyzed in terms of the hydrodynamic free space model for molecular relaxation in liquids ⁶⁰, a theory based on the existence of free space in the hydrodynamic continuum in which the molecule can rotate. Using Desktop Molecular Modeller ⁵⁸ we made an approximation that V1 is a prolate spheroid with semiaxes $a > b$ where $a = 10.8 \text{ \AA}$ and $b = 8.60 \text{ \AA}$, the symmetry parameter α^\perp is defined as b/a . Under stick boundary conditions, the dimensionless rotational friction coefficient can be calculated from Perrin's formula ⁶¹,

$$f_{\text{stick}}^\perp = \frac{(2/3)[1 - (\alpha^\perp)^4]}{\frac{[2 - (\alpha^\perp)^2](\alpha^\perp)^2}{[1 - (\alpha^\perp)^2]^{\frac{1}{2}}} \ln\left\{\frac{1 + [1 - (\alpha^\perp)^2]^{\frac{1}{2}}}{\alpha^\perp}\right\} - (\alpha^\perp)^2} \quad (6.15)$$

where $\alpha^\perp = 0.796$. This gives $f_{\text{stick}}^\perp = 1.08$. The corresponding value of the dimensionless rotational friction coefficient under slip boundary condition, f_{slip}^\perp , is calculated from

$$f_{\text{slip}}^\perp = f_{\text{stick}}^\perp [1 - (f_{\text{stick}}^\perp)^{\frac{-2}{3}}] \quad (6.16)$$

which gives a value of $f_{\text{slip}}^\perp = 0.0540$. From the relation,

$$f_{\text{slip}}^\perp = f_{\text{stick}}^\perp C_{\text{slip}}^{\text{hyd}} \quad (6.17)$$

we can calculate

$$C_{\text{slip}}^{\text{hyd}} = 0.0540 / 1.08 = 0.0500$$

and from equation (6.4) we calculated

$$S = (0.488 - 0.0500) / (1 - 0.0500) = 0.461.$$

Similar analysis is carried for V2, V3, and V4 and the obtained results are presented in table 6.13. One observed that the trends in κ and S are similar, i.e. both κ and S descend in the following trend

$$V2 > V1 > V3 > V4.$$

Thus, in general the interactions are more anisotropic for V1 and V2 vs V3 and V4.

Table 6.13 : Anisotropic Interaction Results

<u>compound.</u> Parameter	V1	V2	V3	V4
a	10.80	11.22	11.50	13.50
b	8.60	11.02	8.60	8.60
α^\perp	0.796	0.982	0.748	0.637
f_{stick}	1.08	1.00	1.11	1.23
f_{slip}	0.0540	0.0027	0.0746	0.1586
C_{slip}^{hyd}	0.0500	0.0027	0.0672	0.1289
K	0.488	0.637	0.408	0.268
S	0.461	0.636	0.365	0.160

Kivelson et al. derived an expression for the parameter κ , which is a measure of the anisotropic ^{62,63} of intermolecular interactions, and found that it is proportional to the ratio of the mean square intermolecular torques of the solute $\langle T^2 \rangle$ to the mean square intermolecular forces of the solvent $\langle F^2 \rangle$

$$\kappa \approx (3/4r_0^2) \langle T^2 \rangle / \langle F^2 \rangle \quad (6.18)$$

where $\langle T^2 \rangle$ is related to the fluctuating intermolecular torque associated with the angular momentum of the solute, and $\langle F^2 \rangle$ is related to the translation shear forces of the solvent. Hence, κ is actually a measure of the anisotropic interactions between the solute and the solvent molecules.

It can be seen from equation 6.18 that κ depends on molecular geometry, r_0 , while in the expression of Kowert and Kivelson ⁶⁴, the stickiness factor, S , is independent of molecular geometry. This concludes that S is a real test of anisotropic interactions independent of molecular geometry. In fact S can be used to differentiate the subtitles of solute solvent interactions independent of molecular geometry. Thus, although κ and S are having similar trends we are going to use the stickiness factors, S , as it is a real test of anisotropic interactions independent of molecular geometry.

The stickiness factor of 1 is valid for a large particle undergoing Brownian motion in a continuous homogeneous medium. While this may be valid for macroscopic bodies, it is less clear that it should hold for a molecule tumbling in a solvent comprising molecules of comparable size. In our system we found that S varies from 0.160 to 0.636, the last value is slowly approaching the value for a Brownian particle, and $S(V2) > S(V1) >$

$S(V3) > S(V4)$. It is remarkable that V2 in toluene approaches the stick boundary condition on a molecular level. In the hydrodynamic limit, it is assumed that there is no lag in the transfer of momentum from the rotating solute molecule to the solvent in the stick boundary condition. We found that quite remarkably that S approaches unity even on the molecular level.

Now, let us investigate the effects of the solute size and shape on the anisotropic interactions. Since the anisotropic interactions are solvent dependent, only system in the same solvent are compared. V1 and V2 are studied in toluene. For V2 S is 0.636 while for V1 it is 0.461, i.e. the anisotropic interaction for V2 are greater than those for V1. At first instance one could expect this is due to the increase in the size since V2 is larger than V1 and the anisotropic interaction are expected to increase with the molecular size. However this contradicts what we observe in the other two systems, namely V3 and V4 in methylene chloride. We found that V3 is having greater anisotropic interactions ($S = 0.365$) than V4 ($S = 0.160$), although V4 is larger in size than V3. When we look closely to the change in the anisotropy (i.e. the shape) of the solute accompanying the size change we found that

(i) in case of V1 and V2, the increase in the size of V2 compared to V1 is perpendicular to the longest axis in a way that V2 shape is approaching the rough hard sphere shape than V1. This change in the shape of the solute could be responsible for the increase in S value, since the anisotropic interactions are expected to be greater in rough sphere compared to rod-like particle.

(ii) While in the case of V3 and V4, the increase in the V4 solute size compared to V3 is along the longest axis i.e. the V4 shape is

deviating from sphere-particle like towards rod-like particle thus resulting in a decrease in the anisotropic interactions. From these results it seems that the anisotropic interactions are correlated to both the size and the shape of the solute.

Next, let us comment on the decrease in the anisotropic interaction in going from V1 and V2 in toluene to V3 and V4 in methylene chloride. In this respect we have to investigate the solvent effects on the anisotropic interaction. With regard to solvent effects, the anisotropic interactions seem to increase with decreasing solvent molecular radius and perhaps with increasing solvent molecular anisotropy. Our result could be understood on the second effect, i.e. the anisotropy of the solvent. This is might be reasonable since these solute molecules are very large compared to the solvent molecules. The shape of toluene is more anisotropic as compared to the methylene chloride, which could lead to higher anisotropic interactions. This may explain our observation that S is larger for V1 and V2 in toluene compared to V3 and V4 in methylene chloride.

CHAPTER VII

CONCLUSION

EPR study was carried out for four vanadium model compounds containing sulfur and nitrogen heteroatoms at the 9GHz. These systems are Bis(S-methyl-3-isopropylidenehydrazinecarbodithioato)oxovanadium (IV); V1; and Bis(S-methyl-3-cyclohexylidenehydrazinecarbodithioato)oxovanadium (IV); V2, in toluene and S-mehtyl-N-salicylidenehydrazinecarbothioatophenanthrolineoxovanadium (IV); V3; and S-mehtyl-N-5-methoxysalicylidenehydrazinecarbothioatophenanthorlineoxovanaium (IV); V4; in methylene chloride.

Rigid limit spectra were taken at 77K and analyzed by computer simulation to yield the magnetic parameters. In fact these are the corner stone for the analysis of the line width in the motional narrowing region and of the line shape in the slow tumbling region. The obtained g & A tensors for the four studied systems are listed in table 4.2

The obtained magnetic parameters are used to obtain information on the geometric and the electronic structures of studied systems. For all the four systems studied,

$$g_e > g_x > g_y > g_z$$

which give support to the five coordinated distorted square pyramidal structure. This is in agreement with optical data and in support of the energy level scheme of Ballhausen and Gray.

The magnetic parameters for V1 and V2 ($g_x \neq g_y$) are showing greater distortion from axial symmetry as compared to v3 and v4 ($g_x \approx g_y$). This is consistent with observed electronic spectra of the systems.

The molecular orbital approach is used to describe the molecular orbital bonding between metal and ligands. The orbit coefficients β_1 , β'_1 , ϵ_1 , ϵ'_1 are calculated from the magnetic and electronic data using Lee and Kivelson's approach. The values are summarized in table 4.3. Our analysis indicates that N_2S_2 systems (V1 and V2) which have larger β_1 value as compared to N_3S systems (V3 and V4) are characterized by a more in-plane σ -bonding. This probably is due to the extreme polarizable electrons on the negatively charged sulphur as they are capable of forming strong bonding with the empty $d_{x^2-y^2}$ orbital on the vanadium which is of high electron deficiency.

In addition, Fermi contact term for the vanadium, K, and the direct dipolar interaction which gives direct information about electron delocalization and covalency, P, are obtained from hyperfine coupling tensors. Closer inspection of both our results and those of others show that there is a good correlation between P and the nature of the coordinating atom. The larger value of P for N_3S systems (V3 & V4) compared to N_2S_2 systems (V1 & V2) studied, 114×10^{-4} and $107 \times 10^{-4} \text{cm}^{-1}$ respectively, indicates that less delocalization of the unpaired electron onto the smaller p_π orbitals on N. Generally P for sulfur coordinating complexes, is much smaller indicating

significant delocalization of the electron in to the π -orbitals on the sulfur ligand while the complexes bonding via N and O have large P values (less delocalization), since involve smaller atoms. Also orbital expansion due to the negative charge and consequent greater delocalization of the unpaired electron is expected.

Also, we found a good correlation between g_{\parallel} and A_{\parallel} values for N_2S_2 and N_3S ligand types which are studied and all agree well with the other ligand types, N_4 and S_4 , studied by Holyk. We observed that there is a linear relationship between g_{\parallel} and A_{\parallel} for ligands made of varying compositions and there is a good correlation for varying complexes with equatorial liquids of the type $VO(N_4)$, $VO(N_3S)$, $VO(N_2S_2)$ and $VO(S_4)$. This will be useful in characterization of the non-porphyrin species of vanadium in asphaltenes.

The translational diffusion constant is determined by the capillary diffusion method at room temperature. The translational diffusion experiment were monitored by electron spin resonance spectral intensities as a function of time. The translational diffusion constants are found to be 6.80×10^{-6} and $6.42 \times 10^{-6} \text{ cm}^2\text{s}^{-1}$ for V1 and V2, respectively, in toluene and 7.12×10^{-6} and $6.61 \times 10^{-6} \text{ cm}^2\text{s}^{-1}$ for V3 and V4, respectively, in methylene chloride. The hydrodynamic radii, r_o , of solvated molecules in solution are obtained from the Stokes Einstein equation for translational diffusion under the stick boundary condition. r_o is determined to be 5.39, 5.70, 7.12 and 7.67 \AA for V1 and V2 in toluene and V3 and V4 in methylene chloride, respectively. These r_o values are essential to the anisotropic interaction analysis.

The variable temperature spectra were recorded and analyzed in both the motional narrowing and the slow motion regions. The motional analysis employing anisotropic rotational diffusion in the fast motion limit suggests that the four systems studied were undergoing axially symmetric rotational diffusion at the y-axis with $N = 2.5, 1.7, 1.5$ and 1.7 ± 0.4 for V1, V2, V3 and V4 respectively. The N values obtained were compared with those calculated from the allowed values equation (AVE) and found to be consistent. From AVE the N values obtained are $2.11 \pm 0.11, 1.99 \pm 0.40, 1.25 \pm 0.30$ and 1.32 ± 0.40 for V1, V2, V3 and V4 respectively.

Also, the obtained N values are compared to the dimensions of the systems studied through the Stokes-Einstein model. Stokes-Einstein Model calculations yield N values of 2.39, 1.54, 1.65 and 1.98 for V1, V2, V3 and V4 respectively. Furthermore, this Stokes-Einstein results describe quantitatively the dependence of the anisotropy of rotation on the dimensions of the molecules. This explains the N values obtained from motional narrowed study. Also, the fast motional analysis yields τ_R values which were analyzed to obtain information about the anisotropic interaction parameters.

The slow tumbling analysis is carried out to test the validity of Stokes-Einstein relation in that region. One of the use of the motional narrowing analysis is that τ_R and N values obtained in the motional narrowing region can be carried over to the slow tumbling region. The spectra in the slow tumbling region were successfully simulated using the Borwnian model. This is important for the calculation of the hydrodynamic molecular radius based on the stick model.

The τ_R values obtained from slow tumbling simulation are found to be linear in η/T in consistent with motional narrowing values, indicating that κ and r_0 are constant in the temperature range studied. The combined results from the fast, slow tumbling and the translational diffusion work were used in the analysis of the solute-solvent interactions using the stickiness factor, S of Hu and Zwanzig.

The stickiness factor, S , which is a real test of anisotropic interactions independent of molecular geometry is found to be 0.461, 0.636, 0.365 and 0.160 for V1, and V2 in toluene and V3 and V4 in methylene chloride respectively. The stickiness factor of 1 is valid for a large particle undergoing Brownian motion in a continuous homogeneous medium. While this may be valid for macroscopic bodies, it is less clear that it should hold for a molecule tumbling in a solvent comprising molecules of comparable size. It is remarkable that V2 in toluene approaches the stick boundary condition on a molecular level. These results indicate that the interactions for V1 and V2 in toluene are more anisotropic versus V3 and V4 in methylene chloride, this might be, at least partially, due to the fact that toluene is more anisotropic than methylene chloride.

In the hydrodynamic limit, it is assumed that there is no lag in the transfer of momentum from the rotating solute molecule to the solvent in the stick boundary condition. We found that quite remarkably that S approaches unity even on the molecular level. Also we found that rough solute spheres exert torques more efficiently than elongated solutes. Furthermore, the solutes exert torques more efficiently when the solvent used is more anisotropic.

REFERENCES

1. Hwang, J. S.; Al-Turabi, M. O. H.; El-Sayed, L. *Energy & Fuels*, **1994**, *8*, 793.
2. Boucher, L. J., Tynan, E. C., and Yen, T. F. In "Electron Spin Resonance of Metal Complexes" ed. Yen, T. F., Plenum, New York, **1969**, 111.
3. a) Dr. El-Sayed, L., Faculty of Science, Alexandria University, Private Communication.
b) Al-Guidhi, H.A., MS thesis, Girl Colleges, Jeddah, Saudi Arabia, **1989**.
4. Miller, G. A. and McClung, R. E. D., *Inorg. Chem.* **1973**, *12*, 2554.
5. Al-Turabi, M. O. H.; MS thesis, King Fahd University of petroleum and Minerals, Dhahran, Saudi Arabia, 1992.
6. Wilson, R.; Kivelson, D. *J. Chem. Phys.* **1966**, *44*, 154.
7. The Rigid limit program, Lefebvre-Maruani, modified by Morsy, M.
8. Campbell, R.F., and Freed, J. H., *J. Phy. Chem.* **1980**, *84*, 2668.
9. Bruno, G. V., Harrington, J. K., and Eastman, M. P., *J. Phy. Chem.* **1977**, *81*, 1111.
10. Hwang, J. S., and Balkhoyor H. B., *J. Phy. Chem.* **1995**, *99*, 8447.
11. a) Hwang, J. S., Kivelson, D., Plachy, W. Z., *J. Phys. Chem.* **1973**, *58*, 1753.

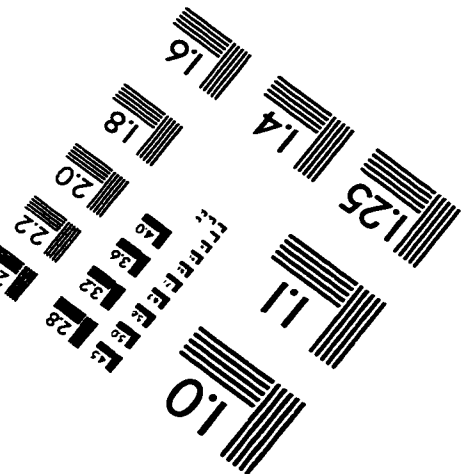
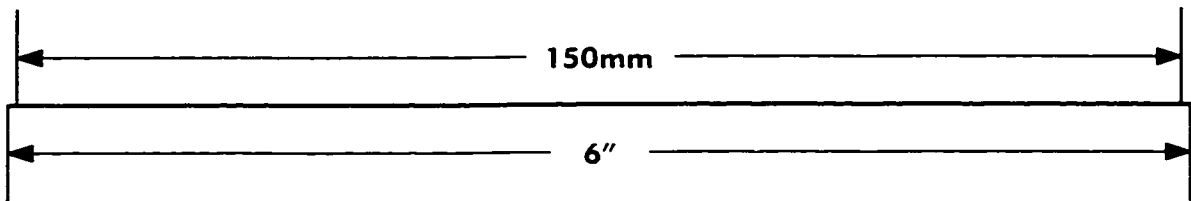
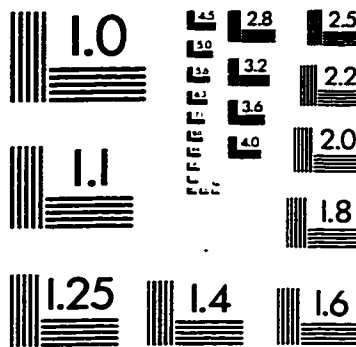
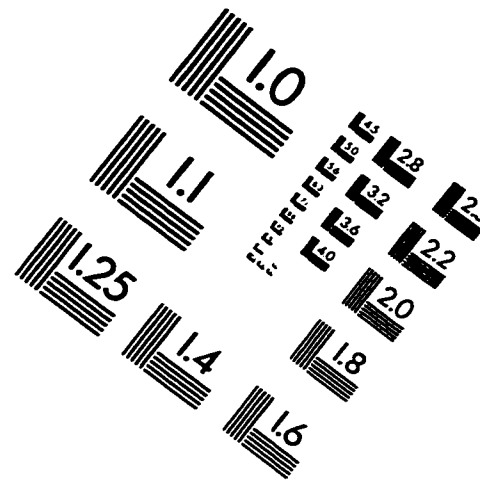
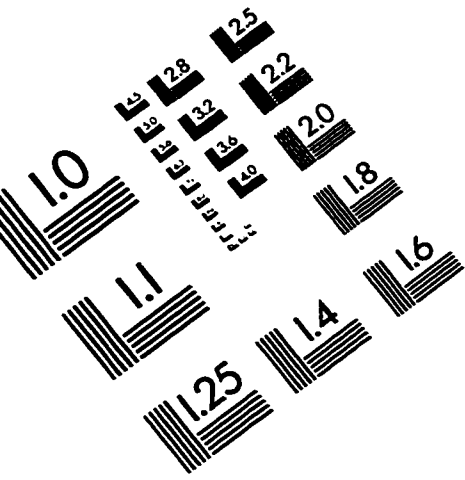
- b) Li, A. S. W., and Hwang, J. S. *J. Phys. Chem.* **1985**, *89*, 2556.
- c) Hwang, J. S., Al-Rashid, W. A., and Saleem, M. M. *J. Phys. Chem.* **1988**, *92*, 3630.
- d) Hwang, J. S., Al-Rashid, W. A., and Saleem, M. M. *J. Phys. Chem.* **1989**, *93*, 1008.
- 12. McClung, R.; Kivelson, D. *J. Chem. Phys.* **1968**, *49*, 3380.
- 13. a) Ahn, M. K.; Derlacki, Z. J. *J. Phys. Chem.* **1978**, *82*, 1930.;
- b) Ahn, M. K.; D. E. Ormond, *J. Phys. Chem.* **1978**, *82*, 1635.
- c) Ahn, M. K. *J. Mag. Reson.* **1976**, *22*, 289.
- 14. Holyk, N. H. M.S. Thesis, University of New Hampshire, Durham, **1979**.
- 15. Chasteen, N. D. In *Biological Magnetic Resonance*, Berliner, L. J., Reuben, J., Eds.; Plenum Press; New York, **1989**, *3*, 53-119.
- 16. Freed, J. H., and Fraenkel, G. K., *J. Chem. Phys.* **1963**, *39*, 326.
- 17. Polnaszek, C. F., and Freed, J. H., *J. Phys. Chem.* **1975**, *79*, 2283.
- 18. Likhtenshein, G. I, "*Spin labeling Methods in Molecular Biology*", John Wiley & Sons, New York, 1976.
- 19. Berliner, L. J., Ed. "*Spin Labelling: Theory and Applications*", Academic Press, New York, 1976.
- 20. Berliner, L. J., Ed. "*Spin Labelling II: Theory and Applications*", Academic Press, New York, 1979.
- 21. Hwang, J. S., Mason, R. P., Hwang, L. P., and Freed, J. H. *J. Phys. Chem.* **1975**, *79*, 489.
- 22. Goldman, S. A., Bruno, G. V., Polnaszek, C. F., and Freed, J. H. *J. Phys. Chem.* **1972**, *56*, 716.

23. Goldman, S. A., Bruno, G. V., and Freed, J. H. *J. Chem. Phys.* **1973**, *59*, 3071.
24. Willigen, H. V., *J. Phys. Chem.* **1983**, *87*, 3366.
25. White, L. K., and Chasteen, N. D., *J. Phys. Chem.* **1979**, *83*, 287.
26. Smith, I. C. P., Swartz, H. M., Botton, J. R. and Borg, D. C., John Wiley and Sons, New York, 1972.
27. Libertini, L. J., and Griffith, O. H. J., *J. Chem. Phys.* **1970**, *53*, 1359.
28. Collison, D., Gohan, B., and Mabbs, F. E., *J. Chem. Soc. Dalton Trans.*, **1987**, *111*.
29. Freed, J. H., and Fraenkel, G. K., *J. Chem. Phys.* **1964**, *40*, 1815.
30. Kevilson, D., *J. Chem. Phys.* **1960**, *33*, 1094.
31. Freed, J. H., *J. Chem. Phys.* **1964**, *41*, 2077.
32. Hwang, J. S.; Rahman, M. H. *Chem. Phys. Lett.* **1992**, *199*, 286.
33. Freed, J. H., Bruno, G. V., and Polnaszek, C. F. *J. Phys. Chem.* **1971**, *75*, 3385.
34. Hwang, J. S.; Pollet P.; Saleem, M. M. *J. Chem. Phys.* **1986**, *84*, 577.
35. Lang, J. C., Jr.; Freed, J. H. *J. Chem. Phys.* **1972**, *56*, 4103.
36. Kovarskii, A. L.; Wasserman, A. M.; Buchachenko, A. L. *J. Mag. Reson.* **1972**, *7*, 225.
37. Kevilson, D., and Lee, S. K. *J. Chem. Phys.* **1964**, *41*, 1896.
38. Atherton, N. M. "Principles of Electron Spin Resonance" Ed. Ellis Horwood-PTR Prentice Hall, 1993.
39. Goodman, b. A. and Raynor, J. B. *In Advances in Inorg. Chem. And Radiochem.*, Ed. AP, **1970**, *13*, 136-362.
40. Ballhausen, C. J.; Gray, H. B. *Inorg. Chem.* **1962**, *1*, 111.

41. Jaffe', H. H. and Doak, G. O. *J. Chem. Phys.* **1953**, *21*, 196.
42. Jaffe', H. H. *J. Chem. Phys.* **1953**, *21*, 258.
43. Clementi, E. and Roetti, C. *At. Data. Nucl. Data*, **1974**, *14*, 177.
44. Casey, A. T. and Raynor. J. B. *J. Chem. soc. Dalton Trans.* **1983**, 2057.
45. Yen, M.F., Tyman, E.C. and Vaughan, G.B. In *Spectroscopy of Fuels*, Friedel, R. A., Ed.; Plenum: New York, 1970, 187.
46. McGarvey, B. R. *J. Phys. Chem.* **1967**, *71*, 51.
47. Gahan, B. and Mabbs, F. E., *J. Chem. soc. Dalton Trans.* **1983**, 1713.
48. Pandeya, K. B. and Khare, D., *Synth. React. Inorg. Met.-Org. Chem.*, **1992**, *22* (5), 521.
49. Jezierski, A. and Raynor. J. B. *J. Chem. soc. Dalton Trans.* **1980**, 1.
50. Yen, T.F. In *The Role of Trace Metals in Petroleum*; Yen, T. F., Ed.; Ann Arbor Science, Ann Arbor, **1975**, 167.
51. Atherton, N. M.; Locke, J.; McCleverty, J. A. *Chem. Ind.* **1965**, 1300.
52. Assour, J. M. *J. Chem. Phys.* **1965**, *43*, 2477.
53. Kuska, H. A. and Rogers, M. T., *Inorg. Chem.* **1966**, *5*, 3113.
54. Miller, G. A. and McClung, R. E. D., *Inorg. Chem.* **1973**, *12*, 2554.
55. Reynolds, J. G.; Biggs, W. R.; Fetzer, J. C.; Gallegos, E.; Fish, R.H.; Komlenic, J. J.; Wines, B. K. In *Characterization of Heavy Crude Oils and Petroleum Residues*; Symposium International, Lyon, France, June 25. Technip, Paris, **1984**. 153.
56. (a) *International Critical Tables*, New York: McGraw-Hill Book Company, Inc. **1929**, *5*, 20.
 (b) *CRC Handbook of Chemistry and Physics*, 72nd Ed., **1991-1992**, 6-157.

57. (a) Kowert B. A., *J. Phys. Chem.* **1981**, 85, 229.
(b) Kowert, B. A. *J. Phys. Chem.* **1981**, 85, 1772.
58. Desktop Molecular Modeller, Version 5.1.
59. Patron, M; Kivelson, D.; Schwartz, R. N., *J. Phys. Chem.* **1982**, 86, 518.
60. Dote, J.; Kivelson, D.; Schwartz, R. N. *J. Phys. Chem.* **1981**, 85, 2169.
61. Dote, J.; Kivelson, D. *J. Phys. Chem.* **1983**, 87, 3889.
62. Kivelson, D., Kivelson, M.G. and Oppenheim, I. *J. Chem. Phys.* **1970**, 52, 1810.
63. Tsay S. and Kivelson, D. *Mol. Phys.* **1975**, 29, 1.
64. Kowert, B. A. and Kivelson, D. *J. Chem. Phys.* **1976**, 64, 5206.

IMAGE EVALUATION TEST TARGET (QA-3)



APPLIED IMAGE, Inc.
1653 East Main Street
Rochester, NY 14609 USA
Phone: 716/482-0300
Fax: 716/288-5989

© 1993, Applied Image, Inc., All Rights Reserved

